

**Georgia Water Resources Institute
Annual Technical Report
FY 2008**

Introduction

INTRODUCTION

The Georgia Water Resources Institute (GWRI) aims to provide interdisciplinary research, education, technology transfer, and information dissemination, and works collaboratively with various local, state, and federal agencies. These include the Georgia Environmental Protection Division/Georgia Dept. of Natural Resources, water and power utilities, environmental organizations, lake associations, California Energy Commission, California Department of Water Resources, National Oceanic and Atmospheric Administration, U.S. Army Corps of Engineers, U.S. Bureau of Reclamation, U.S. Geological Survey, U.S. Environmental Protection Agency, and U.S. Fish and Wildlife Service. Furthermore, GWRI has a significant international involvement in Europe, Africa, China, Middle East, and South America with support from the U.S. Agency for International Development, World Bank, Food and Agriculture Organization of the United Nations, and other international organizations. The Institute strives to bring to bear expertise from a variety of disciplines, including civil and environmental engineering, atmospheric sciences, agriculture, oceanography, forestry, ecology, economics, and public policy. This year's funded activities include:

RESEARCH PROJECTS

- (1) Water Resources Assessment, Planning, and Management In the Southeast US Using Decision Support Systems Driven by Climate-based Hydrologic Forecasts , Aris Georgakakos PI, Georgia Institute of Technology, sponsored by NOAA OGP Climate Prediction Program for the Americas (CPPA) under grant #2006L77.
- (2) Modeling Water Quality Changes in Aquifer Storage Recovery Systems , Chittaranjan Ray, University of Georgia, sponsored by GWRI under grant #1260014025 (Fund #R7113-G7).
- (3) Assessing the Impacts of A Major Wildfire in the Okefenokee Swamp On Mercy Levels in Resident Macroinvertebrates Darold Paul Batzer, University of Georgia, sponsored by GWRI under grant #1260014024 (Fund #R7113-G8).
- (4) A Comprehensive Evaluation of the Mandatory Drought Responses in GA , Susan Cozzens, Susan Cozzens, Georgia Institute of Technology, sponsored by GWRI under grant #51366R2 (Sequence #35334).
- (5) Tidal Streams: A Renewable Energy Source for Georgia , Kevin Haas, Georgia Institute of Technology-Savannah, sponsored by GWRI under grant 2006P10 (Sequence #35266).
- (6) A Decision Support System for Water Resources Planning in the Zhejiang River Basin , Aris Georgakakos PI, Georgia Institute of Technology, sponsored by the Chinese Ministry of Water Resources under grant #2006L89.
- (7) Multi-Scale Investigation of Seawater Intrusion and Application in Coastal Georgia, Jian Luo, PI, Georgia Institute of Technology, sponsored by GWRI under grant #2006P08 (Sub-project #2006P17; Fund #R9261).
- (8) Performance of the Northern California Water System Under Climate Change: INFORM As An Adaptation Tool , Aris Georgakakos, Georgia Institute of Technology, sponsored by the California Energy Commission under grant #2006P32.
- (9) Operational Multiscale Forecast and Reservoir Management in Northern California , Aris Georgakakos, Georgia Institute of Technology, sponsored by NOAA under grant #2006N95.

INFORMATION DISSEMINATION:

Kindsvater Symposium on Drought: Science and Policy, co-sponsored by GWRI, GA EPD, ASCE, USGS in Atlanta, GA, March 25, 2008. There were 125 persons in attendance.

EDUCATIONAL INITIATIVES Africa Water Resources Institute for Education and Applied Research (AWARE). This is a joint institute established by the Georgia Institute of Technology (GT) and the University of Pretoria (UP), through the Georgia Water Resources Institute (GWRI) and the University of Pretoria Water Institute (UPWI). This is the first such initiative between major American and African Universities and focuses on interdisciplinary graduate education, applied research, and technology transfer in the areas of water, energy, and environmental resources planning and management. AWARE was officially launched on June 19, 2008, and is based at the UP campus in Pretoria, South Africa. The first AWARE programs include a Joint Masters Degree Program in Water Resources Management and a Professional Continuing Education Program for water and hydropower professionals.

PROFESSIONAL AND POLICY IMPACT

Georgia:

GWRI continues to provide technical assistance to the Georgia Department of Natural Resources regarding the State Water Plan. In addition to the Georgia Tech River Basin Planning Tool, GWRI has completed a comprehensive study on the impacts of climate change for the Apalachicola-Chattahoochee-Flint River Basin shared with Alabama and Florida. The study indicates that droughts will most likely intensify having serious implications on water supply, energy generation, and ecological flows. The study was discussed at a recent workshop of the National Research Council and has helped to make climate change a matter of key importance in water planning and sharing in the southeast. California: Similar work, collaboratively with the Hydrologic Research Center in San Diego, has focused on climate change impacts on the Northern California water resources system (including the Sacramento and San Joaquin River basins). While the nature of the changes is different, due to hydrologic significance of snow melt, the findings are equally important regarding the need for mitigation and adaptation measures. With funding from the California Energy Commission and the Department of Water Resources, GWRI and HRC have just initiated a second project phase which aims at finalizing and transferring the forecast-decision tools and evaluating alternative climate and demand change mitigation measures. International:

In January 2009, GWRI staff visited the Democratic Republic of the Congo (DRC) and helped formulate and raise funding for a comprehensive assessment and development program. The program focuses on water, environmental, and energy development, as well as institutional and legal reforms, and is a collaborative effort with the United Nations Development Program and the DRC Ministry of the Environment.

Research Program Introduction

None.

Multi-Scale Investigation of Seawater Intrusion and Application in Coastal Georgia

Basic Information

Title:	Multi-Scale Investigation of Seawater Intrusion and Application in Coastal Georgia
Project Number:	2007GA165G
Start Date:	4/1/2008
End Date:	3/31/2011
Funding Source:	104G
Congressional District:	
Research Category:	Ground-water Flow and Transport
Focus Category:	Groundwater, Hydrology, Models
Descriptors:	
Principal Investigators:	Jian Luo, Jian Luo

Publication

ANNUAL REPORT

**GA165G: Multi-Scale Investigation of Seawater Intrusion
and Application in Coastal Georgia**

PI: JIAN LUO

**School of Civil and Environmental Engineering
Georgia Institute of Technology**

May 01, 2009

Content

Summary **2**

Chapter 1. Experimental Design for Seawater Intrusion **3**

Chapter 2. Analysis of stagnation points for a pumping well in recharge areas **5**

Chapter 3. Kinetic mass transfer coupled with periodic tidal activity may widen the transition zone in coastal aquifers **42**

Chapter 4. Influence of anisotropy and stratified heterogeneity on the pumping duration constrained by saltwater upconing **61**

Summary

This report summarizes the research activities conducted during the first year of the project: “Multi-Scale Investigation of Seawater Intrusion and Application in Coastal Georgia”. This report consists of four chapters: the first chapter summarizes the experimental activities for investigating seawater intrusion, the second chapter is an accepted manuscript by Journal of Hydrology, which presents stagnation point analysis for a pumping well in recharge area and will be extended for groundwater flow in coastal aquifers, the third chapter is a manuscript in revision, which discusses a mechanism that may result in wide transitional zones in coastal aquifer with seawater intrusion, and the fourth chapter is a manuscript under preparation, which presents results for upcoming issues in stratified coastal aquifers.

One PhD student, Chunhui Lu, is directly supported by this project. Matching funds from Georgia Institute of Technology include the financial support for another PhD student, Rulan Gong, the PI’s salary support, and experimental facilities.

Chapter 1. Experimental Design for Seawater Intrusion

A 2.4m-long, 1m-high tank was built to simulate quasi-two-dimensional transport in coastal aquifers (Figure 1). The tank walls are made of transparent acrylic material so that the experiments can be visually monitored and captured by digital camera. Glass beads will be packed in the tank as the subsurface porous medium. Salt (NaCl) solutions with a density of 1025kg/m^3 will be used as the seawater. The freshwater head on the left side will be maintained constant through a constant-head cell, and a mobile weir connecting to a driving mechanism is installed at the seawater end (right side) to generate a periodically varying seawater level. Dyes will be mixed with salty water to visualize seawater intrusion and mixed with freshwater or released at the top of tank to serve as contaminants. A computer-based digital camera (Nikon D300) with corresponding software (Camera Control Pro 2) will be employed to record the experiments by taking a time lapse photo series, which will be then processed to convert the color intensity into solute concentration contours. The laboratory chosen has no windows and is surrounded by black curtains to minimize the external light influences. Sampling ports are also installed on the surface of the tank for taking measurements of solute concentrations to validate the color intensity. Experiments will be conducted in the quasi-two-dimensional tank under various settings of hydrogeological conditions and chemical properties. Table 1 summarizes the contaminant property, aquifer type, formation property, and transient effects that may be investigated in the experiments. For example, by mixing glass beads of different sizes, the tank may mimic heterogeneous formations. These visualization experiments will also be used for education purposes.

Table 1. Hydrogeological conditions and chemical property used in quasi-two-dimensional experiments.

Contaminant Property	Aquifer Type	Formation Property	Transient Effects
<ul style="list-style-type: none"> • Conservative • Sorption • Non-soluble 	<ul style="list-style-type: none"> • Confined • Unconfined • Slanted • Stratified 	<ul style="list-style-type: none"> • Homogeneous • Heterogeneous 	<ul style="list-style-type: none"> • Steady state • Tidal Effects • Groundwater withdrawal

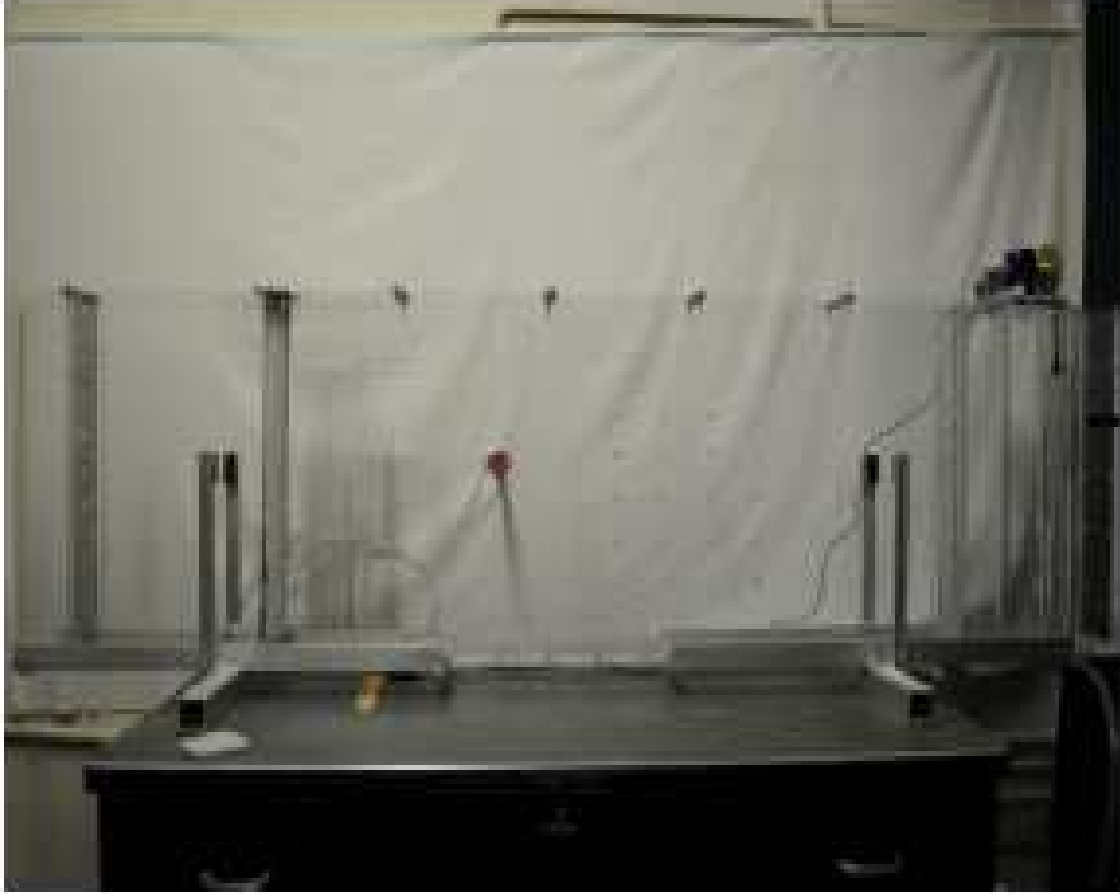


Figure 1. A quasi-two-dimensional experimental facility to simulate coastal hydrogeological systems.

Chapter 2. Analysis of stagnation points for a pumping well in recharge areas (accepted by Journal of Hydrology)

Introduction

Stagnation points are defined as points of zero specific discharge. For two-dimensional potential flow, this condition may be described by

$$\frac{\partial\Phi}{\partial x} = 0, \quad \frac{\partial\Phi}{\partial y} = 0 \tag{1}$$

where Φ is discharge potential, and x and y are spatial coordinates. The number, distribution, and type of stagnation points in the flow domain associated with aquifer features determine the flow pattern (Jin and Steward, 2007). A point satisfying Eq. (1) may be a maximum, a minimum, or a saddle point of the potential field (Fienen et al., 2005). The first two cases are possible only when recharge or drainage is involved, and the Poisson equation is satisfied for a homogeneous medium. In the absence of recharge, Φ is governed by a Laplace equation, and a stagnation point is always a saddle point, by virtue of the mean-value theorem. In all cases, stagnation points can be interpreted as “equilibrium points”, where two or more competing forces balance each other. For example, at the stagnation point between two extraction wells, the pull of one well is exactly opposite from the pull of the other. Stagnation points play an important role in groundwater flow because the separation streamlines passing through them delineate different flow regions. As an example, in flow fields manipulated by pumping well systems, separation streamlines passing through stagnation points delineate capture zones of exaction wells, release zones of injection wells, and boundaries of recirculation zones (Fienen et al., 2005).

Stagnation-point analysis and its applications in groundwater flow have continued for many years. Many researchers have made substantial contributions in this field (e.g. Muskat, 1946; Hantush, 1965; Bear, 1979; Javandel and Tsang, 1986; Newsom and Wilson, 1988; Strack, 1989; Wilson, 1993; Bakker and Strack, 1996; Zhan 1999a and 1999b; Christ and Goltz, 2002; Zhan and Zlotnik 2002; Luo and Kitanidis, 2004; Fienen et al., 2005; Intaraprasong and Zhan, 2007). For example, in flow fields created by

multiple injection-extraction wells, the difference in the value of stream functions at stagnation points may determine the captured flow rate in the capture zones, recirculated flow rate in the recirculation zones, and the flow rate in release zones. These results can then be used to evaluate the capture-zone width, recirculation ratio, and mean residence time, etc., and help design such multiple-well systems for groundwater remediation (Christ et al., 1999; Cunningham et al., 2004; Luo and Kitanidis, 2004; Luo et al., 2006).

Tracing streamlines from stagnation points is another application of stagnation-point analysis. In a flow field where complex potential or stream function can be defined, one can use the stream function to delineate the separation streamlines through stagnation points based on the definition that the value of the stream function is constant along a streamline (Christ and Goltz, 2002; Shan, 1999). Hence, the separation streamlines are contourlines of the stream function value passing through the stagnation point. In scenarios with internal volumetric sources or sinks, however, this method is complicated because each internal source or sink contributes a branch cut, and thus the stream function is discontinuous. Strack (1989) provided a prediction-correction procedure to track particles using stream functions. When particles pass through a branch cut, the stream function needs to be adjusted with a jump. Accounting for many branch cuts it is complicated. In the numerical approach of Cirpka et al. (1999), the stream function was evaluated only element-wise thus avoiding branch-cuts. In this approach, tracing streamlines was based on finding all points at the edges of the element sharing the same local stream function value. The latter authors determined the location of stagnation points by linear interpolation of the velocity field, and employ additional rules to account for stagnation points at element corners. The approach was applied exclusively to numerical flow fields without recharge or drainage. Bakker and Strack (1996) presented a numerical approach based on an analytic element model for the delineation of capture zones in an isotropic, homogeneous aquifer with recharge by determining starting points for tracing separation streamlines. A forward trace at a possible stagnation point is started to locate two forward and two backward points to determine the saddle stagnation points and generate the separation streamlines. Fienen et al. (2005) developed a novel semi-analytical method for quick delineation of streamlines in homogeneous aquifer with anisotropic transmissivity. By investigating the behavior of the potential Hessian matrix

at stagnation points, starting points of separation streamlines at stagnation points can be exactly determined.

In the present study, we present a thorough stagnation-point analysis for a pumping well in uniform regional flow in the presence of recharge or infiltration, which is an extension of the classical scenario of a pumping well in the absence of recharge. It is known that the resulted flow field by the pumping well and recharge is governed by two equations: inside the recharge area, it is the Poisson Equation, outside the recharge area the Laplace Equation. More than one stagnation point may exist as maximum, minimum, or saddle points. This scenario, essentially, can be considered as a combination of two cases studied by Strack (1989). One is that a pumping well is located at the center of a circular island with rainfall, and the other is local infiltration in the presence of regional flow. However, both cases are relatively simpler than ours because they do not include either the regional flow or the pumping well. By neglecting anyone of them, our cases can be simplified to one of these two cases. This combined scenario is of particular interest because it is very common in practice for pumping wells to be located inside or near a recharge area. A typical case is that an irrigation system is fed by groundwater pumped from an inside well. Pumping groundwater for irrigation in most arid and semiarid regions worldwide has experienced a significant increase over the last four decades since it, compared with traditional surface water irrigation systems, offers more reliable supplies, lesser vulnerability to droughts, and ready accessibility for individual user (Garrido et al., 2006). For example, Spain's groundwater irrigation sector represents 27% of 3.3 M ha total irrigated acreage (Garrido et al., 2006). In Northern Territory, Australia, as much as 89% of water used for irrigation is sourced from groundwater in year of 1996-1997 (<http://www.anra.gov.au/topics/irrigation/consumption/nt.html>).

Flow domain and governing equations

Consider an unconfined homogeneous aquifer with a constant infiltration rate N . Note that the infiltration rate is assumed to be an averaged value over the recharge area. Because a well can be drilled almost anywhere in a high-yielding aquifer, it is common to place it at the pivot point for agriculture irrigation systems (http://www.nespal.org/SIRP/awp/2005.03.Fact_Sheet_04SW.pdf). Without loss of

generality, we assume the area with recharge is circular with radius R and centered at the origin. An extraction well inside or near the recharge area with a specific extraction rate Q is arbitrarily located at the x -axis, which is parallel to the regional flow direction. The uniform regional flow is along x direction with intensity q_{x0} . This setup is consistent to the practical scenario, where a well is often the center of an irrigation area or the alignment of wells is parallel to regional flow for optimizing capture zone and containment (Christ and Goltz, 2004).

Fig.1 shows the plane view and cross section of the setup, and the flow field of the case with recharge, regional flow and no pumping well. It is obvious that the pumped water may come from both the regional flow and the recharge area. For example, if the well locates inside the recharge area with a small pumping rate, it is possible that all pumped water may come directly from recharge. At a high pumping rate, however, part of water may also be pumped from the surrounding aquifer, supplied by the regional flow.

The problem is simplified to be two-dimensional by ignoring the vertical infiltration processes and assuming steady-state flow field. As described previously, the flow field is governed by two equations: outside the recharge area, the flow field is analytic and governed by a Laplace equation; by contrast, the flow field inside the recharge area is not analytic due to infiltration, and is governed by a Poisson equation. Thus, a complex potential may be defined in the area without recharge, but is not available in the recharge area. We assume that the location of the well is $(x_w, 0)$, and the coordinates of the center of the infiltration are $(0, 0)$. The discharge potential, Φ , can be formulated as

$$\Phi(x, y) = \frac{Q}{4\pi} \ln\left(\frac{(x-x_w)^2 + y^2}{R^2}\right) - q_{x0}x + \begin{cases} -\frac{x^2 + y^2 - R^2}{4}N + C & \text{for } x^2 + y^2 \leq R^2 \\ -\frac{R^2N}{4} \ln\left(\frac{x^2 + y^2}{R^2}\right) + C & \text{for } x^2 + y^2 \geq R^2 \end{cases} \quad (2)$$

where $\frac{Q}{4\pi} \ln\left(\frac{(x-x_w)^2 + y^2}{R^2}\right)$ is the discharge potential for flow created by a pumping

well; $-q_{x0}x$ is the regional flow potential; $-\frac{x^2 + y^2 - R^2}{4}N$ and $-\frac{R^2N}{4} \ln\left(\frac{x^2 + y^2}{R^2}\right)$

are the discharge potential inside and outside of the recharge area, respectively; C is a constant.

In order to facilitate the interpretation of the analysis, the following dimensionless variables are defined:

$$\begin{aligned} x^* &= \frac{x}{R}, y^* = \frac{y}{R}, x_s^* = \frac{x_s}{R}, y_s^* = \frac{y_s}{R}, x_w^* = \frac{x_w}{R}, y_w^* = \frac{y_w}{R}, Q^* = \frac{Q}{\pi NR^2}, q_{x0}^* = \frac{2q_{x0}}{NR}, \\ H^* &= \frac{H}{N}, \Phi^* = \frac{\Phi}{NR^2} \end{aligned} \quad (3)$$

where x^* , y^* , x_s^* , y_s^* , x_w^* and y_w^* are dimensionless coordinates normalized by recharge area radius; x_s and y_s are stagnation point coordinates; Q^* is dimensionless pumping rate; q_{x0}^* is dimensionless regional flow rate; H^* is dimensionless Hessian matrix of the discharge potential; and Φ^* is dimensionless potential, which is expressed as

$$\Phi^*(x^*, y^*) = \frac{Q^*}{4} \ln\left((x^* - x_w^*)^2 + y^{*2}\right) - \frac{q_{x0}^*}{2} x^* + \begin{cases} -\frac{x^{*2} + y^{*2} - 1}{4} + C & \text{for } x^{*2} + y^{*2} \leq 1 \\ -\frac{1}{4} \ln(x^{*2} + y^{*2}) + C & \text{for } x^{*2} + y^{*2} \geq 1 \end{cases} \quad (4)$$

Stagnation point and critical pumping rate

Stagnation points can be obtained by solving Eq. (1) in dimensionless form

$$0 = \frac{\partial \Phi^*}{\partial x^*} = \frac{Q^*(x^* - x_w^*)}{(x^* - x_w^*)^2 + y^{*2}} - q_{x0}^* + \begin{cases} -x^* & \text{for } x^{*2} + y^{*2} \leq 1 \\ \frac{x^*}{x^{*2} + y^{*2}} & \text{for } x^{*2} + y^{*2} \geq 1 \end{cases} \quad (5)$$

$$0 = \frac{\partial \Phi^*}{\partial y^*} = \frac{Q^* y^*}{(x^* - x_w^*)^2 + y^{*2}} + \begin{cases} -y^* & \text{for } x^{*2} + y^{*2} \leq 1 \\ \frac{y^*}{x^{*2} + y^{*2}} & \text{for } x^{*2} + y^{*2} \geq 1 \end{cases} \quad (6)$$

Thus, the dimensionless coordinates of the stagnation points are given by:

$$x_s^* = \begin{cases} \left(\frac{x_w^* - q_{x0}^*}{2}\right) \pm \sqrt{\left(\frac{x_w^* - q_{x0}^*}{2}\right)^2 + (Q^* + q_{x0}^* x_w^*)} & \text{for } x^{*2} + y^{*2} \leq 1 \\ \frac{(Q^* + q_{x0}^* x_w^* - 1) \pm \sqrt{(Q^* + q_{x0}^* x_w^* - 1)^2 + 4q_{x0}^* x_w^*}}{2q_{x0}^*} & \text{for } x^{*2} + y^{*2} \geq 1 \end{cases}, y_s^* = 0 \quad (7)$$

Eq. (7) indicates that the flow field may have at most four stagnation points, comparing with only one stagnation point without recharge. However, in some cases, the stagnation points may not co-exist or may coincide. Identification of these critical cases may yield critical pumping rates and critical well locations which control the behavior of the flow field. The analysis may also help explain the fate of chemicals and nutrients leached from the field into the groundwater. Detailed analyses about the number and locations of stagnation points can be made based on the dimensionless parameters x_w^* , q_{x0}^* , and Q^* , which are presented in the following sections.

The well locates at the origin

First of all, we consider a special case that the well locates exactly at the origin, namely, $x_w^* = 0$. This will significantly simplify the discussion. According to Eqs. (5) and (6), stagnation points hereby can be obtained by solving

$$0 = \frac{\partial \Phi^*}{\partial x^*} = \frac{Q^* x^*}{x^{*2} + y^{*2}} - q_{x0}^* + \begin{cases} -x^* & \text{for } x^{*2} + y^{*2} \leq 1 \\ \frac{x^*}{x^{*2} + y^{*2}} & \text{for } x^{*2} + y^{*2} \geq 1 \end{cases} \quad (8)$$

$$0 = \frac{\partial \Phi^*}{\partial y^*} = \frac{Q^* y^*}{x^{*2} + y^{*2}} + \begin{cases} -y^* & \text{for } x^{*2} + y^{*2} \leq 1 \\ -\frac{y^*}{x^{*2} + y^{*2}} & \text{for } x^{*2} + y^{*2} \geq 1 \end{cases} \quad (9)$$

Thus, the dimensionless coordinates of the stagnation points are:

$$x_s^* = \begin{cases} -\frac{q_{x0}^*}{2} \pm \sqrt{\frac{q_{x0}^{*2}}{4} + Q^*} & \text{for } x^{*2} + y^{*2} \leq 1 \\ \frac{Q^* - 1}{q_{x0}^*} & \text{for } x^{*2} + y^{*2} \geq 1 \end{cases}, \quad y_s^* = 0 \quad (10)$$

Eq. (10) can not only be used to calculate the dimensionless coordinates of the stagnation points, but also provide a way to determine the dimensionless critical pumping rates by generating the follow inequality set:

$$\left\{ \begin{array}{l} a. -1 \leq -\frac{q_{x0}^*}{2} - \sqrt{\frac{q_{x0}^{*2}}{4} + Q^*} \leq 0 \\ b. 0 \leq -\frac{q_{x0}^*}{2} + \sqrt{\frac{q_{x0}^{*2}}{4} + Q^*} \leq 1 \\ c. \frac{Q^* - 1}{q_{x0}^*} \geq 1 \text{ or } \frac{Q^* - 1}{q_{x0}^*} \leq -1 \end{array} \right. \quad (11)$$

which gives:

$$\left\{ \begin{array}{l} a. \Omega 1: Q^* \leq 1 - q_{x0}^* \\ b. \Omega 2: Q^* \leq 1 + q_{x0}^* \\ c. \Omega 3: Q^* \geq 1 + q_{x0}^* \text{ or } Q^* \leq 1 - q_{x0}^* \end{array} \right. \quad (12)$$

The solutions derived from the inequality set can be used to evaluate the number and locations of stagnation points for different conditions. For example, for the case of two stagnation points where one exists inside the recharge area, and the other locates outside the recharge area, we can derive the dimensionless pumping rate interval by solving

$$Q^* = ((\overline{\Omega 1} \cap \overline{\Omega 2}) \cup (\overline{\Omega 1} \cap \Omega 2)) \cap \Omega 3 \quad (13)$$

where $\overline{\Omega 1}$ and $\overline{\Omega 2}$ represent complements of $\Omega 1$ and $\Omega 2$, respectively. Then, for a given Q^* , we can obtain the stagnation-point locations by solving Eq. (10).

It should be noted that two dimensionless critical pumping rates, $1 + q_{x0}^*$ and $1 - q_{x0}^*$ appear in Eq. (12). Physically speaking, $1 + q_{x0}^*$ denotes sum of the infiltration rate and equivalent regional flow rate on recharge area, while $1 - q_{x0}^*$ represents the difference between these two rates and hereby can be regarded as "over-infiltration rate" on recharge area. Based on the solution set of Eq. (12), the following conclusions about stagnation points can be drawn for different values of Q^* :

1. For $q_{x0}^* \geq 1$:
 - (a) If $0 < Q^* < 1 + q_{x0}^*$, there is only one stagnation point, which is located inside the recharge area.
 - (b) If $Q^* > 1 + q_{x0}^*$, there is only one stagnation point, which is located outside the recharge area.

(c) If $Q^* = 1 + q_{x0}^*$, one stagnation point with dimensionless coordinates (1, 0) is obtained,

$$\text{because } -\frac{q_{x0}^*}{2} + \sqrt{\frac{q_{x0}^{*2}}{4} + Q^*} = \frac{Q^* - 1}{q_{x0}^*} = 1.$$

2. For $q_{x0}^* < 1$:

(a) If $0 < Q^* < 1 - q_{x0}^*$, there are three stagnation points. Two of them are located inside

the recharge area at $\left(-\frac{q_{x0}^*}{2} \pm \sqrt{\frac{q_{x0}^{*2}}{4} + Q^*}, 0\right)$, and one is located outside the recharge

area at $\left(\frac{Q^* - 1}{q_{x0}^*}, 0\right)$.

(b) If $1 - q_{x0}^* < Q^* < 1 + q_{x0}^*$, there is only one stagnation point at

$\left(-\frac{q_{x0}^*}{2} + \sqrt{\frac{q_{x0}^{*2}}{4} + Q^*}, 0\right)$, which is located inside of the recharge area.

(c) If $Q^* > 1 + q_{x0}^*$, there is only one stagnation point at $\left(\frac{Q^* - 1}{q_{x0}^*}, 0\right)$, which is located

outside the recharge area.

(d) If $Q^* = 1 - q_{x0}^*$, there are two stagnation points at (-1, 0) and $(1 - q_{x0}^*, 0)$, because

$$-\frac{q_{x0}^*}{2} - \sqrt{\frac{q_{x0}^{*2}}{4} + Q^*} = \frac{Q^* - 1}{q_{x0}^*} = -1.$$

(e) If $Q^* = 1 + q_{x0}^*$, there is only one stagnation point at (1, 0).

The results above show that the number and position of the stagnation points are determined by the pumping rate and relative magnitude between infiltration rate and equivalent regional flow rate on recharge area.

The well does not locate at the origin

In this section, we will extend the stagnation-point analysis for an arbitrarily located pumping well. We assume $x_w^* > 0$, and the case where $x_w^* < 0$ can be similarly derived.

Eq. (7) can be expressed as the following inequality set subject to the constraint that $x_w^* > 0$:

$$\left\{ \begin{array}{l} a. -1 \leq \left(\frac{x_w^*}{2} - \frac{q_{x0}^*}{2} \right) - \sqrt{\left(\frac{x_w^*}{2} - \frac{q_{x0}^*}{2} \right)^2 + (Q^* + q_{x0}^* x_w^*)} \leq 0 \\ b. 0 \leq \left(\frac{x_w^*}{2} - \frac{q_{x0}^*}{2} \right) + \sqrt{\left(\frac{x_w^*}{2} - \frac{q_{x0}^*}{2} \right)^2 + (Q^* + q_{x0}^* x_w^*)} \leq 1 \\ c. \frac{(Q^* + q_{x0}^* x_w^* - 1) - \sqrt{(Q^* + q_{x0}^* x_w^* - 1)^2 + 4q_{x0}^* x_w^*}}{2q_{x0}^*} \leq -1 \\ d. \frac{(Q^* + q_{x0}^* x_w^* - 1) + \sqrt{(Q^* + q_{x0}^* x_w^* - 1)^2 + 4q_{x0}^* x_w^*}}{2q_{x0}^*} \geq 1 \end{array} \right. \quad (14)$$

Solving these inequalities yields

$$\left\{ \begin{array}{l} a. \Omega 1: Q^* \leq (1 + x_w^*)(1 - q_{x0}^*) \\ b. \Omega 2: Q^* \leq (1 - x_w^*)(1 + q_{x0}^*) \\ c. \Omega 3: Q^* \leq (1 + x_w^*)(1 - q_{x0}^*) \\ d. \Omega 4: Q^* \geq (1 - x_w^*)(1 + q_{x0}^*) \end{array} \right. \quad (15)$$

which provide a tool for calculating the number and locations of stagnation points at a given pumping rate. We define two dimensionless critical pumping rates:

$$Q_{c1} = (1 - x_w^*)(1 + q_{x0}^*) \text{ and } Q_{c1} = (1 + x_w^*)(1 - q_{x0}^*) \quad (16)$$

One can observe from the Eq. (15) that $\Omega 1$ and $\Omega 3$ is the same, which means the dimensionless stagnation points at $[-1, 0)$ and $(-\infty, -1]$ co-exist. On the other hand, $\Omega 2 \cap \Omega 4 = Q_{c1}$ shows that the dimensionless stagnation points at $[0, 1]$ and $[1, +\infty)$ repel each other, except at the critical pumping rate Q_{c1} , which indicates there is one and only one stagnation point located in these two intervals. The results derived for all cases are given in Table 1. It shows that the number and locations of stagnation points are not only related to the magnitudes of x_w^* , q_{x0}^* , and Q^* , but also dependent on the relative magnitude between x_w^* and q_{x0}^* . As an example, consider $q_{x0}^* \leq 1$ and $0 < x_w^* < 1$, the following conclusions about the dimensionless pumping rate, the number and locations of stagnation points can be made.

1. For $x_w^* < q_{x0}^*$:

- (a) If $0 < Q^* < Q_{c2}$, there are three stagnation points, and two of them are inside the recharge area and only one stagnation point is outside the recharge area.
- (b) If $Q_{c2} < Q^* < Q_{c1}$, there is one stagnation point inside the recharge area, and no stagnation point outside the recharge area.
- (c) If $Q^* > Q_{c1}$, there is one stagnation point outside the recharge area, and no stagnation point inside the recharge area.
- (d) Consider critical conditions. If $Q^* = Q_{c2}$, there are two stagnation points, $(-1, 0)$ and

$$\left(\left(\frac{x_w^*}{2} - \frac{q_{x0}^*}{2} \right) + \sqrt{\left(\frac{x_w^*}{2} - \frac{q_{x0}^*}{2} \right)^2 + (Q^* + q_{x0}^* x_w^*)}, 0 \right) \quad \text{because}$$

$$\left(\frac{x_w^*}{2} - \frac{q_{x0}^*}{2} \right) + \sqrt{\left(\frac{x_w^*}{2} - \frac{q_{x0}^*}{2} \right)^2 + (Q^* + q_{x0}^* x_w^*)} = \frac{(Q^* + q_{x0}^* x_w^* - 1) - \sqrt{(Q^* + q_{x0}^* x_w^* - 1)^2 + 4q_{x0}^* x_w^*}}{2q_{x0}^*} = -1$$

- (e) If $Q^* = Q_{c1}$, there is only one stagnation point, namely $(1, 0)$, located at the perimeter of the recharge circle.

2. For $x_w^* > q_{x0}^*$:

- (a) If $0 < Q^* < Q_{c1}$, there are three stagnation points, and two of which are within the recharge area and only one stagnation point is outside the recharge area.
- (b) If $Q_{c1} < Q^* < Q_{c2}$, there are also three stagnation points, and one stagnation point is within the recharge and the rest are outside the recharge area.
- (c) If $Q^* > Q_{c2}$, there is one stagnation point outside the recharge area, and no stagnation point within the recharge area.
- (d) Consider critical conditions. If $Q^* = Q_{c1}$, there are three stagnation points, $(1, 0)$,

$$\left(\left(\frac{x_w^*}{2} - \frac{q_{x0}^*}{2} \right) - \sqrt{\left(\frac{x_w^*}{2} - \frac{q_{x0}^*}{2} \right)^2 + (Q^* + q_{x0}^* x_w^*)}, 0 \right) \quad \text{and}$$

$$\left(\frac{(Q^* + q_{x0}^* x_w^* - 1) - \sqrt{(Q^* + q_{x0}^* x_w^* - 1)^2 + 4q_{x0}^* x_w^*}}{2q_{x0}^*}, 0 \right).$$

(e) If $Q^* = Q_{c2}$, there are two stagnation points with coordinates of

$$\left(\left(\frac{x_w^*}{2} - \frac{q_{x0}^*}{2} \right) + \sqrt{\left(\frac{x_w^*}{2} - \frac{q_{x0}^*}{2} \right)^2 + (Q^* + q_{x0}^* x_w^*)}, 0 \right) \text{ and } (-1, 0).$$

3. For $x_w^* = q_{x0}^*$:

- (a) If $0 < Q^* < Q_{c1}$, there are three stagnation points. Two symmetrical stagnation points are located inside the recharge area and one is outside the recharge area.
- (b) If $Q^* > Q_{c1}$, there is only one stagnation point, which is located outside the recharge area.
- (c) If $Q^* = Q_{c1}$, the two stagnation points locate exactly at the recharge boundary, namely, (1, 0) and (-1, 0).

Type of stagnation points

As described in the introduction, stagnation points may be maximum, minimum, or saddle points when recharge or infiltration is considered. Their roles in characterizing flow pattern have been widely studied (Winter TC, 1978; Anderson and Munte, 1981; Anderson, 2002; Bakker and Strack, 1996; Bear and Jacobs, 1965; Cheng and Anderson, 1994; Christ and Goltz, 2002; Erdmann, 1999; Javandel and Tsang, 1986; Nield et. al, 1994; Smith and Townley, 2002; Steward, 1999; Townley and Trefry, 2000; Fienen et. al, 2002; Jin and Steward, 2007). Since the Laplace equation is not satisfied for the recharge area, $x^{*2} + y^{*2} \leq 1$, we use the Hessian-matrix method of the discharge potential to identify the type of stagnation points and determine the streamline orientations (Fienen et al., 2005). For the sake of completeness, we summarize the Hessian-matrix method in the Appendix A.1.

For simplicity, we identify the type of stagnation points for the case in which the well locates at the origin. Inside the recharge area, the dimensionless Hessian matrix of the discharge potential is given by

$$H^* = \begin{bmatrix} \frac{Q^*}{2} \frac{y^{*2} - x^{*2}}{(x^{*2} + y^{*2})^2} - \frac{1}{2} & \frac{-Q^* x^* y^*}{(x^{*2} + y^{*2})^2} \\ \frac{-Q^* x^* y^*}{(x^{*2} + y^{*2})^2} & \frac{Q^*}{2} \frac{x^{*2} - y^{*2}}{(x^{*2} + y^{*2})^2} - \frac{1}{2} \end{bmatrix} \quad (17)$$

Thus, at the stagnation points,

$$A = -\frac{Q^*}{2x_s^{*2}} - \frac{1}{2}, \quad B = 0, \quad C = \frac{Q^*}{2x_s^{*2}} - \frac{1}{2} \quad (18)$$

For the stagnation point at $\left(-\frac{q_{x0}^*}{2} + \sqrt{\frac{q_{x0}^{*2}}{4} + Q^*}, 0\right)$, we have

$$A < 0, \quad C > 0 \quad (19)$$

The proof of (19) is given in Appendix A.2. According to the properties of the Hessian matrix (see Appendix A.1), this stagnation point is a saddle point and the orientation of the streamlines are x and y direction.

For the stagnation point at $\left(-\frac{q_{x0}^*}{2} - \sqrt{\frac{q_{x0}^{*2}}{4} + Q^*}, 0\right)$, we have

$$A < 0, \quad C < 0 \quad (20)$$

The proof of (20) is given in the Appendix A.3. Thus, this stagnation point is a strict maximum, not a saddle point.

Outside the recharge area, the dimensionless Hessian matrix is given by:

$$H^* = \begin{bmatrix} \left(\frac{Q^*}{2} - \frac{1}{2}\right) \frac{y^{*2} - x^{*2}}{(x^{*2} + y^{*2})^2} & (Q^* - 1) \frac{-x^* y^*}{(x^{*2} + y^{*2})^2} \\ (Q^* - 1) \frac{-x^* y^*}{(x^{*2} + y^{*2})^2} & \left(\frac{Q^*}{2} - \frac{1}{2}\right) \frac{x^{*2} - y^{*2}}{(x^{*2} + y^{*2})^2} \end{bmatrix} \quad (21)$$

Thus, at the stagnation point, $\left(\frac{Q^* - 1}{q_{x0}^*}, 0\right)$, we have:

$$A = -C = \frac{1 - Q^*}{2x_s^{*2}}, B = 0 \quad (22)$$

This stagnation point is a saddle point with streamline orientation in x^* and y^* directions.

Consider the critical condition for pumping rate of the well. If $Q^* = 1 + q_{x0}^*$, two

stagnation points, $\left(-\frac{q_{x0}^*}{2} + \sqrt{\frac{q_{x0}^{*2}}{4} + Q^*}, 0\right)$ and $\left(\frac{Q^* - 1}{q_{x0}^*}, 0\right)$ coincide at $(1, 0)$, and both

are saddle points. Applying the dimensionless Hessian matrix inside of the recharge area, i.e., Eq. (17), we obtain:

$$H^* = \begin{bmatrix} -\frac{q_{x0}^*}{2} - 1 & 0 \\ 0 & \frac{q_{x0}^*}{2} \end{bmatrix} \quad (23)$$

On the contrary, using the Hessian matrix outside the recharge area, i.e., Eq. (21), we get:

$$H^* = \begin{bmatrix} -\frac{q_{x0}^*}{2} & 0 \\ 0 & \frac{q_{x0}^*}{2} \end{bmatrix} \quad (24)$$

Thus, the curvatures at this point are discontinuous although both Hessian matrices define this stagnation point as a saddle point. This discontinuity results from the different governing equation used to solve for the discharge potential. Inside the recharge area, the Poisson equation is applied, but outside the recharge area, the Laplace equation is employed. The analytical solution of the dimensionless discharge potential, Eq. (4), is C1-continuous at the perimeter, but not C2-continuous, that is, the potential curvature is discontinuous. At dimensionless coordinates $(1, 0)$, the curvature is continuous in y^* direction because of the identical element $\frac{q_{x0}^*}{2}$ in the dimensionless Hessian matrices, and discontinuous in x^* direction. Thus, this coincident point can be considered as a transition point between two saddle points, where the potential curvature in direction x^* changes abruptly.

If $Q^* = 1 - q_{x0}^*$ a saddle point $\left(\frac{Q^* - 1}{q_{x0}^*}, 0\right)$ and a maximum point

$\left(-\frac{q_{x0}^*}{2} - \sqrt{\frac{q_{x0}^{*2}}{4} + Q^*}, 0\right)$ coincide at $(-1, 0)$. This point is also a transition point.

Applying Eq. (17), we obtain:

$$H = \begin{bmatrix} \frac{q_{x0}^*}{2} - 1 & 0 \\ 0 & -\frac{q_{x0}^*}{2} \end{bmatrix} \quad (25)$$

Because $Q^* = 1 - q_{x0}^* > 0$ gives $q_{x0}^* < 1$, both eigenvalues are negative. Applying Eq. (21), the dimensionless Hessian matrix becomes

$$H^* = \begin{bmatrix} \frac{q_{x0}^*}{2} & 0 \\ 0 & -\frac{q_{x0}^*}{2} \end{bmatrix} \quad (26)$$

One eigenvalue is positive and the other is negative. Thus, this coincident point is a transition point between a saddle point and a maximum point, where the potential curvature in direction x^* changes abruptly.

Case studies and discussion

To demonstrate the theoretical analyses presented above, we assign some specific values for N , R and q_{x0} to explore the stagnation points and the separation streamlines at different pumping rates for various cases discussed above. We assume that the recharge rate N is 5×10^{-6} m/sec, R is 20 m, and the regional flow rate q_{x0} is 10^{-5} m²/sec. Thus, the value of dimensionless parameter q_{x0}^* is equal to 0.2.

In this case, $q_{x0}^* < 1$, that is, the infiltration rate is larger than equivalent regional flow rate on recharge area, which is more common found in most field conditions. With the changing of well location and pumping rates, the different numbers and locations of stagnation points are obtained, thus forming the different flow fields. The separation

streamline are delineated by tracing streamlines from stagnation points, and the detail regarding this approach is given elsewhere (Fienen et al., 2005).

The well locates at the origin

Fig. 2 shows the stagnation points and the separation streamlines for different pumping rates when the well locates exactly at the origin. Dimensionless well pumping rates and coordinates of stagnation points are listed in Table 2. Fig. 2(a) shows if $Q^* < 1 - q_{x0}^*$, which means the pumping rate is smaller than the difference between the infiltration rate and equivalent regional flow rate on recharge area, there are three stagnation points. The transition point separates a saddle point and a maximum point, located outside and inside the recharge area, respectively. Infiltration not only supplies all the well pumping, but acts as a strong injection, which results in the separation streamlines outside the recharge area, thereby forcing the regional flow to travel outside the separation streamlines. Fig. 2(b) shows when $Q^* = 1 - q_{x0}^*$, two stagnation points can be obtained: one is a saddle point, located inside the recharge circle, and the other is a transition point, where a saddle point and a maxima point coincide. The "over-infiltration" is exactly pumped by the well and therefore separation streamlines form a closed cell. Fig. 2(c) shows if $1 - q_{x0}^* < Q^* < 1 + q_{x0}^*$, a saddle point is located inside the recharge area and the separation streamlines cannot contain the recharge circle. Fig. 2(d) indicates if $Q^* = 1 + q_{x0}^*$, that is, all infiltration and regional flow on recharge area are exactly pumped by the well, a saddle point is located at the perimeter of recharge circle and the separation streamlines are tangent to the recharge circle. Fig. 2(e) indicates if $Q^* > 1 + q_{x0}^*$, there is a stagnation point, which is a saddle point, located outside the recharge area and the separation streamlines contain the recharge circle. It can be physically interpreted as the well capturing all the infiltration and some regional flow because its pumping rate is larger than the total recharge and the regional flow received by the recharge circle.

The well does not locate at the origin

Figs. 3-5 delineate the stagnation points and the separation streamlines at different pumping rates for the wells locating at 2 m, 4 m, and 10 m, respectively. Their

corresponding dimensionless coordinates are (0.1, 0), (0.2, 0) and (0.5, 0). Well pumping rates and coordinates of stagnation points are listed in Tables 3-5. Inspection of these figures and tables leads to the following conclusions.

1. Fig. 6 shows the relationship between the critical pumping rate and well location. As the well moves from the origin to the recharge perimeter, the lower critical pumping rate is linearly increased, and then linearly decreased after passing the well location (0.2, 0), ultimately reaching zero at the perimeter of the recharge area. For the higher critical pumping rate, however, the value is linearly decreased as the well moves from the origin to the dimensionless critical well location (0.2, 0), and then linearly increased after passing this point. Hence, the interval between the higher and lower critical pumping rate initially decreases, and then increases after passing the critical well location. It is noteworthy that at the critical well location, namely the point (0.2, 0), two critical pumping rates are exactly the same being 0.95.
2. An interesting phenomenon can be observed that at the critical well location, namely $x_w^* = 0.2$, two stagnation points obtained inside the recharge area are symmetrical with respect to the origin under the condition that Q^* is less than the critical pumping rate. For example, at $Q^* = 0.56$, there are two symmetrical stagnation points (0.77, 0) and (-0.77, 0); at $Q^* = 0.88$, two symmetrical stagnation points (0.96, 0) and (-0.96, 0) are found; particularly, at critical pumping rate, two stagnation points locates exactly at the perimeter of the recharge circle.
3. At a low pumping rate, namely, for $x_w^* = 0.1$ and $Q^* < 0.88$, $x_w^* = 0.2$ and $Q^* < 0.95$, and $x_w^* = 0.5$ and $Q^* < 0.60$, there are always three stagnation points for each case, and without exception, one locates outside the recharge area and the rest situate inside the recharge area. Like the case where the well locates at the origin, infiltration not only supplies all the well pumping, but serves as a strong injection, which results in the separation streamlines outside the recharge area, thereby forcing the regional flow to travel outside the separation streamlines. At the same pumping rate Q^* where $Q^* \leq 0.60$, as the well moves from the origin to the right, the stagnation point outside the recharge area moves gradually in the negative x^* direction, while two stagnation

points inside the recharge area moves in the positive x^* direction.

4. At a high pumping rate, namely, for $x_w^* = 0.1$ and $Q^* > 1.08$, $x_w^* = 0.2$ and $Q^* > 0.95$, and $x_w^* = 0.5$ and $Q^* > 1.2$, there is always only one stagnation point, which locates outside the recharge area. This phenomenon is due to the fact that at a high pumping rate, all infiltration and partial regional flow are served as a supplier for pumping well, thus no additional infiltration acts on regional flow for resulting in the separation streamline outside the recharge area. Besides, for the condition that the well locates inside the recharge area with the same pumping rate Q^* where $Q^* > 1.2$, as the well moves from the origin to the right, the stagnation point outside the recharge area moves gradually in the positive x^* direction.
5. As well location moves from the origin to the infiltration perimeter, comparing the streamlines and stagnation points at $Q^* = 0.95$ for each case, two “tails” outside the recharge area are becoming more and more closer, and then form a closed circle which surrounds the recharge area under the condition that the well locates at the dimensionless critical well location (0.2, 0); eventually the closed cell moves to the right and includes partial regional flow and excludes some recharge area, which results in the separation streamlines outside the recharge area and forms the third stagnation point.
6. With the exception of the case where the well locates at dimensionless point (0.5, 0), there are two stagnation points obtained at the lower critical pumping rate. For the case where the well locates at the point (0.1, 0), one stagnation point locates at (0.90, 0) and the other locates at (-1, 0). For the well located at the critical well location (0.2, 0), two stagnation point locates at (1, 0) and (-1, 0), respectively. However, at the lower critical pumping rate, as can be seen from Fig. 5(c), there are three stagnation points obtained for the well located at the point (0.5, 0). This may be because the lower critical pumping rate under that condition is so weak that infiltration is surplus for providing the well extraction, which produces the separation streamlines outside the recharge area and eventually forms the third stagnation point. Note that if $x_w^* \geq 0$ and Q^* equals to the lower or higher critical pumping rate, at least one stagnation point locates at the perimeter of recharge circle. On the other hand, except for the well

location of (0.5, 0), at the higher critical pumping rate, there is one stagnation point obtained. For the well located at (0.5, 0), however, there are two stagnation points, as can be seen from Fig. 5(d). The closed cell inside the recharge area denotes a dividing curve of pure infiltration and a mixture of infiltration and regional flow, that is, inside the closed cell, there is only infiltration, and outside the curve, there is a mixture of infiltration and regional flow.

7. As analytically shown previously, the stagnation points in $(-\infty, -1)$ and $(-1, 0)$ co-exist, and there is one, and only one stagnation point in $(0, +\infty)$. For example, as $x_w^* = 0.5$, for $Q^* = 0.48$, there are two stagnation points $(-0.63, 0)$ and $(-2.95, 0)$, located in $(-\infty, -1)$ and $(-1, 0)$, respectively. However, for the interval of $(0, +\infty)$, there is only one stagnation, located at $(0.93, 0)$.

Analyses about the case where the well locates at the left of the origin can be made by the similar method presented above. However, for negative value of x_w^* , we have another constraint for the stagnation point located outside the recharge area, namely,

$(Q^* + q_{x0}^* x_w^* - 1)^2 + 4q_{x0}^* x_w^* \geq 0$. In other words, the pumping rate interval derived for stagnation points outside the recharge area should be implicitly subject to this constraint. As an example, we delineate the stagnation points and separation streamlines for the case where the well locates at $(-0.5, 0)$ with a dimensionless critical pumping rate of 0.40, as can be seen in Fig. 7.

Conclusion

We have presented a thorough stagnation-point analysis for a single pumping well in recharge areas. For the case where the well locates at the origin, we have performed critical pumping rate analysis and calculated the stagnation points for each critical pumping rate interval. According to the characteristics of the Hessian matrix, we also identified the nature of each stagnation point. For the well arbitrarily located, we also presented the critical pumping rate analysis although it appears to be more complicated than the previous case. By performing the stagnation-point analysis, one can realize that

the condition of flow field is determined not only by the magnitude of the single dimensionless parameter such as Q^* , q_{x0}^* , and x_w^* , but also related to the relative magnitude between q_{x0}^* and x_w^* . In the end, we delineated the streamlines for a given case with different well locations and pumping rates. Starting points for tracing separation streamlines are found by offsetting slightly along these directions from the stagnation points. Since the problems that velocity is zero at the stagnation points are eliminated, the separation streamline can be constructed directly by streamline-tracing methods. In summary, for a well inside the recharge area with a relatively low pumping rate, there are always three stagnation points, because the unpumped infiltration produces the separation streamlines outside the recharge area and eventually forms the third stagnation point. However, for the well with a relatively high pumping rate, there is one, and only one stagnation point outside the recharge area, for all infiltration and partial regional flow are extracted by the well.

Acknowledgements

This work was partially funded by Georgia Water Resources Institute, and partially funded by the National Institutes of Water Resources (NIWR) and U.S. Geological Survey (USGS) under project ID 2007GA165G.. The authors would like to thank Dr. M.N. Fienen for his helpful discussion. The authors are very grateful for the helpful review comments from two anonymous reviewers.

Appendix.

A.1 Hessian matrix method for flow field with recharge or drainage (Fienen et al., 2005)

In the presence of regional infiltration or drainage the discharge potential satisfies the Poisson equation, and the complex potential cannot be used to characterize the flow field. On this condition, we use the discharge potential, $\Phi(x, y)$, rather than complex potential, in order to identify the direction of the streamlines passing through stagnation points.

Consider the symmetric matrix formed by the second derivatives of the discharge potential:

$$H = \begin{bmatrix} \frac{\partial^2 \Phi}{\partial x^2} & \frac{\partial^2 \Phi}{\partial x \partial y} \\ \frac{\partial^2 \Phi}{\partial x \partial y} & \frac{\partial^2 \Phi}{\partial y^2} \end{bmatrix} \quad (\text{A1})$$

This matrix is known as the Hessian of $\Phi(x, y)$ and describes the curvature of Φ at a specific point. The larger the absolute value of the second derivative, the more curved the surface $\Phi(x, y)$. The sign determines convexity or concavity. A positive second derivative means convexity, \cup , while a negative one means concavity, \cap . If the first derivative is zero, then the diagonal elements determine whether we have a maximum, a minimum, or an inflection point along a certain direction.

In order to interpret the application of the Hessian matrix, we choose the origin of the coordinate system at a stagnation point. Then, in the vicinity of the stagnation point, where $\frac{\partial \Phi}{\partial x} = \frac{\partial \Phi}{\partial y} = 0$, the potential can be approximated by truncated Taylor expansion:

$$\begin{aligned} \Phi(x, y) &= \Phi(0, 0) + \frac{1}{2} \frac{\partial^2 \Phi}{\partial x^2} x^2 + \frac{1}{2} \frac{\partial^2 \Phi}{\partial y^2} y^2 + \frac{\partial^2 \Phi}{\partial x \partial y} xy \\ &= \frac{A}{2} x^2 + Bxy + \frac{C}{2} y^2 + D \end{aligned} \quad (\text{A2})$$

and thus the Hessian matrix is

$$H = \begin{bmatrix} A & B \\ B & C \end{bmatrix} \quad (\text{A3})$$

This matrix has eigenvalues

$$\lambda_1 = \frac{A}{2} + \frac{C}{2} + \frac{1}{2} \sqrt{A^2 - 2AC + C^2 + 4B^2} \quad (\text{A4})$$

$$\lambda_2 = \frac{A}{2} + \frac{C}{2} - \frac{1}{2} \sqrt{A^2 - 2AC + C^2 + 4B^2} \quad (\text{A5})$$

with corresponding eigenvectors that define lines with the following slopes:

$$\tan(\theta_1) = \frac{A - C + \sqrt{A^2 - 2AC + C^2 + 4B^2}}{2B} \quad (\text{A6})$$

$$\tan(\theta_2) = \frac{A - C - \sqrt{A^2 - 2AC + C^2 + 4B^2}}{2B} \quad (\text{A7})$$

Transforming the system if coordinates are different from the x and y directions to the direction of the eigenvectors, the Hessian matrix becomes a diagonal matrix with eigenvalues λ_1 and λ_2 as entries. Thus, the eigenvalues, λ_1 and λ_2 reveal the nature of the potential at the stagnation point. According to the properties of the Hessian matrix, the following conclusions can be drawn:

1. $\lambda_1 \lambda_2 < 0$: The point is a saddle point.
2. $\lambda_1 < 0$ and $\lambda_2 < 0$: The point is a strict maximum.
3. $\lambda_1 > 0$ and $\lambda_2 > 0$: The point is a strict minimum.
4. $\lambda_1 = 0$ or $\lambda_2 = 0$: The point is an inflection point along the direction of the corresponding eigenvalue.
5. $\lambda_1 = \lambda_2 = 0$: No conclusion about the nature of the potential at the point can be drawn.

However, this is a rare case, and is not considered further.

A.2 Proof of Inequality (19)

At the stagnation point $\left(-\frac{q_{x0}^*}{2} + \sqrt{\frac{q_{x0}^{*2}}{4} + Q^*}, 0 \right)$,

$$q_{x0}^* < \sqrt{q_{x0}^{*2} + 4Q^*} \quad (\text{A.8})$$

which can be written as

$$2q_{x0}^{*2} < 2q_{x0}^* \sqrt{q_{x0}^{*2} + 4Q^*} \quad (\text{A.9})$$

Thus,

$$q_{x0}^{*2} - 2q_{x0}^* \sqrt{q_{x0}^{*2} + 4Q^*} + q_{x0}^{*2} + 4Q^* < 4Q^* \quad (\text{A.10})$$

Then,

$$\left(-q_{x0}^* + \sqrt{q_{x0}^{*2} + 4Q^*} \right)^2 < 4Q^* \quad (\text{A.11})$$

and

$$x_s^{*2} = \left(-\frac{q_{x0}^*}{2} + \sqrt{\frac{q_{x0}^{*2}}{4} + Q^*} \right)^2 < Q^* \quad (\text{A.12})$$

For element A in the Hessian matrix, $A = -\frac{Q^*}{2x_s^{*2}} - \frac{1}{2}$, is always negative because Q^*

and x_s^{*2} are positive. For element C , replacing with inequality (A.12), we have

$$C = \frac{Q^*}{2x_s^{*2}} - \frac{1}{2} > 0 \quad (\text{A.13})$$

A.3 Proof of Inequality (20)

At the stagnation point $\left(-\frac{q_{x0}^*}{2} + \sqrt{\frac{q_{x0}^{*2}}{4} + Q^*}, 0\right)$, we have

$$x_s^{*2} = \left(-\frac{q_{x0}^*}{2} + \sqrt{\frac{q_{x0}^{*2}}{4} + Q^*}\right)^2 > Q^* \quad (\text{A.14})$$

Thus,

$$C = \frac{Q^*}{2x_s^{*2}} - \frac{1}{2} < 0 \quad (\text{A.15})$$

References

Aderson, E.I., 2002. An analytic solution representing groundwater-surface water interaction. *Water Resour. Res.* 39(3), 1071-1078.

Aderson, M.P., Munter, J.A., 1981. Seasonal reversals of groundwater flow around lakes and the relevance to stagnation points and lake budget. *Water Resour. Res.* 17(4), 1139-1150.

Bear, J., 1979. *Hydraulics of Groundwater*. New York: McGraw-Hill Book Co.

Bear, J., Jacobs, M., 1965. On the movement of water bodies injected into aquifers. *J. Hydrol.* 32(5), 1309-1315.

Bakker, M., Strack, O.D.L., 1996. Capture zone delineation in two-dimensional groundwater flow models. *Water Resour. Res.* 32 (5), 1309-1315.

- Bair, E.S., Springer, A.E., Roadcap, G.S., 1991. Delineation of travel-time-related capture areas of wells using analytical flow models and particle-tracking analysis. *Ground Water* 29 (3), 387-397.
- Cheng, X., Anderson, M.P., 1994. Simulating the influence of lake position on groundwater fluxes. *Water Resour. Res.* 30(7), 2041-2049.
- Christ, J.A., Goltz, M.N., 2004. Containment of groundwater contamination plumes: minimizing drawdown by aligning capture wells parallel to regional flow. *J. Hydrol.* 286, 52-68.
- Cunningham, J.A., Hoelen, T.P., Hopkins, G.D., Lebron C.A., Reinhard, M., 2004. Hydraulics of recirculating well pairs for ground water remediation. *Ground Water* 42(6), 880-889.
- Cirpka, O.A., Frind, E.O., Helming, R., 1999. Streamline-oriented grid-generation for transport modeling in two-dimensional domains including wells. *Adv. Water Resour.* 22 (7), 697-710.
- Christ, J.A., Goltz, M.N., Huang, J., 1999. Development and application of an analytical model to aid design and implementation of *in situ* remediation technologies. *J. Contam. Hydrol.* 37(3-4), 295-317.
- Christ, J.A., Goltz, M.N., 2002. Hydraulic containment: analytical and semi-analytical models for capture zone curve delineation. *J. Hydrol.* 262 (1-4), 224-244.
- Cole, B.E., Silliman, S.E., 2000. Utility of simple models for capture zone delineation in heterogeneous unconfined aquifers. *Ground water* 38 (5), 665-672.
- Erdmann, J., 1999. On capture width and capture zone gaps in multiple-well systems. *Ground Water* 38(4), 497-504.
- Fienen, M.N., Luo, J., Kitanidis, P.K., 2005. Semi-analytical homogeneous anisotropic capture zone delineation. *J. Hydrol.* 312 (1-4), 39-50.
- Garrido, A., Martinez-Santos, P., Llamas, M.R., 2006. Groundwater irrigation and its implications for water policy in semiarid countries: the Spanish experience. *Hydrol. J.* 14(3), 340-349.
- Hantush, M.S., 1965. Wells near streams with semipervious beds. *J. Geophys. Res.* 70, 2829-2838.
- Intaraprasong, T., Zhan H., 2007. Capture zone between two streams. 338, 297-307.
- Javandel, I., Tsang, C.F., 1986. Capture zone type curves: a tool for aquifer cleanup. *Ground water* 24 (5), 616-625.

- Jin, W., Steward, D.R., 2007. The transition of flow patterns through critical stagnation points in two-dimensional groundwater flow. *Adv. Water Resour.* 30, 16-28.
- Lerner, D.N., 1992. Well catchments and time-of-travel zones in aquifers with recharge. *Water Resour. Res.* 28 (10), 2621-2628.
- Luo J., Kitanidis P.K., 2004. Fluid residence times within a recirculation zone created by an extraction-injection well pair. *J. Hydrol.* 295(1-4), 149-162.
- Luo J., Wu, W.M., Fienen, M.N., Jardine, P.M., Mehlhorn, T.L., Watson, D.B., Cirpka, O.A., Criddle, C.S., Kitanidis P.K., 2006. A nested-cell approach for in situ remediation. *Ground Water* 44(2), 266-274.
- Muskat, M., 1946. *The Flow of Homogeneous Fluids through Porous Media.* J.W. Edwards, Ann Arbor, USA.
- Nield, S.P., Townley, L.R., Barr, A.D., 1994. A framework for quantitative analysis of surface water-groundwater interaction: flow geometry in a vertical section. *Water Resour. Res.* 30(8), 2461-2475.
- Newsom, J.M., Wilson, J.L., 1988. Flow of ground water to a well near a stream-effect of ambient ground-water flow direction. *Ground Water* 26 (6), 703-711.
- Shan, C., 1999. An analytical solution for the capture zone of two arbitrarily located wells. *J. Hydrol.* 222 (1-4), 123-128.
- Steward, D.R., 1999. Three-dimensional analysis of the capture of contaminated leachate by fully penetrating, partially penetrating, and horizontal wells. *Water Resour. Res.* 35(2), 461-468.
- Strack, O.D.L., 1989. *Groundwater Mechanics.* Englewood Cliffs, NJ: Prentice-Hall.
- Smith, A.J., Townley, L.R., 2002. Influence of regional setting on interaction between shallow lakes and aquifers. *Water Resour. Res.* 38(9), 1170.
- Schaferperini, A.L., Wilson, J.L., 1991. Efficient and accurate front tracking for two-dimensional groundwater models. *Water Resour. Res.* 27 (7), 1471-1485.
- Townley, L.R., Trefry, M.G., 2000. Surface water-groundwater interaction near shallow circular lakes: flow geometry in three dimensions. *Water Resour. Res.* 36(4), 935-949.
- Winter T.C., 1978. Numerical simulation of steady state three-dimensional groundwater flow near lakes. *Water Resour. Res.* 4(2), 245-254.

Wilson J.L., 1993. Induced infiltration in aquifers with ambient flow. *Water Resour. Res.* 29 (10), 3503-3512.

Zhan, H., 1999a. Analytical and numerical modeling of a double-well capture zone. *Math. Geol.* 31 (2), 175-193

Zhan, H., 1999b. Analytical study of capture time to a horizontal well. *J. Hydrol.* 217, 46-54.

Zhan, H., Zlotnik, V.A., 2002. Ground water flow to horizontal and slanted wells in unconfined aquifers. *Water Resour. Res.* 38 (7), 1108, doi: 10.1029/2001WR000401.

Zheng, C., Bennett, G., 2002. *Applied Contaminant Transport Modeling, Theory and Practice* (Second ed.). New York: John Wiley and Sons, Inc.

Table 1

Well Pumping rates associated with the number and location of the stagnation points.

			Pumping rate Q^*	Location of the stagnation point (x_s^*)						TSP ^a
				$(-\infty, -1)$	-1	$(-1, 0)$	$(0, -1)$	1	$(1, -\infty)$	
$q_{x0}^* \leq 1$	$0 < x_w^* < 1$	$x_w^* < q_{x0}^*$	$0 < Q^* < Q_{c2}$	x		x	x			3
			$Q^* = Q_{c2}$		x		x			2
			$Q_{c2} < Q^* < Q_{c1}$				x			1
			$Q = Q_{c1}$					x		1
			$Q^* > Q_{c1}$						x	1
			$Q^* > Q_{c1}$							
	$x_w^* > q_{x0}^*$	$x_w^* > q_{x0}^*$	$0 < Q^* < Q_{c1}$	x		x	x			3
			$Q = Q_{c1}$	x		x		x		3
			$Q_{c1} < Q^* < Q_{c2}$	x		x			x	3
			$Q^* = Q_{c2}$		x				x	2
			$Q^* > Q_{c2}$						x	1
	$x_w^* = q_{x0}^*$	$x_w^* = q_{x0}^*$	$0 < Q^* < Q_{c1}$	x		x	x			3
			$Q = Q_{c1}$		x			x		2
			$Q^* > Q_{c1}$						x	1
	$x_w^* \geq 1$	$x_w^* \geq 1$	$0 < Q^* < Q_{c2}$	x		x			x	3
$Q^* = Q_{c2}$				x				x	2	
$Q^* > Q_{c2}$								x	1	
$q_{x0}^* > 1$	$0 < x_w^* < 1$	$0 < Q^* < Q_{c1}$				x			1	
		$Q = Q_{c1}$					x		1	
		$Q^* > Q_{c1}$						x	1	
	$x_w^* = 1$	$Q^* > 0$						x	1	

^a TSP = Total number of stagnation points.

Table 2

Dimensionless well pumping rates and coordinates of stagnation points ($x_w^* = 0$)

	Q^*	(x_s^*, y_s^*)
(a). $Q^* < 1 - q_{x0}^*$	0.53	(0.64, 0), (-0.84, 0), (-2.33, 0)
(b). $Q^* = 1 - q_{x0}^*$	0.8	(0.8, 0), (-1, 0)
(c). $1 - q_{x0}^* < Q^* < 1 + q_{x0}^*$	0.95	(0.88, 0)
(d). $Q^* = 1 + q_{x0}^*$	1.2	(1, 0)
(e). $Q^* > 1 + q_{x0}^*$	1.44	(2.20, 0)

Table 3

Dimensionless well pumping rates and coordinates of stagnation points ($x_w^* = 0.1$)

	Q^*	(x_s^*, y_s^*)
(a). $Q^* < Q_{c2}$	0.56	(0.71, 0), (-0.81, 0), (-2.33, 0)
(b). $Q^* = Q_{c2}$	0.88	(0.90, 0), (-1, 0)
(c). $Q_{c2} < Q^* < Q_{c1}$	0.95	(0.94, 0)
(d). $Q^* = Q_{c1}$	1.08	(1, 0)
(e). $Q^* > Q_{c1}$	1.44	(2.47, 0)

Table 4

Dimensionless well pumping rates and coordinates of stagnation points ($x_w^* = 0.2$)

	Q^*	(x_s^*, y_s^*)
(a). $Q^* < Q_{c1}$	0.56	(0.77, 0), (-0.77, 0), (-2.43, 0)
(b). $Q^* < Q_{c1}$	0.88	(0.96, 0), (-0.96, 0), (-1.23, 0)
(c). $Q^* = Q_{c1}$	0.95	(1, 0), (-1, 0)
(d). $Q^* > Q_{c1}$	1.08	(1.35, 0)
(e). $Q^* > Q_{c1}$	1.44	(2.73, 0)

Table 5

Dimensionless well pumping rates and coordinates of stagnation points ($x_w^* = 0.5$)

	Q^*	(x_s^*, y_s^*)
(a). $Q^* < Q_{c1}$	0.48	(0.93, 0), (-0.63, 0), (-2.95, 0)
(b). $Q^* = Q_{c1}$	0.60	(1, 0), (-0.70, 0), (-2.50, 0)
(c). $Q_{c1} < Q^* < Q_{c2}$	0.95	(1.73, 0), (-0.89, 0), (-1.45, 0)
(d). $Q^* = Q_{c2}$	1.2	(2.50, 0), (-1, 0)
(e). $Q^* < Q_{c2}$	1.44	(3.40, 0)

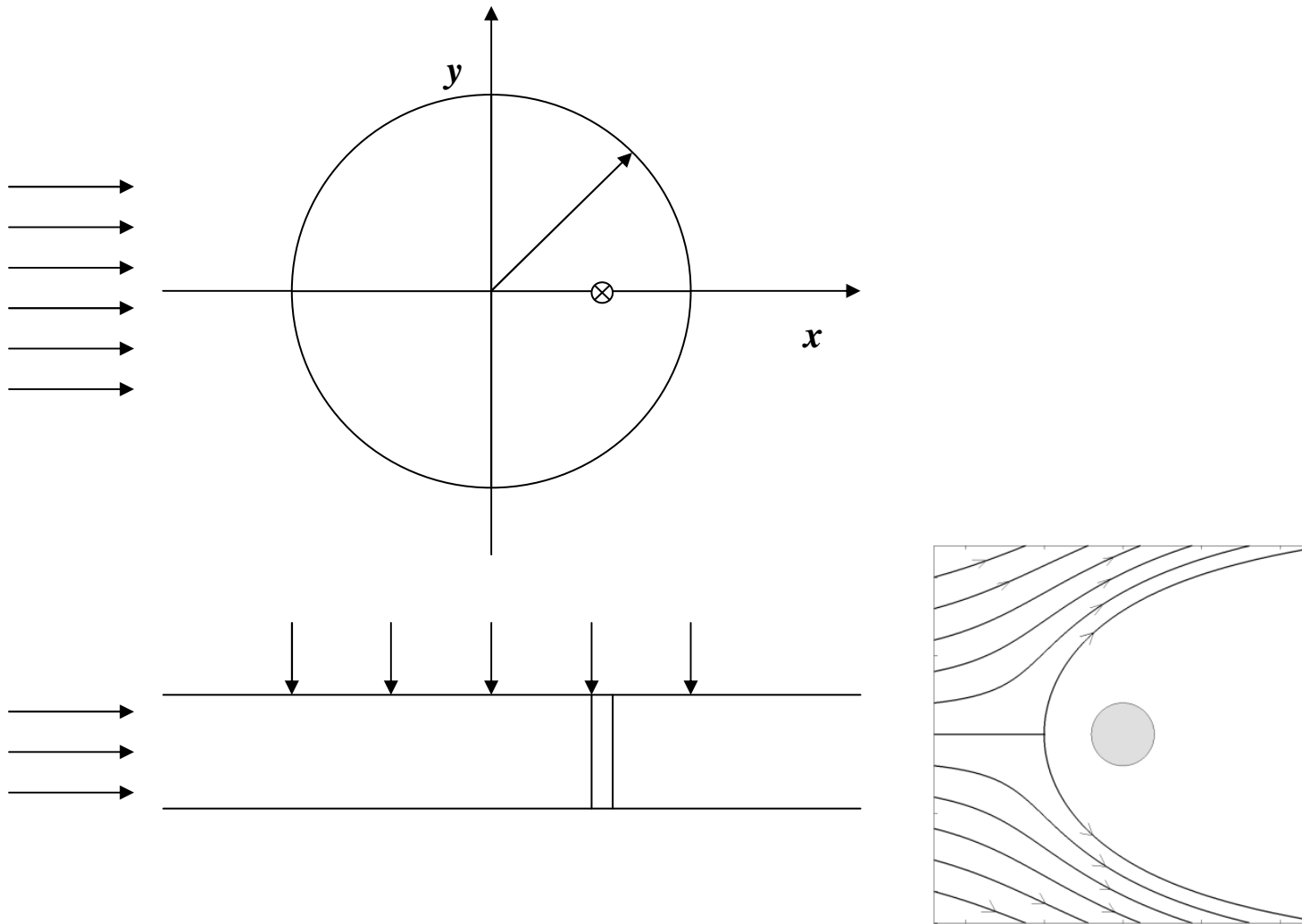


Fig. 1. Plan view and cross section of an extraction well in a uniform regional flow with constant infiltration rate. The right figure shows a flow field with recharge, regional flow and no pumping well. The gray circle represents the infiltration zone.

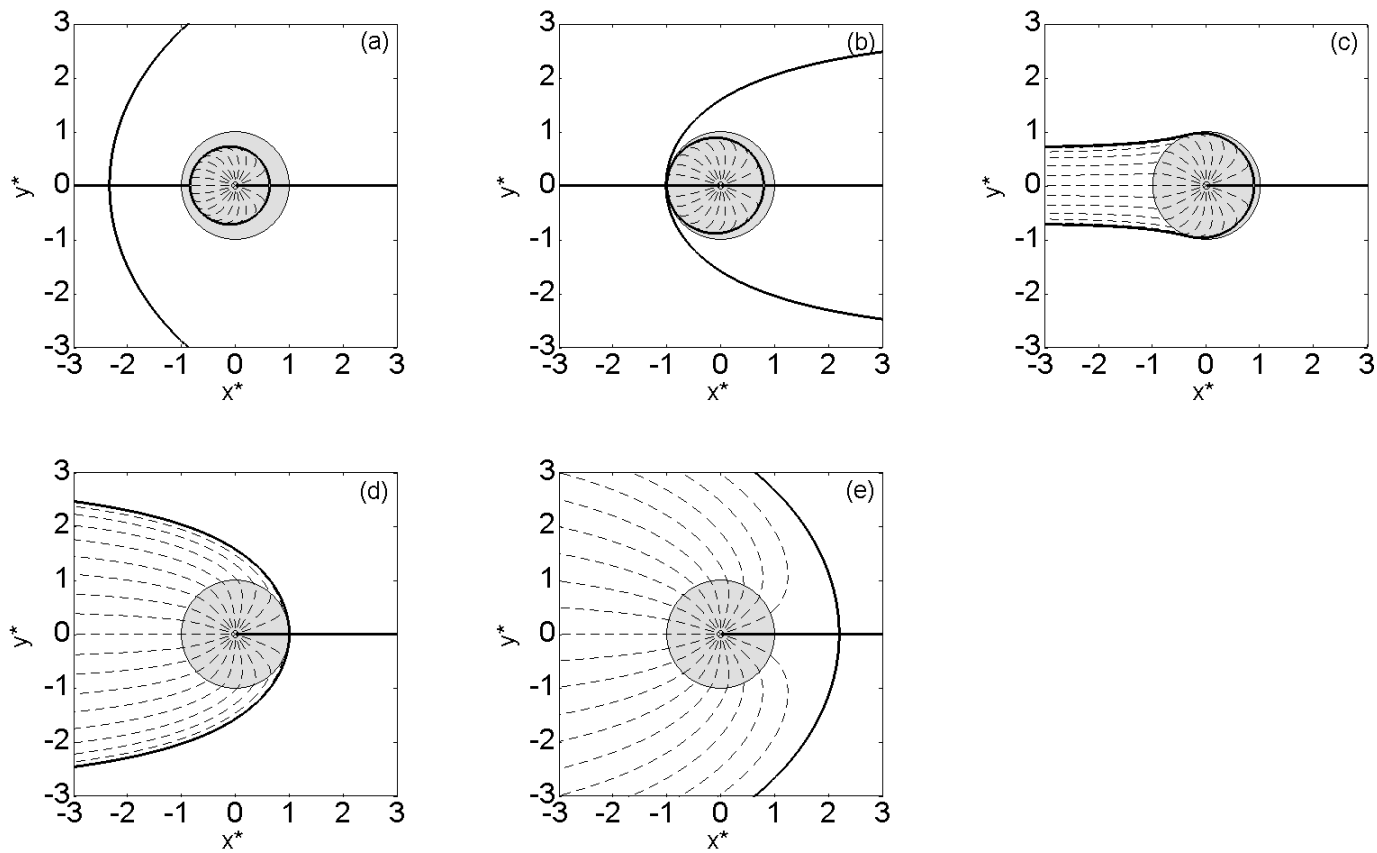


Fig. 2. Stagnation points and separation streamlines for the case where the well locates at the origin. The dark solid lines are separation streamlines, the dashed lines are streamlines plotted by backward tracing from the extraction. The gray circle represents the infiltration zone. (a) $Q^* = 0.53$, (b) $Q^* = 0.8$, (c) $Q^* = 0.95$, (d) $Q^* = 1.2$, and (e) $Q^* = 1.44$.

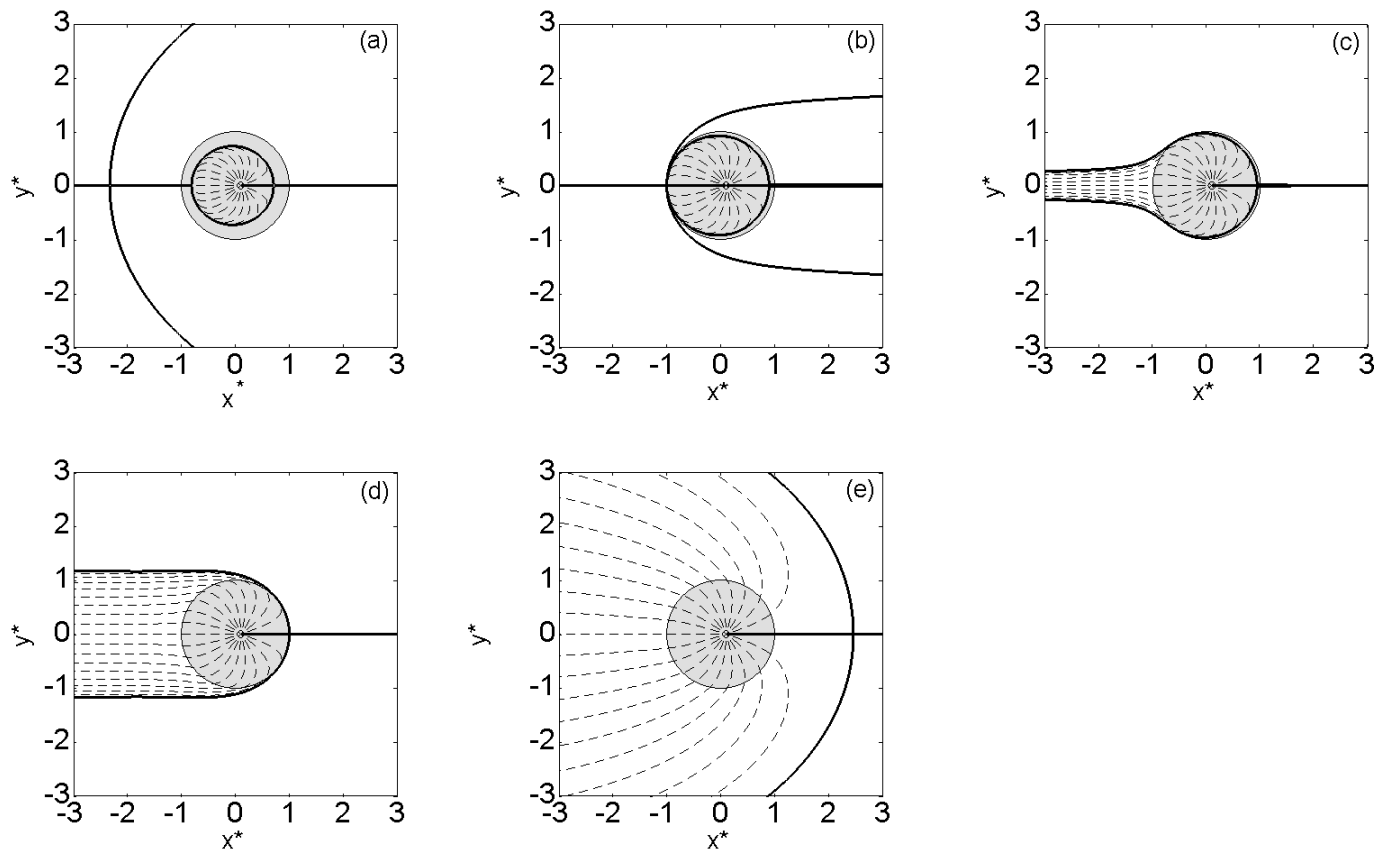


Fig. 3. Stagnation points and separation streamlines for the case where the well locates at the dimensionless point $(0.1, 0)$. The dark solid lines are separation streamlines, the dashed lines are streamlines plotted by backward tracing from the extraction. The gray circle represents the infiltration zone. (a) $Q^* = 0.56$, (b) $Q^* = 0.88$, (c) $Q^* = 0.95$, (d) $Q^* = 1.08$, and (e) $Q^* = 1.44$.

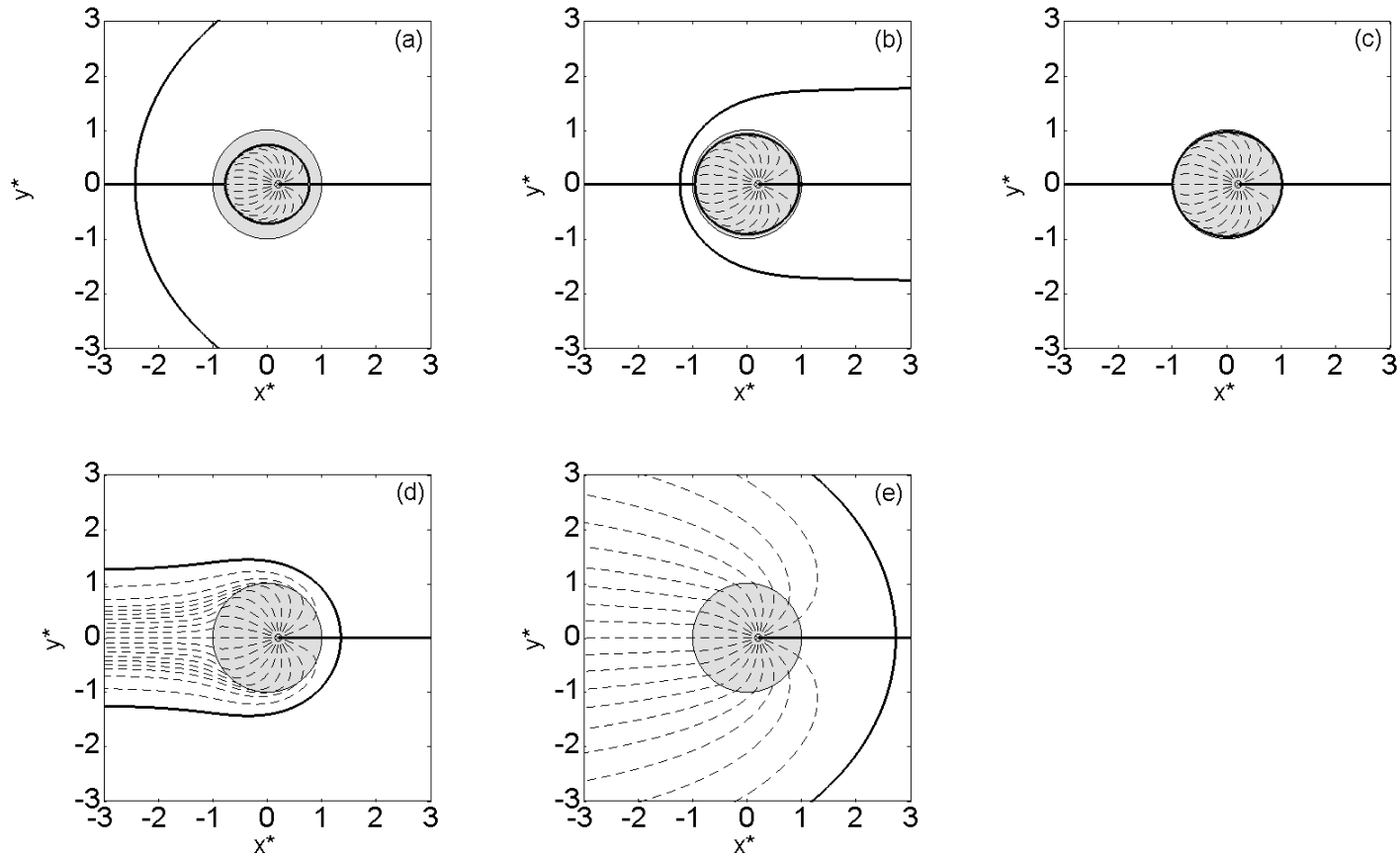


Fig. 4. Stagnation points and separation streamlines for the case where the well locates at the dimensionless point (0.2, 0). The dark solid lines are separation streamlines, the dashed lines are streamlines plotted by backward tracing from the extraction. The gray circle represents the infiltration zone. (a) $Q^* = 0.56$, (b) $Q^* = 0.88$, (c) $Q^* = 0.95$, (d) $Q^* = 1.08$, and (e) $Q^* = 1.44$.

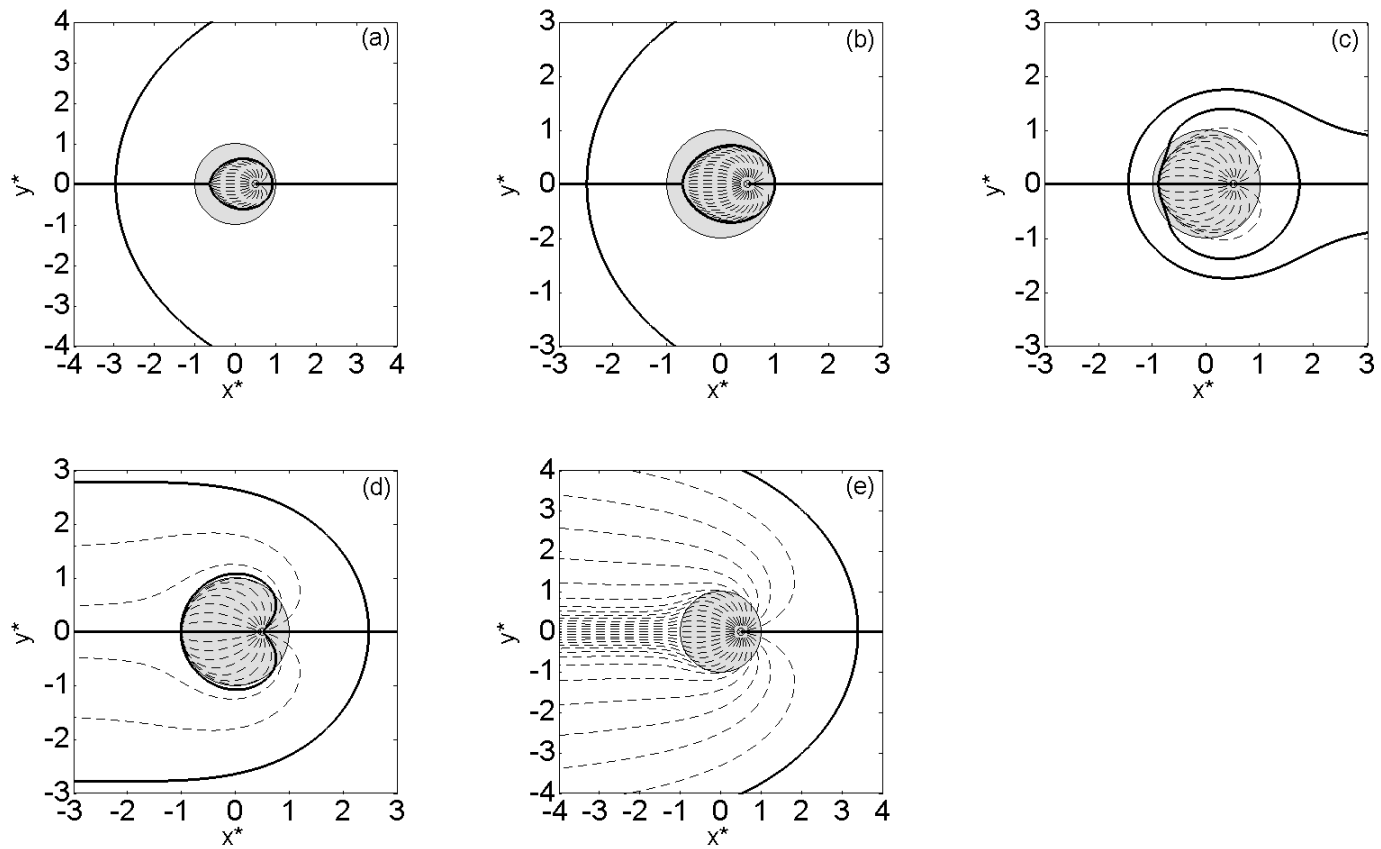


Fig. 5. Stagnation points and separation streamlines for the case where the well locates at the point (10, 0). The dark solid lines are separation streamlines, the dashed lines are streamlines plotted by backward tracing from the extraction. The gray circle represents the infiltration zone. (a) $Q^* = 0.48$, (b) $Q^* = 0.60$, (c) $Q^* = 0.95$, (d) $Q^* = 1.2$, and (e) $Q^* = 1.44$.

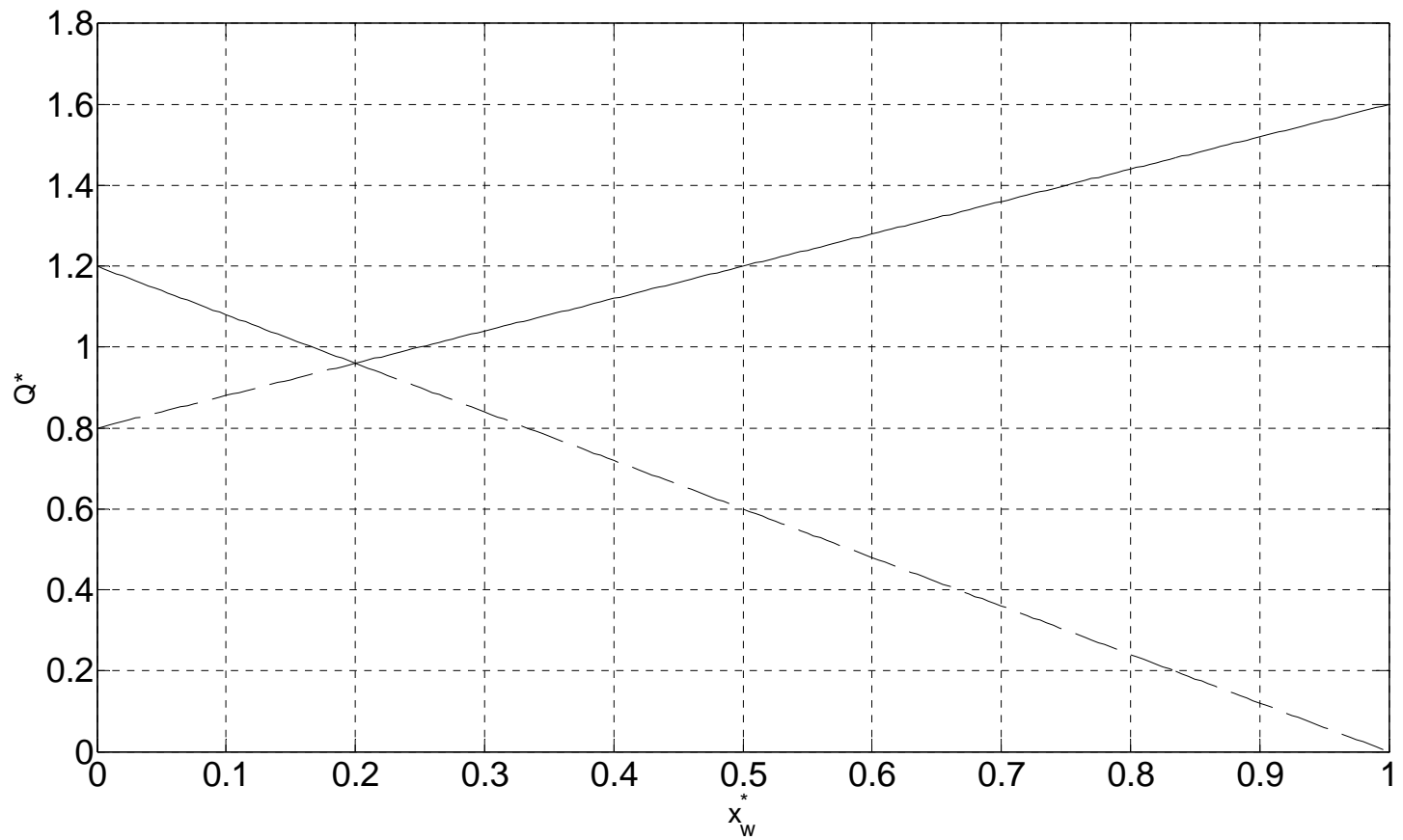


Fig.6. The relationship between the dimensionless critical pumping rate and well location. The dashed line denotes the lower critical pumping rate, and the solid line represents the higher critical pumping rate.

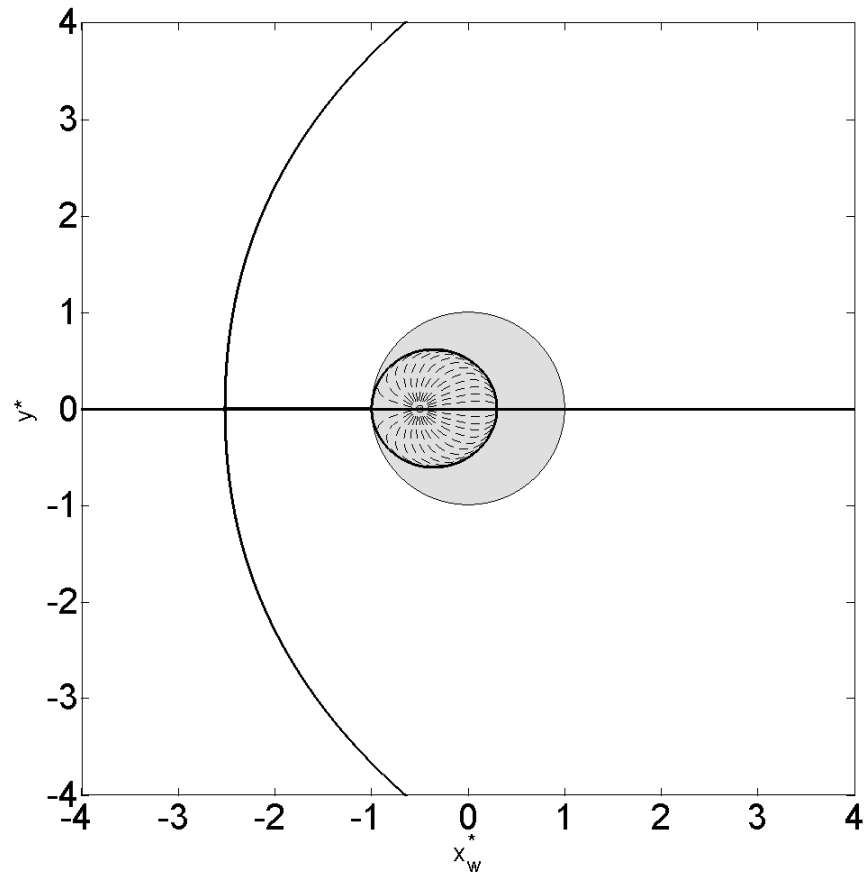


Fig. 7. Stagnation points and separation streamlines for the case where the well locates at the point $(-0.5, 0)$ with a critical pumping rate of $2.5 L/sec$. The dark solid lines are separation streamlines, the dashed lines are streamlines plotted by backward tracing from the extraction. The gray circle represents the infiltration zone.

Chapter 3. Kinetic mass transfer coupled with periodic tidal activity may widen the transition zone in coastal aquifers (a manuscript in revision)

Introduction

Seawater intrusion is the movement of seawater into freshwater aquifers, characterized by the heavier seawater flowing below the lighter freshwater in geologic formations. A variable-density transition zone is developed between freshwater and seawater. Wide transition zones have been observed in many aquifers [Xue *et al.*, 1993; Wu *et al.*, 1993; Cherry, 2006]. The width of the transition zone is of particular interest because (1) seawater intrusion may be described by the growth and decay of the transition zone; (2) the size of the transition zone may reflect the impact area during seawater intrusion; and (3) a wider transition zone indicates stronger mixing, and consequently enhances reactive transport processes in coastal aquifers [Rezaei *et al.*, 2005]. The extent of transition zone depends not only on hydrogeological properties of the aquifer, but also on the hydrodynamic fluctuations of groundwater and seawater levels. However, the key mechanisms responsible for wide transition zones are not well understood and still remain debatable [Volker and Rushton, 1982; Ataie-Ashtiani *et al.*, 1999; Abarca *et al.*, 2006].

In the present research, we provide a plausible explanation for wide transition zones in coastal aquifers. The hypothesis is that the combination of periodic tidal activities and kinetic mass transfer may widen the transition zone. This study is motivated by (1) periodic tidal activities have been found to have great impacts on seawater intrusion [Ataie-Ashtiani *et al.*, 1999, 2001;

Kim et al., 2006]; and (2) kinetic mass transfer can significantly increase the residence time and enhance solute mixing [*Michalak and Kitanidis*, 2000]. To the best of our knowledge, almost all studies that have been done for seawater intrusion did not consider mass transfer processes. As it is well-known, mass transfer occurs in almost all fractured and porous heterogeneous media over various scales ranging from pore scale to field scale. *Langevin et al.* [2003] conducted a simulation of variable-density flow coupled with dual-domain transport for the well-known Henry problem. Without the consideration of tidal effects, they found that the steady-state salinity distribution was roughly the same as the salinity distribution for the classical Henry problem. However, we expect that the combination of periodic tidal activities and kinetic mass transfer may widen transition zones in coastal aquifers. The hypothesis will be tested by a scaled tank model solved using numerical models for miscible-fluid systems.

Numerical model

The governing equation for saturated variable-density groundwater flow in terms of freshwater head is described by [*Langevin et al.*, 2003]:

$$\nabla \cdot \left[\rho K_f \left(\nabla \cdot h_f + \frac{\rho - \rho_f}{\rho_f} \cdot \nabla z \right) \right] = \rho S_f \frac{\partial h_f}{\partial t} + \theta_e \frac{\partial \rho}{\partial t} - \rho_s q_s \quad (1)$$

where z [L] is the vertical coordinate directed upward; K_f [LT^{-1}] is the equivalent freshwater hydraulic conductivity; h_f [L] is the equivalent freshwater head; ρ [ML^{-3}] is the fluid density; ρ_f [ML^{-3}] is the freshwater density; S_f [L^{-1}] is the equivalent freshwater storage coefficient; t [T] is the time; θ_e is the effective porosity; and ρ_s [ML^{-3}] and q_s [T^{-1}] are the density and flow rate per unit volume of aquifer of the source/sink, respectively. It should be noted that many existing

codes used for variable-density groundwater simulation formulate the equations in terms of pressure rather than equivalent freshwater hydraulic head. To facilitate the use of MODFLOW routines to solve for flow fields, the equation presented above is formulated in terms of equivalent freshwater head [Langevin and Guo., 2006].

Transport models with mass transfer descriptions usually conceptualize a porous or fractured heterogeneous medium as consisting of two overlapping continuous media: a mobile domain, where advective-dispersive transport occurs, and an immobile one with a continuous withdrawal and return of solute mass [Coats and Smith, 1964; van Genuchten and Wierenga, 1976]. The dual-domain model considered in the present research involves advection, molecular diffusion, mechanical dispersion, and first-order mass transfer, and is described by:

$$\theta_m \frac{\partial c_m}{\partial t} + \theta_{im} \frac{\partial c_{im}}{\partial t} = \nabla \cdot (\theta_m \mathbf{D} \nabla c_m) - \nabla \cdot (\theta_m \vec{v} c_m) \quad (2a)$$

$$\theta_{im} \frac{\partial c_{im}}{\partial t} = \zeta (c_m - c_{im}) \quad (2b)$$

where θ_m is the porosity of the mobile domain, which is equal to the effective porosity used in Eq. (1); θ_{im} is the porosity of the immobile domain; c_m [ML⁻³] is the dissolved concentration in the mobile; c_{im} [ML⁻³] is the dissolved concentration in the immobile; ζ [T⁻¹] is the first-order mass transfer rate constant; \mathbf{D} [L²T⁻¹] is the hydrodynamic dispersion coefficient tensor; and \vec{v} [LT⁻¹] is the velocity vector, which can be evaluated based on Darcy's law and the equivalent freshwater heads.

The relationship between the fluid density and salt concentration is represented by the linear function of state:

$$\rho = \rho_f + \epsilon C_m \quad (3)$$

where ϵ is a dimensionless constant with a value of 0.7143 for salt concentrations ranging from zero to 35 kg m^{-3} , a typical concentration value for seawater [Langevin *et al.*, 2003]; and ρ is expressed in kg m^{-3} .

A scaled tank model is designed to simulate the growth and decay of transition zones under the consideration of kinetic mass transfer and periodic tidal effects. A schematic representation of the seawater intrusion problem is shown in Figure 1. The geometry, hydrogeological, and transport parameters for the scaled tank model are summarized in Table 1. The size of the tank model and parameters are all comparable to previous numerical simulations for a tank model on seawater intrusion [Zhang *et al.*, 2001; Volker *et al.*, 2002; Brovelli *et al.*, 2007]. The selected hydrogeological and transport parameters are typical for homogeneous mixed-sand materials [Nowak and Cirpka, 2006]. A triangular periodic head boundary is imposed at the seaward boundary to simulate transient seawater-level fluctuations caused by periodic tidal activities [Brovelli *et al.*, 2007]. The period used in our simulations is 40 minutes, and the amplitude is 0.04 m (see Figure 2). Note the intention of the present research is to study the synergistic effect of periodic variability in flow and kinetic mass transfer. Although the proposed triangular periodic function may not reflect the real tidal activities, it will not influence the results. Parameters of kinetic mass transfer, including the mobile and immobile porosity and the first-order rate constant, will be varied in order to investigate the effects of kinetic mass transfer.

The numerical model is solved by the density-dependent groundwater flow code SEAWAT-2000 implemented in a graphic user interface software, Groundwater Vista 5.20, developed for 3D groundwater flow and transport modeling. The simulation domain is discretized into 10800 cells

in order to satisfy the accuracy and convergence requirement for grid spacing in terms of the local Péclet number [Voss and Souza, 1987; Zhang *et al.*, 2001; Volker *et al.*, 2002; Brovelli *et al.*, 2007]. To simplify the numerical simulation, a large hydraulic conductivity is assigned to the free seawater area above the slope so that the whole simulation domain is idealized as an aquifer [Winter, 1976; Anderson *et al.*, 2002; Mao *et al.*, 2006; Brovelli *et al.*, 2007; Robinson *et al.*, 2007]. In this work, we assign a value of 0.3 m s^{-1} , 75 times that of the saturated aquifer hydraulic conductivity, for the seawater area. A porosity of 1 and a constant salt concentration of 35 kg m^{-3} are enforced in the free seawater area. In addition, a horizontal strip of cells with a variable-head boundary condition are added onto the seawater surface to reproduce the flat surface of the sea [Brovelli *et al.*, 2007]. Simulations start from steady-state conditions which are calculated by assuming the mean seawater level. The simulation period for each case that will be discussed in the next section is twenty periods of tidal cycles, a sufficiently long period for the flow field to reach a dynamic equilibrium state, a state without significant change in salinity distribution in consecutive periods.

Results and Discussion

Control Cases

In order to demonstrate the effects of combining kinetic mass transfer and tidal activities on the growth and decay of the transition zone, we first generate steady-state control cases that neglect kinetic mass transfer or tidal activities. By assuming a constant seawater level of 0.520 m and a constant freshwater level of 0.545 m, a simulation was first conducted to obtain the steady-state solution in the absence of mass transfer. Figure 3A shows the transition zone, where the contourlines delineate the normalized concentrations 0.1, 0.5, and 0.9. Rather than a sharp

interface, a thin transition zone is formed due to density gradient and local dispersion. We also evaluated the transition zone by including mass transfer but neglecting tidal activity. Similar to the observation by *Langevin et al.* [2003], the resulting transition zone is almost the same as the one neglecting mass transfer. For steady-state analyses, mass transfer does not make significant contributions in altering salinity distribution. In fact, by forcing the transient terms in Eq. (2) to be zero, the transport model reduces to the case without mass transfer. That is, the steady-state salinity distributions will become identical for cases with and without mass transfer, although the timescales to reach the steady state may be different.

Figure 4 shows the transition zones with the consideration of tidal activities but neglecting mass transfer. A thicker transition zone, particularly at the toe, is observed compared to the transition zone shown in Figure 3. With tidal activities forcing the seawater back and forth in the costal aquifer, the equilibrium state shown in Figure 3 is disturbed, yielding a transient velocity field and a fluctuated density distribution, which result in enhanced mixing and a thicker transition zone. Figure 4 also shows that the transition-zone position varies at different periods of tidal activities because the variable hydraulic-head gradients during a period determine the position of the transition zone. Thus, we can only define a dynamic-equilibrium state instead of a steady state for the transient case. Here, the dynamic-equilibrium state is defined as the state where the transition-zone position has no significant variations between two consecutive periods of tidal activities, which is achieved in our numerical simulations after ten tidal periods. In addition, although the position of the transition zone varies, the width during the tidal period does not change noticeably. *Ataie-Ashtiani et al.* [1999] found that a larger tidal amplitude may force the seawater to intrude further inland. For the given tidal amplitude in our case, we do not observe a

more intruded transition zone than the steady state shown in Figure 3. This phenomenon is consistent with that found by *Chen and Hsu* [1999] for the Henry problem.

Mass Transfer Coupled with Tidal Activity

Figure 5 shows the transition zones with the consideration of both mass transfer and tidal activities. Mobile porosity and immobile porosity both are set to be 0.2. The first-order mass transfer rate coefficient is 0.025 min^{-1} . Figure 5 clearly shows that the mass transfer effect leads to significantly wider transition zones at any moment of the tidal period compared with those shown in Figure 4. In particular, the spreading is more pronounced at the moments of low tide and falling tide. As already mentioned, in the absence of tidal activities, mass transfer has no effect on the steady-state salinity distribution because there is no concentration gradient between the mobile and immobile domains and Eq. (2) can be simplified to the classical advection-dispersion equation, although the timescale to reach the steady state may be changed. However, in transient cases, e.g., tidal activities included, the transition zone is pushed back and forth by tidal energy, resulting in non-equilibrium in the salt concentrations in the mobile and immobile domains and an enhanced mass exchange between them. The immobile domain here essentially acts as a sink or source for solutes in the mobile zone, determined by the direction of concentration gradient between two domains. Specifically, salts in the mobile domain are withdrawn to the immobile domain as the transition zone is dragged inland, while salts are released from the immobile domain to the mobile domain driven by inversed concentration gradients when the transition zone is towed toward the sea. The disturbed concentration and density gradient field leads to enhanced mixing and a wider transition zone than would occur in the absence of mass transfer. Moreover, Figure 5 shows that the combination of mass transfer and tidal activities has greater influence on the high concentration contourlines (see the

contourlines of normalized concentration 0.9), which become closer to the seaward boundary. Certainly, if a lowering freshwater head or increasing tidal amplitude is considered, one may expect to observe an expanding transition zone moving further inland.

Sensitivity Analysis

In order to interpret the results concisely and produce a meaningful generalization, the following dimensionless variables are defined:

$$\tau = \zeta^{-1}/T_{\text{tidal}} \quad (5)$$

$$\beta = \theta_{\text{im}}/\theta_{\text{m}} \quad (6)$$

$$w = W/W_{\text{ss}} \quad (7)$$

where T_{tidal} is the tidal period; ζ^{-1} represents a characteristic mass transfer time in the immobile domain; β is known as the capacity ratio; W_{ss} is the transition-zone width under steady-state condition; and W is the width of the transition zone under the coupled effect of mass transfer and tidal activities. For simplicity, W is represented by the horizontal distance between concentration contourlines of 0.1 and 0.9. Here, we choose the width of the transition zone at the height of 300 mm at the high tidal moment to calculate W . Similar results will be obtained for the width of the transition zone at other heights and tidal moments. By assuming a constant total porosity for the mobile and immobile domain, the effects of mass transfer parameters and tidal activities on the dimensionless width of the transition zone, w , can be investigated by varying the dimensionless variables, τ and β .

Figure 6 shows the simulated results for the sensitivity analysis. With a given mean retention time, i.e., a constant first-order mass transfer rate coefficient, the width of the transition zone increases with the capacity ratio, indicating that a larger immobile domain may cause a wider transition zone. With a given capacity ratio, i.e., a constant porosity of the immobile domain, the width of the transition zone is maximized when the retention timescale of the mass transfer and the tidal period become comparable, i.e., at the same order of magnitude. In such cases, the effects of the capacity ratio will also be maximized. In addition, the left and right tails of the curves shown in Figure 6 indicate that the mass transfer may not have significant impacts on the width of the transition zone when there is a several orders of magnitude difference between the retention timescale and the tidal period. In fact, both the limiting cases of very small and large mass transfer rate coefficients can be simplified to a classical advective-dispersive transport problem. For a small mass transfer rate coefficient, it is equivalent to the transport problem in a medium with a smaller total porosity, i.e., practically no mass transfer occurs. For a large mass transfer rate coefficient, the kinetic mass transfer may be considered as an instantaneous process, which simplifies the two-domain model into a one-domain model with a retardation factor, $1 + \beta$. Thus, for both limiting cases, the width of the transition zone will approach the steady-state result presented in control cases. In our tank model, the transition zone is significantly widened for τ between 0.1 and 100, and the width reaches maximum for τ to be about 2, i.e., τ^{-1} is equal to $2T_{tidal}$. For example, the width of the transition zone triples for the case of $\beta = 1$ and $\tau = 2$. We may expect that the width of the transition zone will become much larger for a higher β .

Conclusions

Wide transition zones have been observed in many aquifers all over the world. However, no agreement has been reached in terms of the responsible mechanisms. In the present work, we explore the hypothesis that the combination of periodic tidal activities and kinetic mass transfer may widen transition zones in coastal aquifers. The hypothesis is tested by conducting a numerical study based on the variable-density groundwater model for a scaled tank model. From the simulated cases and sensitivity analyses of dimensionless variables, the following conclusions can be drawn:

- tidal activity alone with constant period and amplitude may cause a slightly wider transition zone compared with steady-state results, although it does not change the location of seawater intrusion into the freshwater aquifer;
- the consideration of both tidal activities and kinetic mass transfer may significantly widen the transition zone;
- a larger capacity ratio of mass transfer leads to a wider transition zone, and the maximum width may be reached when the mean retention times in the immobile domain and the tidal period become comparable.

As it is well-known, no natural geological media are truly homogenous, and mass transfer occurs in almost all fractured and porous heterogeneous media over various scales ranging from pore scale to field scale. Our findings provide a plausible explanation for wide transition zones in coastal aquifers which may consist of low-permeability zones, dead-end pores, porous particles, aggregates, and rock matrix between fractures. In such aquifers, the effects of kinetic mass transfer and tidal activities must be considered to evaluate seawater intrusion and the growth and decay of the variable-density transition zone. Certainly, other hydrogeological factors, such as

the amplitude of the periodic tidal function, the rate of freshwater flow, the heterogeneity of the geological formations, the recirculation between the seawater and freshwater, may also influence the growth and decay of the transition zone. The research about the relative importance of these mechanisms is undergoing and will be discussed elsewhere.

Acknowledgements:

This research was sponsored by the National Institutes of Water Resources (NIWR) and U.S. Geological Survey (USGS) under project ID 2007GA165G. This article has not been reviewed by the agency, and no official endorsement should be inferred. Any opinions, findings, and conclusions or recommendations expressed in this material are those of the authors and do not necessarily reflect the views of NIWR and USGS. We also thank David Hochstetler for his comments on a preliminary version of the manuscript.

References:

- Ataie-Ashtiani, B., R. E. Volker, and D. A. Lockington (1999), Tidal effects on sea water intrusion in unconfined aquifers, *J. Hydrol.*, 216, 17-31.
- Ataie-Ashtiani, B., R. E. Volker, and D. A. Lockington (2001), Tidal effects on groundwater dynamics in unconfined aquifers, *Hydrol. Process.*, 15, 655-669.
- Anderson, M. P., R. J. Hunt, J. T. Krohelski, and K. Chung (2002), Using high hydraulic conductivity nodes to simulate seepage lake, *Ground Water*, 40(2), 117-122.
- Abarca, E., M. Pool, J. Carrera, and M. Dentz (2006), Can seawater intrusion modeling be simplified, *Eos Trans. AGU*, 87(52), Fall Meet. Suppl., Abstract H54E-05.
- Brovelli A., X. Mao, D. A. Barry (2007), Numerical modeling of tidal influence on density-dependent contaminant transport, *Water Resour. Res.*, 43, W10426, doi:10.1029/2006WR005173.
- Coats, K. H., and B. D. Smith (1964). Dead-end pore volume and dispersion in porous media, *Soc. Pet. Eng. J.*, 4, 73-81.

- Chen, B. F., and S. M. Hsu (2004), Numerical study of tidal effects on seawater intrusion in confined and unconfined aquifer by time-independent finite-difference method. *J. Waterw. Port Coastal Ocean Eng.*, 130(4), 191-206.
- Kim, K. Y., H. Seong, T. Kim, K. H. Park, N. C. Woo, Y. S. Park, G. W. Koh, and W. B. Park (2006), Tidal effects on variations of fresh-saltwater interference and groundwater flow in a multilayered coastal aquifer on a volcanic island (Jeju Island, Korea). *J. Hydrol.*, 330, 525-542, doi: 10.1016/j.jhydrol.2006.04.022.
- Luszczynski, N. J. (1961), Head and flow of ground water of variable density. *J. Geophys. Res.*, 66, 4247-4256.
- Langevin, C. D., and W. Guo (2006), MODFLOW/MT3DMS-based simulation of variable-density ground water flow and transport. *Ground Water*, 44, 339-351.
- Langevin, C. D., W. B. Shoemaker, and W. Guo (2003), Modflow-2000, The U.S. Geological Survey modular ground-water flow model: Documentation of the Seawat-2000 version with the variable density flow process (VDF) and the integrated MT3DMS transport process (IMT), U.S. Geol. Surv. Open File Rep., 03-426, 43 p.
- Michalak, A. M., and P. K. Kitanidis (2000), Macroscopic behavior and random-walk particle tracking of kinetically sorbing solutes, *Water Resour. Res.*, 36(8), 2133–2146.
- Mao, X., P. Enot, D. A. Barry, L. Li, A. Binley, and D.-S. Jeng (2006), Tidal influence on behavior of a coastal aquifer adjacent to a low-relief estuary, *J. Hydrol.*, 327, 110-127, doi: 10.1016/j.jhydrol.2005.11.030.
- Novak, W., and O.A. Cirpka (2006), Geostatistical inference of hydraulic conductivity and dispersivities from hydraulic heads and tracer data, *Water Resour. Res.*, 42, W08416.
- Paster A., G. Dagan, and J. Guttman (2006), The salt-water body in the Northern part of Yarkon-Tanimim aquifer: field data analysis, conceptual model and prediction. *J. Hydrol.*, 323, 154-167, doi: 10.1016/j.jhydrol.2005.08.018
- Paniconi C., I. Khlaifi, G. Lecca, A. Giacomelli, and J. Tarhouni (2001), Modeling and analysis of seawater intrusion in the coastal aquifer of eastern Cap-Bon, Tunisia. *Transport Porous Med.* 43, 3-28.
- Qahman K., and A. Larabi (2006), Evaluation and numerical modeling of seawater intrusion in the Gaza aquifer (Palestine), *Hydrogeol. J.*, 14, 713-728.
- Robinson C., L. Li, H. Prommer (2007), Tide-induced recirculation across the aquifer-ocean interface, *Water Resour. Res.*, 43, W07428, doi:10.1029/2006WR005679.
- Rezaei, M., E. Sanz, E. Raeisi, C. Ayora, E. Vazquez-Sune, and J. Carrera (2005), Reactive transport modeling of calcite dissolution in the fresh-salt water mixing zone. , *J. Hydrol.*, 311, 282-298, doi: 10.1016/j.jhydrol.2004.12.017.

Van Genuchten, M. T., and P. J. Wierenga (1976), Mass-transfer studies in sorbing porous-media: 1. Analytical solution, *Soil Sci. Soc. Am. J.*, 40, 473-480.

Volker, R. E., and K. R. Rushton (1982), An assessment of the importance of some parameters for seawater intrusion in aquifers and a comparison of dispersive and sharp-interface modelling approaches. *J. Hydrol.*, 56, 239-250.

Voss, C. I., and W. R. Souza (1987), Variable density flow and solute transport simulation of regional aquifers containing a narrow freshwater-seawater transition zone, *Water Resour. Res.*, 23, 1851-1866.

Volker, R. E., Q. Zhang, and D. A. Lockington (2002), Numerical modeling of contaminant transport in coastal aquifers, *Math. Comput. Simul.*, 59(1-3), 35-44.

Winter, T. C. (1976), Numerical simulation analysis of the interaction of lakes and groundwater, *U. S. Geol. Surv. Prof.*, 1001.

Zhang Q., R. E. Volker, and D. A. Lockington (2001), Influence of seaward boundary condition on contaminant transport in unconfined coastal aquifer, *J. Contam. Hydrol.*, 49(3-4), 201-215.

Zhang Q., R. E. Volker, and D. A. Lockington (2004), Numerical investigation of seawater intrusion at Gooburrum, Bundaberg, Queensland, Australia. *Hydrogeol. J.*, 12, 674-687.

Table

Table 1. Geometry, hydrogeological, and transport parameters used in the scaled tank model

Parameter	Variable Symbol	Value
Domain length [m]	L	1.8
Domain height [m]	H	0.6
Domain width [m]	W	0.1
Beach slope [-]	φ	1 : 6
Horizontal saturated hydraulic conductivity [m s^{-1}]	K_h	4×10^{-3}
Vertical saturated hydraulic conductivity [m s^{-1}]	K_v	4×10^{-3}
Longitudinal dispersivity [m]	α_L	1×10^{-3}
Transverse dispersivity [m]	α_T	1.25×10^{-4}
Total effective porosity [-]	θ	0.4
Mean seawater level [m]	h_s	0.520
Constant freshwater level [m]	h_f	0.545
Seawater density [kg m^{-3}]	ρ_s	1025
Freshwater density [kg m^{-3}]	ρ_f	1000
Salt concentration [kg m^{-3}]	C_s	35

Figure Captions:

Figure 1. Conceptual model and schematic representation of the flow domain and boundary conditions for the scaled tank model.

Figure 2. Periodic seawater levels to simulate tidal activities. The arrows indicate different moments during one period.

Figure 3. The variable-density transition zone between the freshwater and seawater for steady-state conditions in the absence of tidal activities and kinetic mass transfer. The solid lines are the contourlines of normalized salt concentrations.

Figure 6. Sensitivity analysis for the effects of combining tidal activities and kinetic mass transfer.

Figure 1

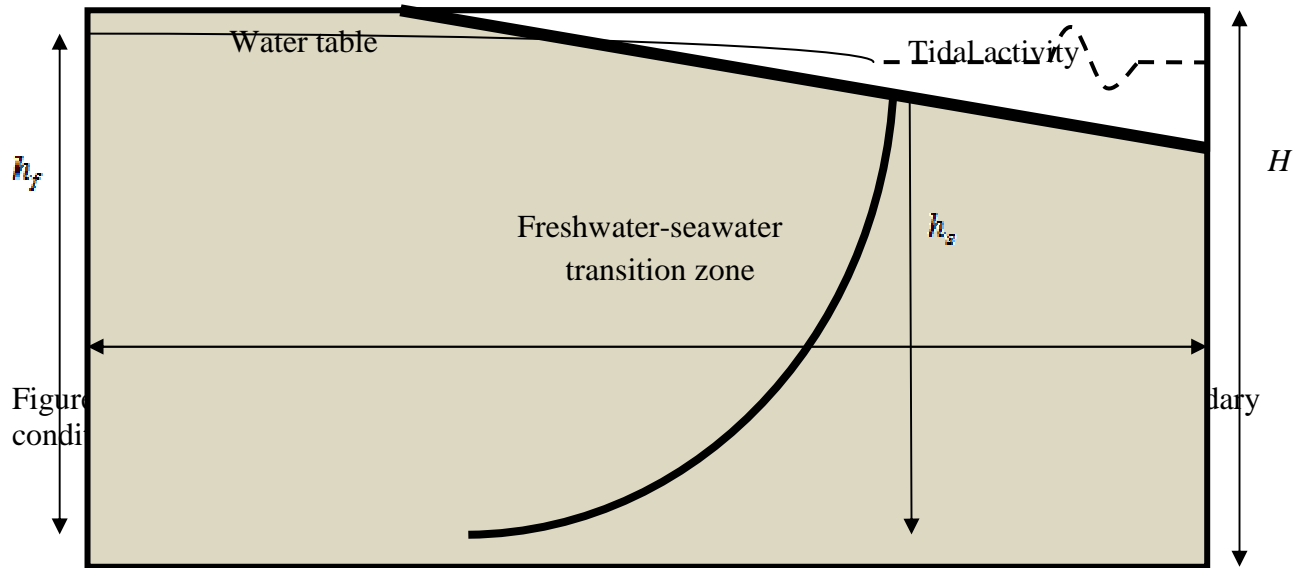


Figure 2

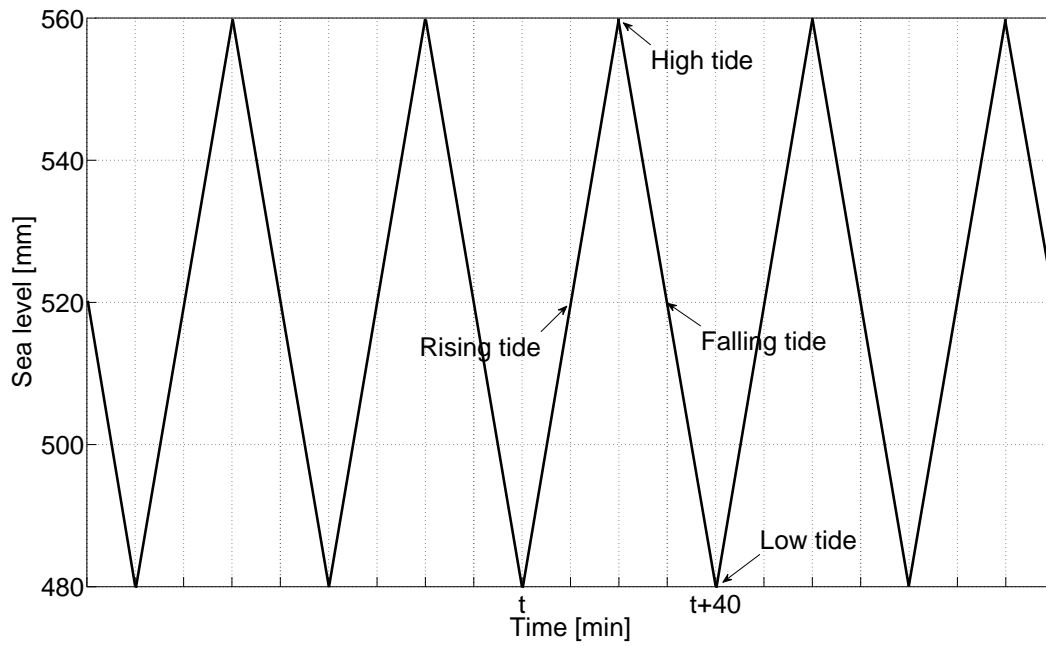


Figure 2. Transient seawater levels caused by tidal activities. The tidal period is 40 minutes. The arrows indicate different moments during one tidal period.

Figure 3

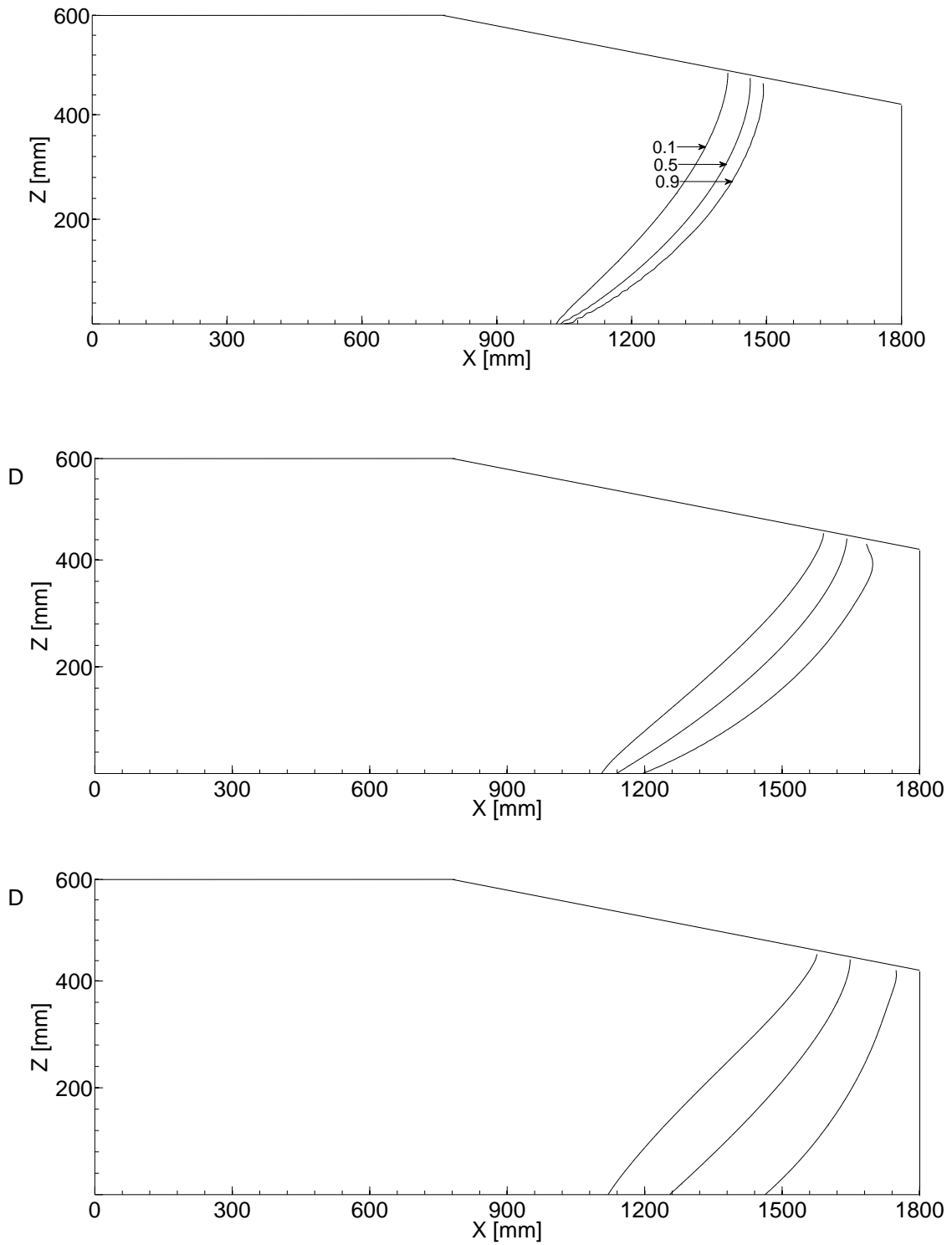


Figure 3. The variable-density transition zone between the freshwater and seawater for steady-state conditions in the absence of tidal activities and kinetic mass transfer. The solid lines are the contourlines of normalized salt concentrations.

Figure 6

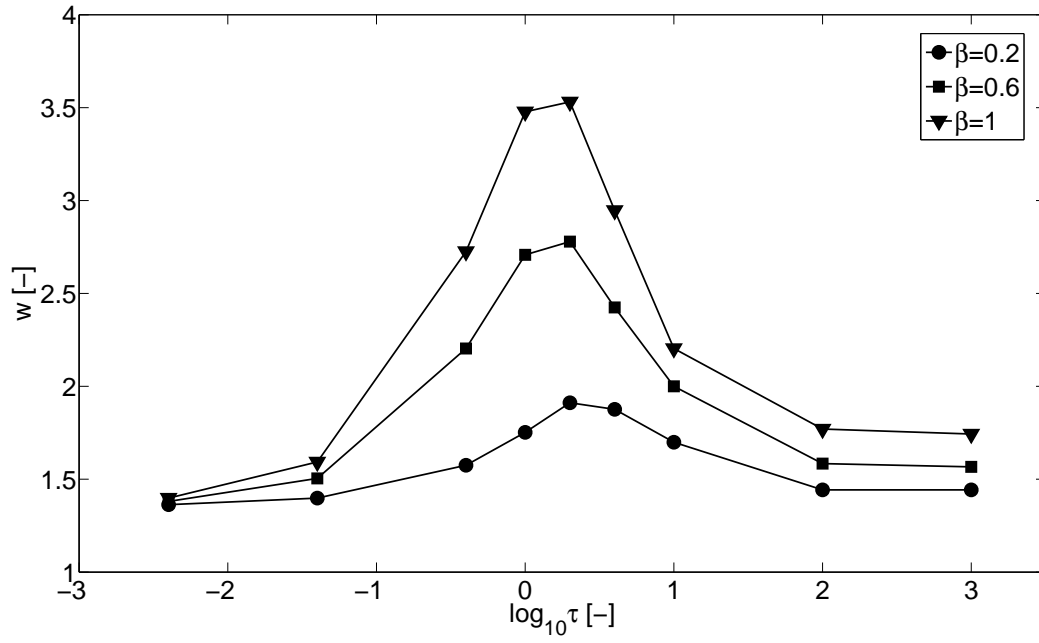


Figure 6. Sensitivity analysis for the effects of combining tidal activities and kinetic mass transfer.

Chapter 4. Influence of anisotropy and stratified heterogeneity on the pumping duration constrained by saltwater upconing (a manuscript in preparation)

Introduction

Coastal aquifers are becoming more and more important for water resources supply due to the rapid urbanization and industrialization in coastal areas. Because of seawater intrusion problem, saltwater underlies freshwater with an interface separating them, which is found in many inland aquifers as well as most coastal aquifers. In reality, this interface may be disturbed by a pumping well installed in a freshwater zone. In response to pumping, the freshwater-saltwater interface moves vertically toward the well (see figure 1), which refers to saltwater upconing. When the pumping rate is below a certain critical value, the well may always pump essentially fresh groundwater. However, this situation may be changed with an increased pumping rate. With a higher pumping rate, the interface will rise abruptly, and the pumping well will gradually become more and more saline, and finally have to be abandoned [Bear *et al.*, 1999].

The studies of saltwater upconing, including analytical, experimental, and numerical methods, have continued for several decades [Muskat, 1937; Bear and Dagan, 1964; Schmorak and Mercado, 1969; Reilly and Goodman, 1987; Reilly *et al.*, 1987, Dagan and Zeitoun, 1998; Bower *et al.*, 1999, Voss and Koch, 2001, Johannsen *et al.*, 2002; Nassereddin and Mimi, 2005; Zhou *et al.*, 2005; Nordbotten and Celia, 2006; Paster and Dagan, 2008]. There are two ways to describe the seawater-freshwater interface in studying seawater upconing problems. The first method is based on a sharp interface approximation assuming freshwater and saltwater to be immiscible, where the transition zone between freshwater and saltwater zones is relatively narrow compared

to the thickness of the aquifer. *Muskat* [1937] defined a critical rise of the sharp interface, above which the cone becomes unstable. In steady of assuming a fixed value for the critical rise of the interface, *Bower et al.* [1999] determined its location by using an analytical expression in terms of aquifer and confining unit properties, well geometry and the critical interface rise ratio. An analytical solution for interface upconing in a stratified aquifer with a random hydraulic conductivity is presented by *Dagan and Zeitoun* [1998].

In reality, a transition zone forms between the two fluids due to mixing by molecular diffusion and by transverse pore-scale dispersion [*Paster and Dagan*, 2008]. As the pumping rate is increased, the thickness of this transition zone is enlarged and the sharp interface approximation will no longer be justify. Therefore, a more realistic model of the transition zone through a system of variable-density flow and the advection-dispersion equations should be considered, which describes the distribution of salinity in a more precise way. The presence of the nonlinearity in coupled flow and salt transport equations, however, can be only solved by numerical techniques. *Reilly and Goodman* [1987] applied the SUTRA code to a local upconing problem. By comparing with their results with the sharp interface approximations obtained by *Bennett et al.* [1968], they found that the sharp interface model overestimates the critical pumping rate. A radial simulation model (RASIM), developed by *Aliewi* [1993], was used to predict the movement of saline upconing under a skimming well in the Pleistocene aquifer of Jericho, and simulations were carried out under different hydrogeological and operational conditions [*Nassereddin and Mimi*, 2005].

Zhou et al. [2005], using the FEAS code, investigated a hypothetical upconing problem where a partially penetrating well extracts water from the upper freshwater zone of a confined aquifer. In their study, the effects of longitudinal and transversal dispersivities, and density on the saltwater

upconing-decay process are examined based on a homogeneous and anisotropic aquifer. It is necessary to extend the investigation to examine more realistic stratified heterogeneous aquifer scenarios. In this work, a perfectly stratified confined aquifer with two layers is assumed to examine the effect of stratified heterogeneity on pumping duration constrained by the saltwater upconing. The relative and absolute magnitudes of hydraulic conductivity of two layers are expected to have a great effect on saltwater upconing process, and thus exercise a great influence on pumping duration. In addition, the influence of the anisotropy is also investigated in this study.

Governing Equation

In this study, the MODFLOW/MT3DMS-based SEAWAT-2000 code [Guo and Langevin, 2002; Langevin et al., 2003; Langevin and Guo, 2006] is used to simulate the saltwater upconing process.

The governing equation for density-dependent groundwater flow in terms of freshwater head is expressed as follows [Langevin et al., 2003]:

$$\nabla \cdot \left[\rho K_f \left(\nabla \cdot h_f + \frac{\rho - \rho_f}{\rho_f} \cdot \nabla z \right) \right] = \rho S_f \frac{\partial h_f}{\partial t} + \theta_e \frac{\partial \rho}{\partial t} - \rho_s q_s \quad (1)$$

where z [L] is the vertical coordinate directed upward; K_f [LT^{-1}] is the equivalent freshwater hydraulic conductivity; h_f [L] is the equivalent freshwater head; ρ [ML^{-3}] is the fluid density; ρ_f [ML^{-3}] is the freshwater density; S_f [L^{-1}] is the equivalent freshwater storage coefficient; t [T] is time; θ_e is the effective porosity; and ρ_s [ML^{-3}] and q_s [T^{-1}] are the density and flow rate per unit volume of aquifer of the source/sink, respectively. The governing equation for salt transport is

$$\frac{\partial c}{\partial t} = \nabla \cdot (D \cdot \nabla c) - \nabla \cdot (\vec{v}c) - \frac{q_s}{\theta} c_s \quad (2)$$

where C [ML⁻³] is the concentration of dissolved salt; D [L²T⁻¹] is the hydrodynamic dispersion coefficient tensor; \vec{v} [LT⁻¹] is the pore water velocity; and C_s [ML⁻³] is the concentration of dissolved salt from source/sink [Zheng and Bennett, 2002]. the hydrodynamic dispersion coefficient tensor; and \vec{v} [LT⁻¹] is the pore water velocity vector. The relationship between the fluid density and salt concentration is represented by the linear function of state:

$$\rho = \rho_f + \epsilon C_m \quad (3)$$

where ϵ is a dimensionless constant depending on the units and mass concentration used in the simulation, which is set to be 0.7143 for salt concentrations ranging from zero to 35 kg m⁻³, a typical concentration value for seawater; and ρ is expressed in kg m⁻³.

Numerical model

The hypothetical domain in our study is like the one used by Zhou *et al.* [2005], which is shown in Figure 2. The confined aquifer is 120 m thick. Upper 98 m is freshwater and the lower 20 m is saltwater. The freshwater and saline groundwater is separated by a 2-m-thick transition zone. A partially penetrating well with 20 m long is centered 10 m below the aquifer top. The porosity is set to be 0.2. The value of pumping rate is 2400 m³/d. With the pumping process, water is recharged from the external radial boundary located at $r = 2000$ m. The densities of freshwater and saltwater are 1000 kg / m³ and 1025 kg / m³, respectively. Molecular diffusion is neglected. The parameters used above are exactly the same as those used in Zhou *et al.* [2005]. In the study of Zhou *et al.* [2005], however, the domain is homogeneous and anisotropic, while ours is isotropic and stratified. Assumption of a perfectly stratified aquifer is usually a first step to explore new theoretical issues in subsurface hydrology. Therefore, a perfectly stratified aquifer

with two layers is assumed. The aquifer and transport parameters are listed in Table 1. The hydraulic conductivities of upper 60 m and lower 60 m are specified as K_1 and K_2 . The corresponding values of permeability, k_1 and k_2 , are listed in Table 2 for different cases.

We employ a similar resolution level of the finite-difference grid spacing as the finite-element mesh used by *Zhou et al.* [2005]. The grid involves 113 columns and 60 layers. The dimensions of the grid vary from 0.5 m near the well to 25 m at the distant boundary. Each layer is 2 m thick. This scheme of the discretization is exactly the same as that used by *Langevin* [2008], who takes the *Zhou et al.*'s [2005] upconing problem to validate the applicability of studying an axially symmetric groundwater flow and transport problem by a unmodified version of SEAWAT.

Results and discussion

Langevin [2008] pointed out that the SEAWAT code using Cartesian geometry can accurately simulate an axially symmetric groundwater flow and solute transport problem. The proposed approach is straightforward and implemented by adjusting several input parameters to account for the increase in flow area with radial distance from the injection or extraction. It should be noted that the proposed method works for layered heterogeneous media.

First of all, our isotropic case (Case 1) is compared with *Zhou et al.*'s anisotropic case. Likewise, we assume that the pumping well must be shut off when the normalized salt fraction in the extracted water reaches 2% [*Zhou et al.*, 2005]. Figure 3 shows the variation of the salt fraction in extracted water with pumping time for two cases. At $t = 2.89$ years, for isotropic case the salinity of extracted water reaches the criteria where the pumping well should be shut off. However, for anisotropic case, the concentration of the extracted water reaches 2% of the saline water after about 5.55 years. *Zhou et al.* [2005] predicted that the pumping duration for the same anisotropic case is 3.95 years. *Langevin* [2008] inferred that the discrepancy may be caused by

different solute boundary conditions. Therefore, pumping well in anisotropic case can extract 92% more water than in isotropic case, which is caused by a smaller value of vertical hydraulic conductivity. Transient distributions of normalized salt fraction at $t = 2.89$ years in two cases are exhibited in Figure 4. As can be seen, the thickness of the transition zone in two cases are similar at this moment. However, the distribution of the salt contours are changed. The accelerated upconing of salt for isotropic case can be seen from comparing the location of 0.2 concentration contour in two subfigures. The analysis above indicates aquifer hydraulic conductivity have a significant effect on how long the pumped water reaches the criteria where the pumping well should be shut off.

For aquifers in coastal areas, stratified heterogeneity is usually found and therefore, expected to have great effects on well-induced saltwater upconing. To demonstrate the effect of stratified heterogeneity on the saltwater upconing, we simulate other six different cases listed in Table 2. When a pumping well extracts groundwater, the lost water of the aquifer will be recharged by the distal boundary. Hence, the values of hydraulic conductivity in upper freshwater layer and lower saltwater layer determine the pumping duration. Figure 5 presents the variation of the salt fraction in extracted water with pumping time for Case 1, 2 and 3. For these three cases, the hydraulic conductivities of the upper half domain, K_1 , are all the same, while K_1/K_2 are different being 1, 2 and 5 for Case 1, 2 and 3, respectively, where K_2 is hydraulic conductivity of the lower half domain. Pumping durations for above three cases are 2.89, 6.79 and 38.21 years, respectively. It is clearly shown that a lower hydraulic conductivity of the lower half domain increases the pumping duration provided that the hydraulic conductivity of the upper half domain is constant. However, the results are reverse when values of hydraulic conductivity are reverse for two half domains, which are demonstrated in Figure 6 showing the variation of the salt

fraction in extracted water with pumping time for Case 1, 4 and 5. For these three cases where K_1/K_2 are 1, 1/2 and 1/5, pumping durations are 2.89, 1.05 and 0.59 years, respectively. This indicates that a lower hydraulic conductivity of the upper half domain decreases the pumping duration when the hydraulic conductivity of other half domain keeps constant. On the other hand, cases where $K_1 > K_2$ can obtain much more water than cases where $K_1 < K_2$.

As K_1/K_2 keeps constant, one expects the pumping well to extract different amounts of water for different absolute hydraulic conductivities. For this purpose, we examine the pumping duration for two case groups (Case 2 and Case 6, and Case 4 and Case 7), where K_1/K_2 are 2 and 1/2, respectively. Figure 7 indicates that under same ratio of K_1 and K_2 , a higher hydraulic conductivity could obtain more water from the aquifer. For instance, the pumping durations of Case 6 and Case 7 are 2.73 and 0.71 years, respectively, which are both less than corresponding Case 2 and Case 4 being 6.79 and 1.05.

Conclusions

Saltwater upconing that occurs in many aquifers in response to pumping from a well in freshwater zone can salinize the extracted freshwater. The pumping well should be shut off when the normalized salt fraction of the pumped water reaches a certain criteria (2%). For a given well, the pumping duration is effected by many factors including pumping rate, transport and aquifer parameters as well as density difference of two fluids. In this work, we investigate the influence of anisotropy and stratified heterogeneity on the pumping duration. The numerical simulations were run using the SEAWAT-2000 code.

It is found that the pumping duration of the homogeneous case (Case 1) extracts less water than that of *Zhou et al.*'s [2005] anisotropic case because of a higher vertical hydraulic conductivity. Importance of stratified heterogeneity on the pumping duration is studied by simply defining a

perfectly two-layer homogeneous confined aquifer with same height. For cases where K_1 is constant and $K_1/K_2 = 1, 2$ and 5 , the pumping duration is increased with the increasing ratio of K_1/K_2 . Similarly, if K_2 keeps constant and $K_1/K_2 = 1, 1/2$ and $1/5$, the pumping duration is decreased with the decreasing ratio of K_1/K_2 . It should be noted that cases where $K_1 > K_2$ can obtain much more water than cases where $K_1 < K_2$. On the other hand, provided that K_1/K_2 keeps constant, the well can extract more water from the aquifer with higher hydraulic conductivities. In reality, the stratification of the aquifer would be more complex than our studied scenarios. A simply layered aquifer, however, is often applied to the first step of the theoretical analysis of stratified heterogeneity [Ward *et al.*, 2008]. Our preliminary investigations demonstrate that stratified heterogeneity have significant influence on pumping duration constrained by the saltwater upconing problem. For pumping-induced saltwater upconing under the effect of random heterogeneity, the study is undergoing.

Acknowledgements. This research was sponsored by the National Institutes of Water Resources (NIWR) and U.S. Geological Survey (USGS) under project ID 2007GA165G. This article has not been reviewed by the agency, and no official endorsement should be inferred. Any opinions, findings, and conclusions or recommendations expressed in this material are those of the authors and do not necessarily reflect the views of NIWR and USGS. The authors thank Dr. C. D. Langevin for providing the assistance in numerical simulations.

References

- Aliewi, A. (1993), Numerical simulation of the behavior of the fresh/saline water transition zone around a scavenger well. Ph. D. Thesis, University of Newcastle Upon Tyne, UK.
- Bear, J., A. H. -D. Cheng, S. Sorec, D. Ouazar, and I. Herrera (1999), *Seawater Intrusion in Coastal Aquifers- Concepts, Methods and Practices*. Springer, New York.

- Bear, J., and G. Dagan (1964), The unsteady interface below a coastal collector. *Hydraul. Lab. Progr. Rep. No. 3*, Israel Institute of Technology, Haifa, Israel.
- Bower, J.W., L. H. Motz, and D. W. Durden (1999), Analytical solution for determining the critical condition of saltwater upconing in a leaky artesian aquifer. *J. Hydrol.* , 221, 43-54.
- Dagan, G., and D. G. Zeitoun (1998), Free-surface flow toward a well and interface upconing in stratified aquifers of random conductivity, *Water Resour. Res.*, 34, 3191-3196.
- Guo W. X., and C. D. Langevin (2002), User's guide to SEAWAT: a program for the simulation of three-dimensional variable-density ground-water flow. USGS Techniques of Water Resources Investigations, Book 6, chap A7.
- Johannsen, K., W Kinzelbach, S Oswald, and G. Wittum (2002), The saltpool benchmark problem-numerical simulation of saltwater upconing in a porous medium. *Adv. Water Resour.* 25, 335-348.
- Langevin, C. D. (2008), Modeling axisymmetric flow and transport. *Ground Water*, 46, 579-590.
- Langevin, C. D., and W. Guo (2006), MODFLOW/MT3DMS-based simulation of variable-density ground water flow and transport. *Ground Water*, 44, 339-351.
- Langevin, C., W. B. Shoemaker, and W. Guo (2003), Modflow-2000, The U.S. Geological Survey modular ground-water flow model □ Documentation of the Seawat-2000 version with the variable density flow process (VDF) and the integrated MT3DMS transport process (IMT), U.S. Geol. Surv. Open File Rep., 03-426, 43 p.
- Muskat, M. (1937), *The flow of homogeneous fluids through porous media*, McGraw-Hill, Inc. New York.
- Motz, L. H. (1992), Salt-water upconing in an aquifer overlain by a leaky confining bed. *Gound Water*, 30, 192-198.
- Nassereddin, K. M., and Z. A. Mimi (2005), Numerical simulation of saline upconing in the Pleistocene aquifer of Jericho area, *Water Environ. J.*, 19, 25-29.
- Nordbotten, J. M., and M. A. Celia (2006), An improved analytical solution for interface upconing around a well, *Water Resour. Res.*, 42, W08433, doi:10.1029/2005WR004738.
- Paster, A., and G. Dagan (2008), Mixing at the interface between two fluids in aquifer well upconing steady flow, *Water Resour. Res.*, 44, W05408, doi:10.1029/2007WR006510.
- Reilly, T. E., and A. S. Goodman (1987), Analysis of saltwater upconing beneath a pumping well. *J. Hydrol.*, 89, 169-204.
- Reilly, T. E., M. H. Frimpter, D. R. LeBlance, and A. S. Goodman (1987), Analysis of steady state saltwater upconing with application at Truro well field, Cape Cod, Mass. *Gound Water*, 25, 194-206.
- Schmorak, S., and A. Mercado (1969), Cupconing of fresh water-sea water interface below pumping wells, field study, *Water Resour. Res.*, 5, 1290-1311.
- Voss, C. I., and W. R. Souza (1987), Variable density flow and solute transport simulation of regional aquifers containing a narrow freshwater-seawater transition zone, *Water Resour. Res.*, 23, 1851-1866.

Voss, A. and M. Koch (2001), Numerical simulations of topography-induced saltwater upconing in the state of Brandenburg, Germany, *Phys. Chem. Earth(B)*, 26, 353-359.

Ward, J. D., C. T. Cimmons, and P. J. Dillon (2008), Variable-density modelling of multiple-cyc aquifer storage and recovery (ASR): Importance of anisotropy and layered heterogeneity in brackish aquifers. *J. Hydrol.* 356, 93-105.

Zhou, Q.L., J., Bear, and J. Bensabat (2005), Saltwater upconing and decay beneath a well pumping above an interface zone. *Transport Porous Med.*, 61, 337-363.

Table 1 Model input parameters

Parameter	Variable	Value
Porosity	θ	0.2
Longitudinal dispersivity, m	α_L	1.0
Transversal dispersivity, m	α_T	0.5
Molecular diffusion coefficient, $m^2 d^{-1}$	D_m	0
Dynamic viscosity, $kg m^{-1}s^{-1}$	μ	1.0×10^{-3}
Density of freshwater, $kg m^{-3}$	ρ_f	1000
Density of saltwater, $kg m^{-3}$	ρ_s	1025
Pumping rate, $m^{-3}d^{-1}$	Q_w	2400

Table 2 Permeability for different studied cases

Permeability	Case 1	Case 2	Case 3	Case 4	Case 5	Case 6	Case 7
$k_1 \times 10^{11}, \text{m}^2$	2.56	2.56	2.56	1.28	0.512	1.28	0.64
$k_2 \times 10^{11}, \text{m}^2$	2.56	1.28	0.512	2.56	2.56	0.64	1.28

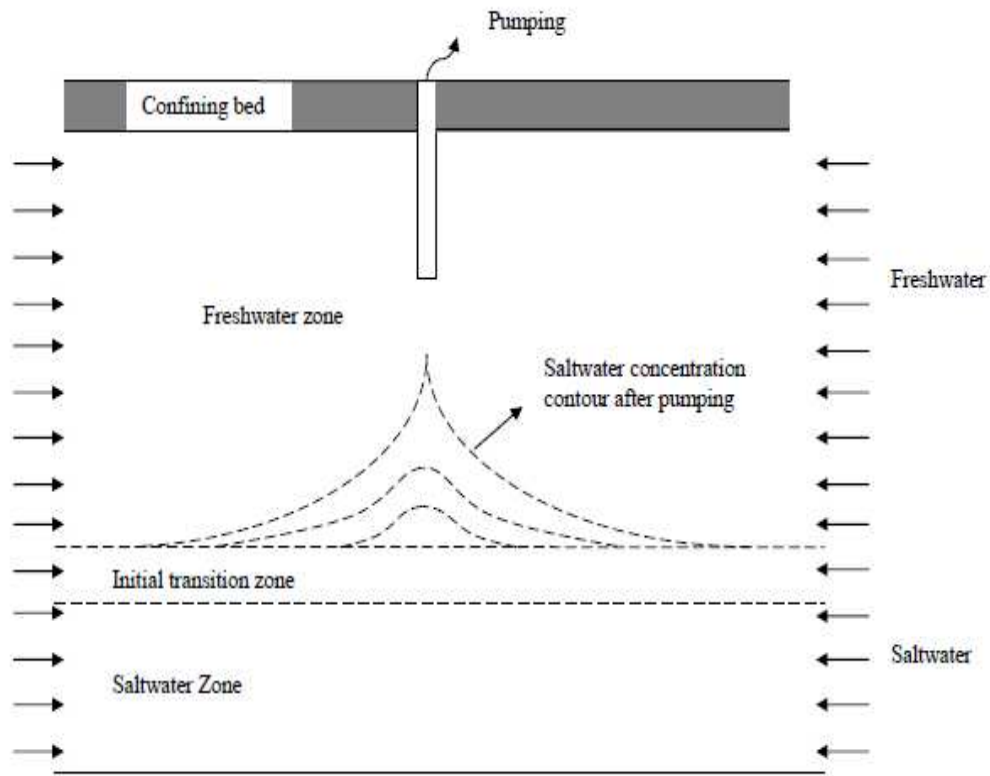


Figure 1. Pumping-well induced saltwater upconing.

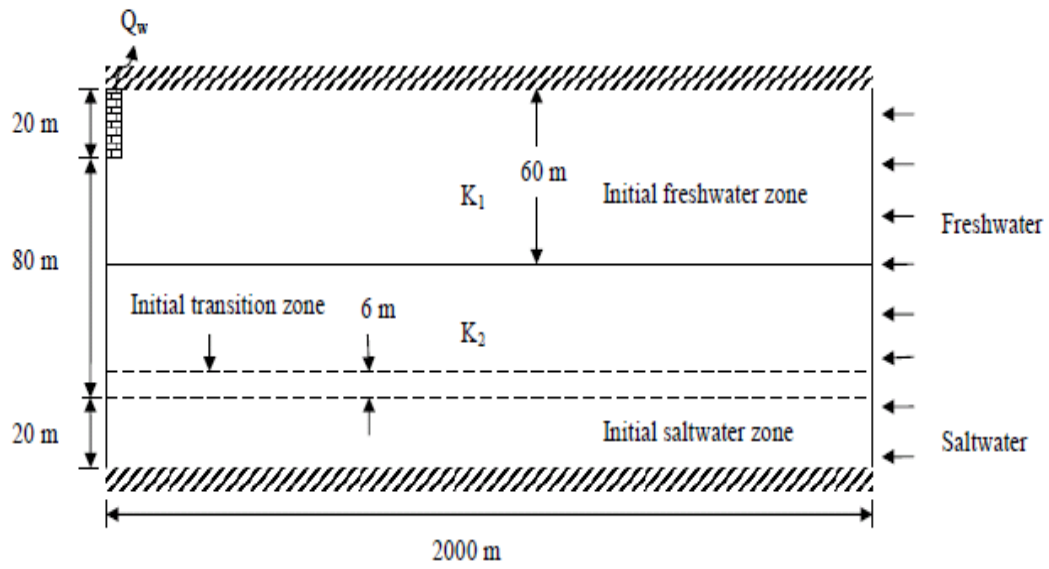


Figure 2. Configuration of the model domain with initial and boundary conditions.

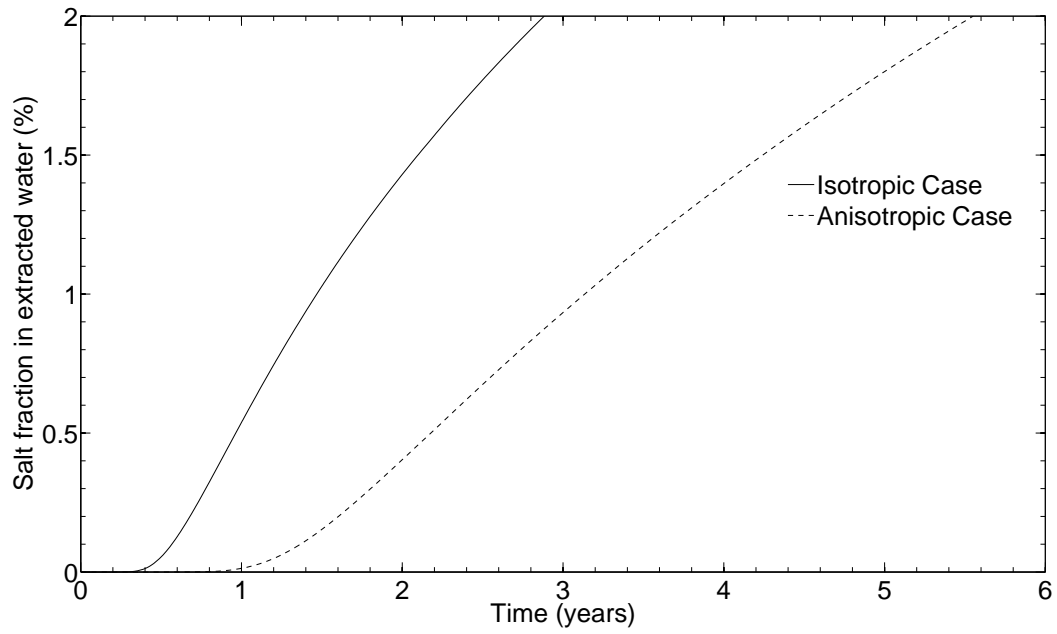


Figure 3. Salt fraction in extracted water vs. time since pumping started for isotropic and anisotropic cases.

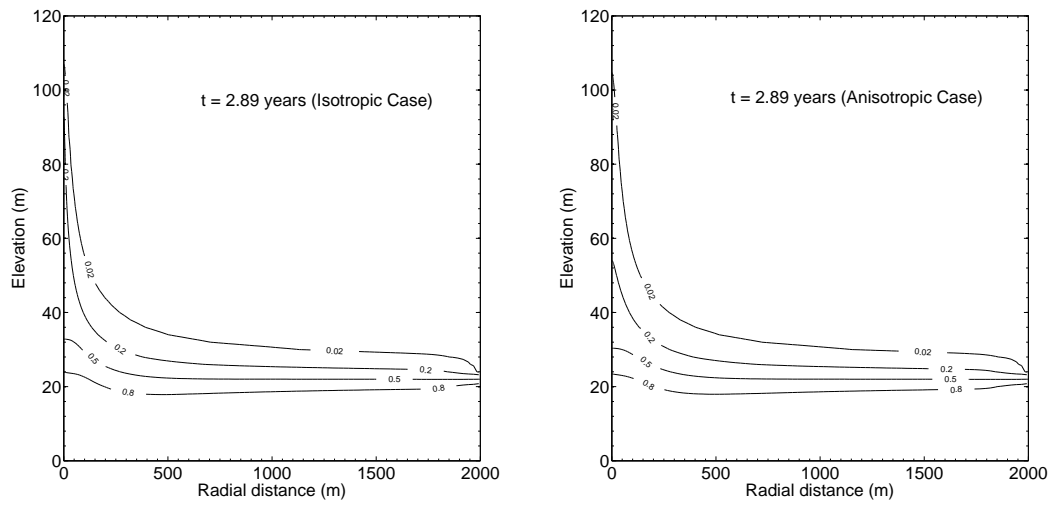


Figure 4. Transient distribution of slat concentration contours after 2.89 years of pumping for isotropic and anisotropic cases.

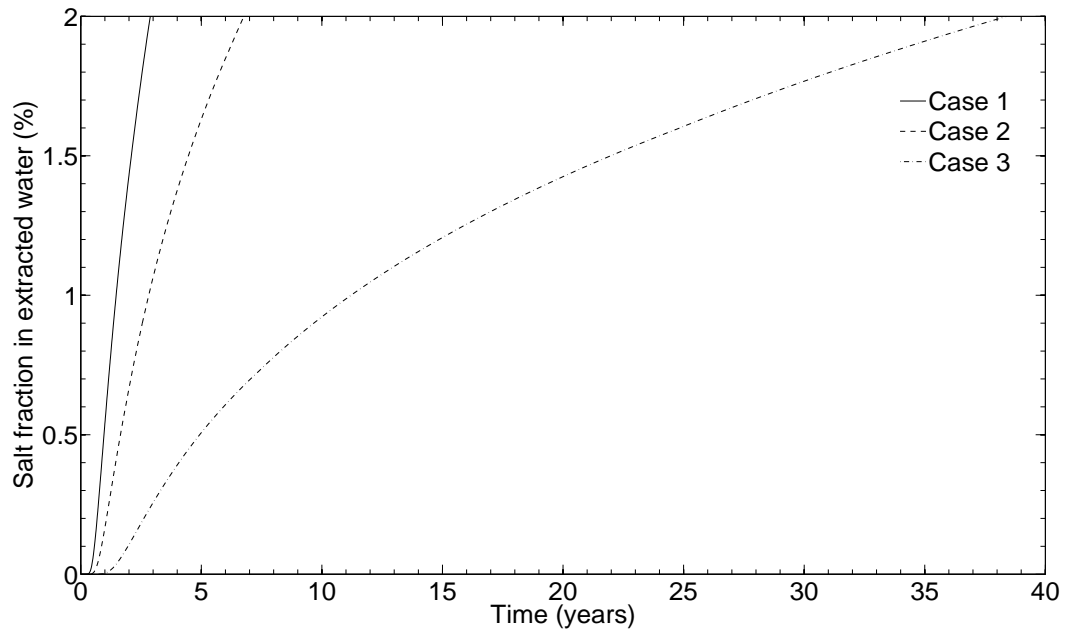


Figure 5. Salt fraction in extracted water vs. time since pumping started for Case 1, 2 and 3.

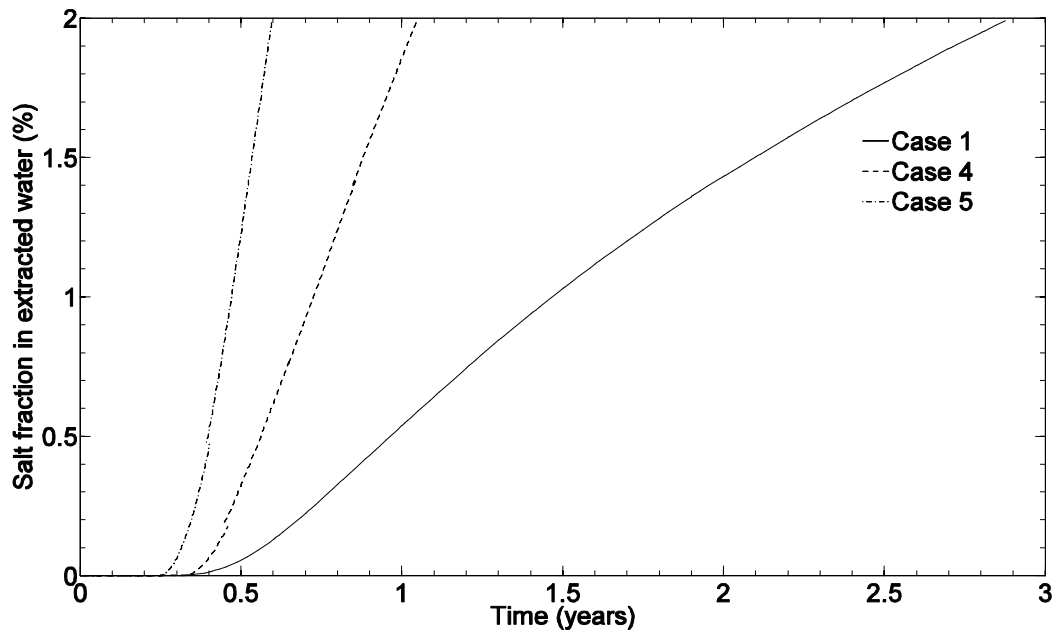


Figure 6. Salt fraction in extracted water vs. time since pumping started for Case 1, 4 and 5.

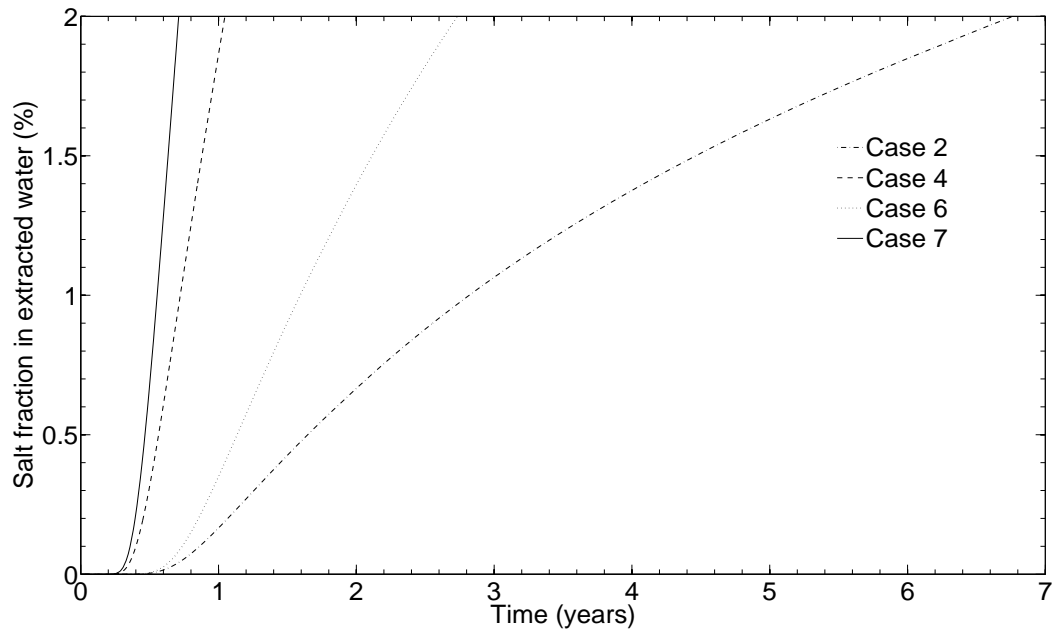


Figure 7. Salt fraction in extracted water vs. time since pumping started for Case 2, 4, 6 and 7.

Assessing the impacts of a major wildfire in the Okefenokee Swamp on mercury levels in resident macroinvertebrates

Basic Information

Title:	Assessing the impacts of a major wildfire in the Okefenokee Swamp on mercury levels in resident macroinvertebrates
Project Number:	2008GA175B
Start Date:	3/1/2008
End Date:	2/28/2009
Funding Source:	104B
Congressional District:	10
Research Category:	Water Quality
Focus Category:	None, None, None
Descriptors:	
Principal Investigators:	Darold Paul Batzer, Darold Paul Batzer

Publication

Title: Assessing the impacts of a major wildfire in the Okefenokee Swamp on mercury levels in resident macroinvertebrates

Author: Darold P. Batzer, Professor of Entomology, University of Georgia, Athens

Period of Performance: March 1, 2008 to February 28, 2009.

Executive Summary

In 2007, a major wildfire swept through most of Okefenokee Swamp in southeastern Georgia. That habitat has a history of elevated mercury levels in aquatic biota (invertebrates, fish), and concerns developed that the fire may exacerbate the problem. This study assessed mercury levels in key aquatic invertebrates (amphipod crustaceans, dragonfly nymphs, crayfish) in areas that burned versus areas that did not burn; a study conducted prior to the wildfire provided additional reference data for comparison. Preliminary analyses do not indicate that mercury levels increased in invertebrates residing in burned areas. The study has been extended for an additional year to provide sufficient data for valid conclusions to be drawn, and has been expanded to include mosquitofish, to assess responses beyond the invertebrate community.

List of Figures

Figure 1. Map of the extent of June 2007 fires across the Okefenokee Swamp. The Big Turnaround Fire burned the northern half, and the Bugaboo Scrub Fire burned the southern half.
Figure 2. Mercury levels (mean \pm SE) in 1998-2000 for amphipods, odonates, and crayfish across the Okefenokee Swamp, with levels being significantly higher in amphipods than other taxa (ANOVA, Tukey test, $P < 0.05$).
Figure 3. Locations of sites sampled in 2007 and 2008, and proposed for 2009. Closed circles are in areas that burned and open circles are in areas that did not (see Figure 1).
Figure 4. Preliminary data on post-fire total mercury levels in amphipods in areas that burned vs. residual areas that did not burn.

PROJECT SCOPE AND OBJECTIVES

Prolonged drought conditions have emerged as the major concern affecting water resources in Georgia. If increasing prevalence of drought is symptomatic of on-going climate change, then an understanding of consequences will be imperative to effective management of Georgia's water resources. For wetlands, an important impact of drought is an increased prevalence of wildfire. In June 2007, the most expansive wildfires in recorded history occurred in the Okefenokee Swamp of southeast Georgia, and more than 75% of that wetland burned (Figure 1, Beganyi and Batzer 2009).

In terms of water quality, wildfires could have significant consequences because many wetlands, including the Okefenokee, are important sinks for mercury contaminants. Elemental mercury and methyl mercury are of particular concern for environmental safety. The methylated form of mercury is a potent neurotoxin and poses serious problems to animals in many ecosystems (Morel et al. 1998), and potentially to humans. Understanding how wildfire and drought affect mercury bioavailability in wetlands would have substantial benefits for assessing increased risk.

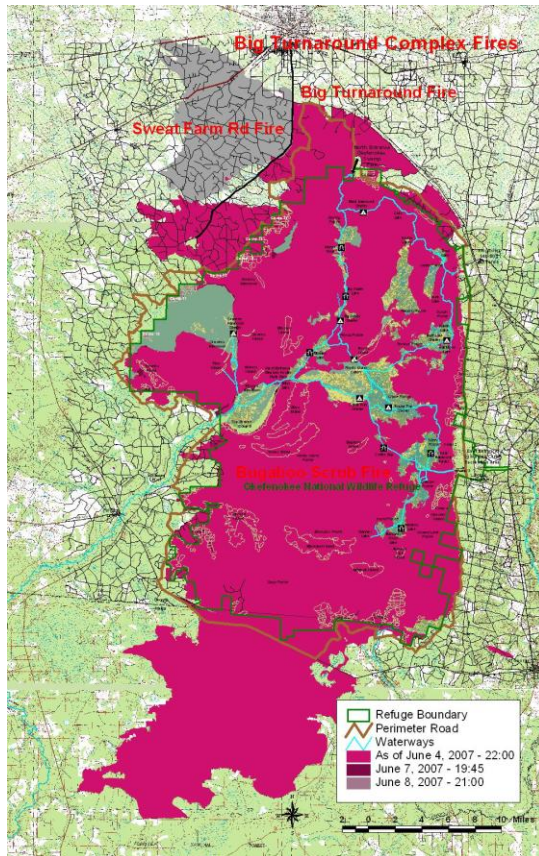


Figure 1. Map of the extent of June 2007 fires across the Okefenokee Swamp. The Big Turnaround Fire burned the northern half, and the Bugaboo Scrub Fire burned the southern half.

Even prior to the 2007 fires, the Georgia Department of Natural Resources had placed restrictions on the consumption of fish from the Okefenokee (bowfin, *Amia calva*; flier, *Centrarchus* sp.; pickerel, *Esox* spp.) due to high levels of mercury. My own laboratory established that unusually high levels of mercury occur in Okefenokee invertebrates (George and Batzer 2007), and fish probably derive mercury from these organisms. It is possible that mercury problems could become even more severe after the wildfire (Garcia and Carignan 1999, 2000).

The goal of this project is to assess whether mercury levels in Okefenokee Swamp invertebrates have increased as a result of the 2007 wildfire. That goal can be achieved because an expansive data set on mercury levels in Okefenokee invertebrates already exists, gathered from 1998 to 2000 (George and Batzer 2007), and this data set can be used as a baseline to assess fire induced change. Thus far we have collected post-fire invertebrate samples in December 2007, May 2008, September 2008, and December 2008.

REVIEW OF PAST RELEVANT WORK

Past Work on Mercury Contaminant in Wetlands

Burning of fossil fuels, medical waste incineration, agriculture, and mining are all important sources of mercury to the environment (Rood et al. 1995). Emissions significantly increase mercury levels in precipitation (Rolfhus and Fitzgerald 1995, Keeler et al. 1995), and the material accumulates in wetlands (Moore et al. 1995, Rood

1996, St. Louis et al. 1996, Heyes et al. 1998, Niamo et al. 2000). Fire and direct drying of sediments from drought may remobilize mercury from sediments and peat, increasing mercury bioavailability to biota (Hall et al. 1998, Lamontagne et al. 2000, Snodgrass et al. 2000).

Bioaccumulation of mercury by invertebrates allows mercury to become available to organisms higher in the food chain (Liu et al. 2008). Wetland fish can bioaccumulate particularly high levels of methyl mercury (Bloom 1992, Mason et al. 1994, Kannan et al. 1997, Wong et al. 1997, Hall et al. 1998). As a result, piscivorous birds are exposed to bioavailable mercury (Gariboldi et al. 1997). Since alligators are long-lived wetland predators, there are also concerns about the potential to bioaccumulate mercury in their tissues (Jagoe et al. 1998, Khan and Tansel 2000). Game fish, birds, and alligators are all organisms of concern in the Okefenokee, and invertebrates and mosquitofish are likely involved in the food chains for each.

Past Work in the Okefenokee

Invertebrates are useful bioindicators of environmental conditions (Rader et al. 2001), and thus in 1998 a project was initiated to assess spatial and temporal variation of mercury levels in Okefenokee invertebrates (George and Batzer 2007). In that two year study, 32 sites were chosen in the Okefenokee that were distributed across the range of hydrological units and vegetative communities present in the swamp. They included sites centered around Chesser/Grand Prairie, Double Lakes, Durden Prairie, Chase Prairie, Floyd's Prairie, and Billy's Lake. At each site, sampling was stratified to include shrub thickets, marsh prairies, cypress stands, boat trails, and deepwater lakes or canals. Sampling was conducted in December 1998, May 1999, August 1999, December 1999, May 2000, and August 2000. At each sampling location, amphipods (Crangonyctidae) were collected as available for 30 minutes using sweep nets. Beginning in May 1999, Odonata nymphs (primarily Anisoptera) were collected, and beginning in December 1999, crayfish (Cambaridae) were added to collections. Invertebrates were placed in plastic vials and transported on ice back to the laboratory, and then frozen. Total mercury levels were determined using Atomic Absorption Spectrophotometry (AAS) as described by Waldrop (1999). Validation trials were conducted and lower detection limit was 0.25 ppb.

Mercury levels varied dramatically among sample pools (averaged 1.6 ppm, but ranged from 0 to 86 ppm), and a 4-way ANOVA model concurrently addressing location, sub-habitat, sample date, and study organism accounted for 65.1% of this variation. However, the kind of organism ($F_{2, 184} = 93.07$, $P < 0.0001$) and the sample date ($F_{5, 184} = 16.16$, $P < 0.0001$) were the only significant factors in the model, with the study organism and sample date accounting for 43.3% and 18.8% of variation, respectively. Mercury concentrations were dramatically higher in amphipods than either odonates or crayfish (Figure 2). Levels varied temporally with the highest levels of mercury occurring in May 2000. Overall levels of mercury were similar among all six locations ($F_{5, 184} = 1.67$, $P = 0.1448$) and all five subhabitats ($F_{4, 184} = 1.67$, $P = 0.3527$). These analyses suggest that, while no "hot spots" for mercury were detected, there were "hot times" and "hot organisms" (see also Liu et al. 2008). The lack of spatial variation in mercury across the Okefenokee is consistent with aerial deposition of the material relatively evenly across the wetland (Fitzgerald et al. 1998).

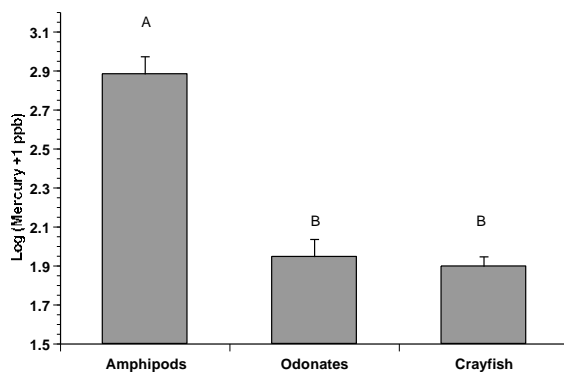


Figure 2. Mercury levels (mean \pm SE) omn 1998-2000 for amphipods, odonates, and crayfish across the Okefenokee Swamp, with levels being significantly higher in amphipods than other taxa (ANOVA, Tukey test, $P < 0.05$)

Levels of mercury detected in Okefenokee aquatic invertebrates seemed unusually high, even for wetlands. We frequently encountered mercury levels in excess of 20 ppm, and levels averaged 1.6 ppm. In comparison, mercury levels in invertebrates of the Florida Everglades averaged 0.3 ppm (Scheidt 2000), and levels averaged 0.1 ppm in small depressional wetlands in South Carolina (Snodgrass et al. 2000). However, the higher than normal mercury levels detected in this study may not necessarily indicate a uniquely severe problem for the Okefenokee Swamp. The high levels occurred almost exclusively in amphipods, and these organisms are often not collected in other studies of mercury in wetland invertebrates. Amphipods might be especially useful for detecting high levels of mercury because, as Sferra et al. (1999) reported, mercury toxicity in amphipods can exceed 4.1 ppm. Many organisms might die before accumulating such high levels. It follows that since amphipods are often a major source of food for fish they might be contributing to the high levels of mercury in Okefenokee Swamp fish.

METHODS

The Okefenokee Swamp is one of the largest freshwater wetlands in North America. It is approximately 3,800 km² and provides habitat for a variety of aquatic organisms including fish, reptiles, birds, and invertebrates (Porter et al. 1999, Kratzer and Batzer 2007). The Okefenokee Swamp has many characteristics that could lead to mercury accumulation and bioavailability problems, including high water temperature, frequent anoxic conditions, low pH (< 4.0), intermittent hydrology, peat deposits, and periodic fire (Mason et al. 2000).

After the 2007 wildfire, I selected 21 sites for post-fire sampling, all located in the same six general areas sampled before the fire (Figure 3, Beganyi and Batzer 2009). Thirteen of the sites had burned (5 cypress stands, 5 scrub-shrub thickets, 3 marsh prairies) and 8 had not (3 cypress stands, 3 shrub-shrub thickets, 2 prairies). Sites were sampled in December 2007, May 2008, September 2008, and December 2008, which corresponds to the seasonal schedule of past efforts. Amphipods (Cragonictidae), odonates (Libellulidae), and crayfish (Cambaridae) were collected with nets and dip pans for 1 person/ hour. Total mercury levels in these samples are being determined by the UGA CAES Soils and Environmental Testing Laboratory using Atomic Absorption

Spectrophotometry (AAS), although the procedures have been up-dated from those used previously. Standard quality control steps are being conducted including validation trials in conjunction with each sampling run.

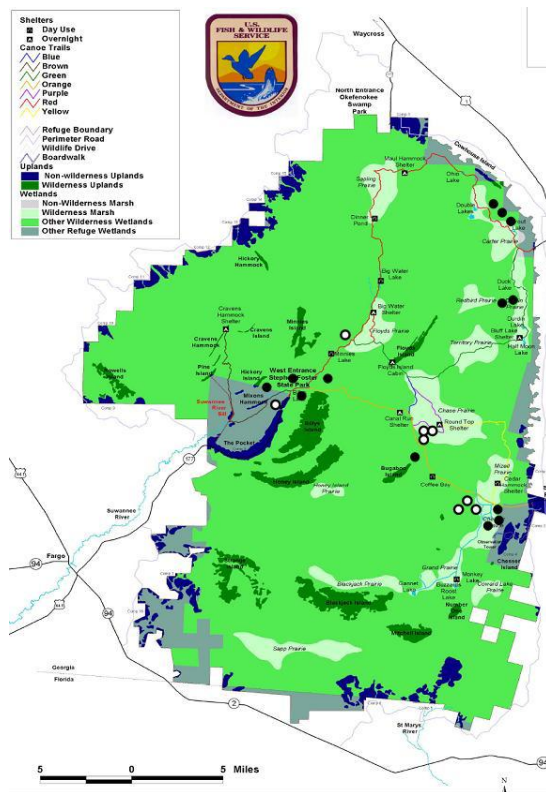


Figure 3. Locations of sites sampled in 2007 and 2008, and proposed for 2009. Closed circles are in areas that burned and open circles are in areas that did not (see Figure 1).

RESULTS

Analyses of mercury levels are on-going, but I can provide some preliminary findings (see also Beganyi and Batzer 2009). All data on mercury levels in invertebrates collected from December 2007 through December 2008 are listed in Appendix 1. As prior to the fire, total mercury levels appear higher in amphipods than in odonates or crayfish. Also as earlier, temporal variation is pronounced, with levels varying from December 2007 to September 2008 ($P = 0.0002$, Figure 4). However, at this point, I have no compelling evidence that mercury levels are higher in invertebrates living in burned areas compared to residual non-burned areas (Figure 4, Appendix). Additionally the high levels of mercury in invertebrates detected in baseline sampling in 1998-2000 do not seem to be re-occurring in 2007-2008. The possibility that mercury levels in aquatic invertebrates declined, rather than increased, after the fire needs further exploration. Also because temporal variation in mercury levels is natural, additional sampling planned for 2008-2009 will provide a more complete picture.

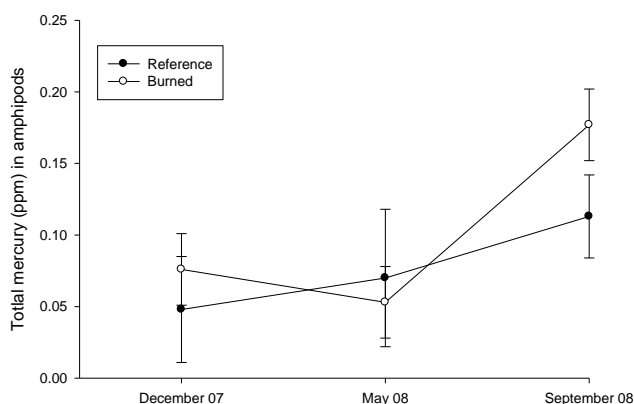


Figure 4. Preliminary data on post-fire total mercury levels in amphipods in areas that burned vs. residual areas that did not burn.

CONCLUSIONS AND RECOMMENDATIONS

Preliminary analyses do not indicate significant change in total mercury levels in any of the invertebrates sampled. The project has been extended to include May and September 2009 to enable analysis of a full two-year-long invertebrate data set. Additionally sampling in May and September 2009 will be extended to include mosquitofish (*Gambusia* spp.) to begin to assess possible mercury bioaccumulation problems in the fish community of the Okefenokee. Finally, analyses of the responses of overall invertebrate communities to the fire are also now part of the continuing project.

References Cited

- Beganyi SR, Batzer DP. 2009. The effects of fire on the community composition and mercury concentrations of aquatic macroinvertebrates in the Okefenokee Swamp, Southeast Georgia: Study design. Proceedings of the 2009 Georgia Water Resources Conference, April 27-29, 2009, University of Georgia, Athens. <www.gwrc2009.org>
- Bloom NS. 1992. On the chemical form of mercury in edible fish and marine invertebrate tissue. *Canadian Journal of Fisheries and Aquatic Sciences* 49:1010-1017.
- Fitzgerald WF, Engstrom DR, Mason RP, Nater EA. 1998. The case for atmospheric mercury contamination in remote areas. *Environmental Science & Technology* 32:1-7.
- Garcia E, Carignan R. 1999. Impacts of wildfire and clear-cutting in the boreal forest on methyl mercury in zooplankton. *Journal of Canadian Fisheries and Aquatic Sciences* 56:339-345.
- Garcia E, Carignan R. 2000. Mercury concentrations in northern pike (*Esox lucius*) from boreal lakes with logged, burned, or undisturbed catchments. *Journal of Canadian Fisheries and Aquatic Sciences* 57:129-135.
- Gariboldi CH, Jagoe AL, Bryan A. 1997. Dietary exposure to mercury in nestling wood storks. *Archives Environmental Contamination and Toxicology* 34:398-405.
- George BM, Batzer, DP. 2007. Spatial and temporal variations of mercury levels in Okefenokee invertebrates: Southeast Georgia. *Environmental Pollution*, in press.
- Hall BD, Rosenberg DM, Wiens AP. 1998. Methyl mercury in aquatic insects from an experimental reservoir. *Canadian Journal of Fish and Aquatic Sciences* 55:2036-2047.

- Heyes A, Moore TR, Rudd JWM. 1998. Mercury and methyl mercury in decomposing vegetation of a pristine and impounded wetland. *Journal of Environmental Quality* 27:591-599.
- Jagoie CH, Arnold-Hill B, Yanochko GM, Winger PV, Brisbin Jr. IL. 1998. Mercury in alligators (*Alligator mississippiensis*) in the southeastern United States. *The Science of the Total Environment* 213:255-262.
- Kannan K, Smith RG, Lee RF, Windom HL, Heitimuller PT. 1997. Distribution of total mercury and methyl mercury in water sediment, and fish from south Florida estuaries. *Archives of Environmental Contamination and Toxicology* 34:109-118.
- Keeler G, Glinsorn G, Pirrone N. 1995. Particulate mercury in the atmosphere: its significance, transport, transformation and sources. *Water Air Soil Pollution* 80:159-168.
- Khan B, Tansel B. 2000. Mercury bioconcentration factors in American alligators. *Ecotoxicology and Environmental Safety* 47:54-58.
- Kratzer, E., Batzer, DP. 2007. Spatial and temporal variation in aquatic macroinvertebrates in the Okefenokee Swamp, Georgia, USA. *Wetlands* 27:127-140.
- Lamontagne S, Carignan R, Praire YT, Pare D. 2000. Elemental export in runoff from eastern Canadian Boreal Shield drainage basins following forest harvesting and wildfires. *Canadian Journal of Fish and Aquatic Sciences* 57:118-128.
- Liu GL, Cai Y, Philippi T, Kalla P, Scheidt D, Richards J, Scinto L, Gaiser E, Appleby C. 2008. Mercury mass budget estimates and cycling seasonality in the Florida Everglades. *Environmental Science and Technology* 42:1954-1960.
- Mason RP, Reinfelder JR, Morel FM. 1994. Bioaccumulation of mercury and methyl mercury. *Water Air Soil Pollution* 80:915-921
- Mason RP, Laporte JM, Andres S. 2000. Factors controlling the bioaccumulation of mercury, methyl mercury, arsenic, selenium, and cadmium by freshwater invertebrates and fish. *Environmental Contamination and Toxicology* 38:283-297.
- Moore TR, Bubier JL, Heyes A, Flett RJ. 1995. Methyl and total mercury in boreal wetland plants, Experimental Lake Area, Northwestern Ontario. *Journal of Environmental Quality* 24:845-850.
- Morel FM, Kraepiel AM, Amyot M. 1998. The chemical cycle and bioaccumulation of mercury. *Annual Review Ecology and Systematics* 29:543-566.
- Niamo TJ, Wiener JG, Cope WG, Bloom NS. 2000. Bioavailability of sediment-associated mercury to *Hexagenia* mayflies in a contaminated floodplain river, *Canadian Journal of Fisheries and Aquatic Science* 57:1092-1102.
- Pickhardt PC, Stepanova M, Fisher NS. 2006. Contrasting uptake routes and tissue distributions of inorganic and methylmercury in mosquitofish (*Gambusia affinis*) and redear sunfish (*Lepomis microlophus*). *Environmental Toxicology and Chemistry* 25:2132-2142.
- Porter KG, Bergstedt A, Freeman MC. 1999. The Okefenokee Swamp: invertebrate communities and food webs. Pages 121-136; D.P Batzer, R.B Rader, & S.A Wissinger (Eds.). *Invertebrates in Freshwater Wetlands of North America; Ecology and Management*. John Wiley & Sons, Inc.
- Rader, R. B., D. P. Batzer, and S. A. Wissinger (eds.). 2001. *Biomonitoring and Management of North American Freshwater Wetlands*. John Wiley and Sons, New York.
- Rolfhus KR, Fitzgerald WF. 1995. Linkages between atmospheric mercury deposition and the methyl mercury content of marine fish. *Water Air Soil Pollution* 80:915:921.

- Rood BE, Gottgens JF, Delfino JJ, Earle CD, Crisman TL. 1995. Mercury accumulation trends in Florida Everglades and savannas marsh flooded soils. *Water Air Soil Pollution* 80:981-990.
- Rood BE. 1996. Wetland mercury research: a review with case studies. *Current Topics in Wetland Biogeochemistry* 2:73-108.
- Scheidt D. 2000. Ecologic and precursor success criteria for South Florida ecosystem restoration. Report to the Working Group of the South Florida Ecosystem Restoration Taskforce. Ch. 10.
- Sferra JC, Fuchsman PC, Wenning RJ, Barber TR. 1999. A site-specific evaluation of mercury toxicity in sediment. *Archives of Environmental Contamination and Toxicology* 37:488-495.
- St. Louis VL, Rudd JW, Kelly CA, Beaty KG, Flett RJ, Roulet NT. 1996. Production and loss of methylmercury and loss of total mercury from boreal forest catchments containing different types of wetlands. *Environmental Science and Technology* 30: 2719-2729.
- Snodgrass JW, Jagoe CH, Bryan AL, Brant HA, Burger J. 2000. Effects of trophic status and wetland morphology, hydroperiod, and water chemistry on mercury concentrations in fish. *Canadian Journal Fish and Aquatic Sciences* 57:171-180.
- Waldrop CV. 1999. Extraction of soil and/or biological tissue for determination of mercury by atomic absorption spectrophotometry. Technical Report CIET/SOP 401-67-01. Clemson University, Clemson, SC.
- Wong AH, McQueen DJ, Williams DD, Demers E. 1997. Transfer of mercury from benthic invertebrates to fishes in lakes with contrasting fish community structures. *Canadian Journal of Fisheries and Aquatic Sciences* 54:1320-1330.

APPENDIX. Total mercury (Hg) levels (ppm) in individual sample pools of invertebrates (amphipods, odonates, crayfish) collected from in burned and non-burned reference habitats (12/2007 to 12/2008).

	Burned Hg (ppm)			Reference Hg (ppm)		
	Amphipods	Odonates	Crayfish	Amphipods	Odonates	Crayfish
Prairie	0.555	0.012	0.018	0.045	0.011	0.032
	0.141	0.012	0.015	0.065	0.038	0.041
	0.149	0.021		0.065	0.035	0.020
	0.017			0.000	0.016	
	0.046			0.018		
	0.032			0.023		
	0.000					
	0.000					
	0.027					
Shrub	0.101	0.024	0.028	0.077	0.022	0.018
	0.194	0.024	0.009	0.108	0.030	0.022
	0.102	0.021	0.035	0.088	0.027	0.021
	0.028	0.014	0.008	0.019	0.033	0.013
	0.068	0.017	0.011	0.077	0.012	0.000
	0.058	0.021	0.015	0.044	0.028	0.034
	0.062	0.003	0.010	0.057		
	0.058	0.026	0.014	0.035		

	0.000	0.046				
	0.036	0.012				
	0.025	0.019				
	0.029	0.019				
		0.014				
		0.022				
Cypress	0.186	0.028	0.029	0.103	0.053	0.046
	0.097	0.030	0.018	0.283	0.109	0.080
	0.073	0.018	0.014	0.138	0.035	0.061
	0.104	0.040	0.032	0.036	0.023	0.016
	0.245	0.020		0.045	0.042	0.028
	0.068	0.015		0.166	0.034	0.041
	0.050	0.010		0.034	0.021	0.031
	0.167	0.018		0.052	0.032	
	0.132	0.015			0.031	
	0.172	0.000			0.047	
	0.076	0.031				
	0.181	0.022				
	0.027	0.031				
	0.025					
	0.103					
	0.023					
	0.062					
	0.028					
	0.055					
Average	0.090	0.020	0.018	0.072	0.034	0.032
SD	(0.097)	(0.010)	(0.009)	(0.062)	(0.021)	(0.020)

Modeling Water Quality Changes in Aquifer Storage Recovery Systems

Basic Information

Title:	Modeling Water Quality Changes in Aquifer Storage Recovery Systems
Project Number:	2008GA176B
Start Date:	3/1/2008
End Date:	2/28/2009
Funding Source:	104B
Congressional District:	10
Research Category:	Ground-water Flow and Transport
Focus Category:	Hydrogeochemistry, Water Supply, Models
Descriptors:	
Principal Investigators:	

Publication

Title: Modeling Water Quality Changes in Aquifer Storage Recovery Systems

Principal Investigator: Chittaranjan Ray

Start Date 3/1/2008

End Date 2/28/2009

Table of Contents

Executive Summary 2

List of Tables 2

List of Figures 2

Project Scope and Research Objectives 3

Research Objectives 5

Review of Past Relevant Work 5

Methods, Procedures and Facilities Used 6

Results/Findings 12

Conclusions and Future Research Recommendations 16

References 16

Disclaimer

The contents of this report are those of the authors and do not necessarily reflect the views of the Georgia Water Resources Institute, the United States Geological Survey, or the State of Georgia.

Executive Summary

A novel combination of riverbank filtration and aquifer storage recovery was investigated to elucidate possible changes in water quality. Aquifer storage and recovery (ASR) options are being sought out to address temporal water shortage problems in the Albany region of Georgia. Riverbank filtration (RBF) is sought to be used as source water to inject water into the deeper aquifer during times of excess flows in the Flint River and extract it during the drier seasons (ASR). RBF taps the Flint River through the Upper Floridan Aquifer and the available data shows that it can produce water that can be injected into the deeper Clayton Aquifer, saving on conventional water treatment costs. This study tests the conceptual framework of having such RBF and ASR schemes coupled together and, more importantly, looks at the geochemical changes that are likely to occur during its commission. It is concluded that in-situ geohydrological and chemical conditions will affect the actual outcome of the quality of water.

List of Tables

Table 1: Aqueous components as model inputs from charge balanced data set

Table 2: Pumping Schedule

Table 3: Aqueous components of extracted water

List of Figures

Fig 1: Possible location of the ASR site east/north-east of Albany.

Fig 2: Aquifers in the Albany area (source: <http://ga.water.usgs.gov/projects/albany/stratcol.html>)

Fig 3: Two dimensional model depicting riverbank filtration.

Fig 4: Rectangular grid model with a finer mesh of cells near the injection/extraction well at right and observation wells at 50 feet and 400 feet from the well.

Fig 5: Hydraulic head exerted on the well head. (-150 ft bgs is the ambient condition)

Fig 6: Concentration time series data at the RBF pumping well.

Fig 7: Concentration time series plot at the ASR well.

Fig 8: Successive fronts of Ca^{2+} ions showing dissolution of the Calcite Aquifer.

Project Scope and Research Objectives

The Georgia State Water Plan (EPD, 2008) outlines surface water storage, interbasin transfer, and aquifer storage and recovery (ASR) as three main water supply management practices. ASR is a process in which water is recharged into an aquifer using wells, trenches, or other surface methods. Later, the stored water is withdrawn (and may or may not be additionally treated) for supply. In the Southeast, the well method is most common. ASR implementation in Georgia is currently prohibited in areas underlain by the Floridan Aquifer within counties governed by the Georgia Coastal Zone Management Program. As cited in the State Water Plan, the Environmental Protection Division (EPD) has been charged to develop protocols for assessing the viability of ASR. Protocols could include identifying the aquifers and sources of recharge water which can be potential candidates for ASR, comparing the potential costs of ASR to other water resource management options (as stated above), and studying the legal issues related to ASR. Protocols may include environmental assessments to i) study the hydrogeologic and hydrochemical properties of target aquifers for understanding the flow path dynamics and the chemical changes occurring during injection, storage, and extraction of the recharge water, ii) conduct bench-scale studies and chemical equilibrium modeling to understand hydro-geochemistry changes during ASR operation, iii) conduct pilot-scale studies of ASR wells(s) in permitted areas to collect basic information for the design and operation of full-scale systems, and iv) make quantitative analysis of the environmental effects of ASR in target aquifer and possibly conducting computer modeling to evaluate such effects, especially in complex aquifer settings.

It is a well-known fact that geochemical reactions in the subsurface affect the quality of the stored water. Some of these reactions are beneficial while others can have adverse effects. In terms of benefits, ASR has the potential to remove pathogens, disinfection byproducts (from chlorinated water), dissolved organic carbon (DOC), and pharmaceutical residues (Water Science and Technology Board report; NRC, 2007). The NRC report also points to case studies where trihalomethanes have been formed by injecting chlorinated drinking water to aquifers that have some amount of DOC. Recently, arsenic (As) dissolution from the Floridan aquifer (Arthur et al., 2002) has caught the attention and resulted in a temporary ban on the operation of several ASR systems in Florida. At the Punta Gorda ASR site in Florida, these authors showed that arsenic concentrations significantly increased during the recovery periods (and it exceeds the current As standard). Similar mobilization of arsenic has also been observed at the Peace River ASR site in Florida. The limestone matrix in the Floridan Aquifer contains small amounts of As (often adsorbed to iron (hydro)oxide surfaces) along with a few other trace metals. Under normal conditions, this As is in equilibrium with the native ground water. However, during ASR operation, especially when the system experiences iron-reducing conditions and the iron oxides dissolve, sorbed As is released (Smedley and Kinniburgh, 2002). With the recent lowering of As standard to 10 µg/L (from 50 µg/L), about 13 ASR systems in Florida are in violation of the drinking water standard (NRC, 2007).

Despite earlier qualitative concerns of ASR from the point of view of hydrodynamics and water quality, Georgia state legislature may allow the development of ASR in limited settings. Conducting comprehensive studies will take several years of planning and execution. Without the benefit of data from pilot or full-scale systems, it will be prudent to conduct limited modeling exercises to evaluate the effect of ASR systems on ground water quality.

ASR is considered as a useful water management option in areas of water scarcity or where the seasonal demands fluctuate widely. ASR systems are expanding in a rapid pace worldwide. In some areas, they may be the only option to reuse water for water supply. The knowledge base is limited to only certain parts of the World (Australia, Europe, and some areas of the United States). The United States is a relatively young player in this effort; however, a number of ASR systems are expected to come on line within this decade. Before widespread implementation of ASR in the United States, modeling studies will be useful to elucidate the impact of the quality of the dissolved constituents (e.g., oxygen, organic carbon, dissolved ions) of the injected water on the redox, precipitation, dissolution, sorption, ion exchange, and complex formation reactions. Additionally, the rate of microbially-mediated reactions, the impact of seasonal temperature variation on reactions, and impact of seasonal variations in DOC and dissolved oxygen (DO) of the injected waters can be examined through sophisticated models that have been developed in recent years. Such information will not only be useful to consultants and ASR system designers, but will be able to answer many “what if?” questions of regulators.

The search for alternative sources of water will receive increased attention from the legislative and regulatory community in Georgia during the next several years. In the past statutes did not allow the use of ASR in Georgia. However, recent drought conditions provide a reason to consider ASR as one of the alternatives for drinking water supply to the growing population of Georgia.

As the State Water Plan is implemented in Georgia, ASR is likely to be tested out at least on a limited scale as a potential alternative water supply management option. If not in coastal counties, ASR wells might be installed in interior areas of the state for storing excess water during periods of low demand. Greatest potential exist for areas in southwest Georgia where water from rivers can be taken out during high flows, treated naturally through natural filtration systems (e.g., riverbank filtration systems, e.g., RBF) or through standard water treatment operations and injected into deeper drinking water supply aquifers for later use. The recent findings from the NRC (2007) has delineated the challenges of managed aquifer recharge (MAR) operations (here ASR is considered as a MAR) in terms of site hydrogeology, water quality, legal, economic, and operation issues. One of the conclusions of this study is the modeling of ground water at regional and high-resolution local scales can be a cost-effective tool for the planning, design, and operation of MAR systems. It suggests additional studies be conducted to understand geochemical processes and potential removal processes of microbial pathogens and emerging chemicals (such as pharmaceuticals and personal care products). The report also concludes that research should focus on monitoring relevant parameters during the operational cycles of the MAR systems.

Unlike Australia, California, or Arizona, the injection water in Georgia and other Southeastern states is expected to experience extreme temperature variations between the winter and summer seasons. Also, the DOC of the injected water and the DO content will vary with season. So far, limited literature exists on the evaluation of the impact of these variations on water quality. A modeling study of this nature, combining RBF and ASR will be able to answer some of these questions.

Research Objectives

The objectives of this research were to:

- (a) Examine areas of Georgia where ASR can be practiced outside areas of Georgia Coastal Zone Management Program,
- (b) Develop a conceptual model of RBF and ASR for storing excess water during periods of high flows in the river, and
- (c) Simulate water quality changes during extraction from the river using RBF and storage in the aquifer.

Review of Past Relevant Work

ASR is increasingly becoming a popular technique to augment drinking water supplies as well as to enhance the recharge of aquifers with reclaimed water (Pyne, 2005). There are more than 300 ASR systems operating (NRC, 2007). The quality of the injected water undergoes a complex set of physico-chemical and biological reactions (Greskowiak et al., 2005). These processes not only alter the quality of the water during storage and recovery, they may alter the hydraulic properties (permeability and porosity) of the aquifer due to mineral precipitation/dissolution (Meyer, 1999) and/or by biological clogging (Rinck-Pfeiffer et al., 2000). Injecting oxygen-rich potable water and nutrient-rich reclaimed water into an anaerobic aquifer lead to a variety of water quality changes (Greskowiak et al., 2005; Vanderzalm et al., 2006). This process leads to the production or consumption of protons and other reactants which in turn triggers the precipitation and dissolution of minerals, ion exchange, and surface complexation reactions (Eckert and Appelo, 2002).

In field settings, quality changes during the injection of high quality water have been observed by several authors (Mirecki et al., 1998; Stuyfzand, 1998). However, only a limited number of studies report water quality changes during the injection of reclaimed water. Australia and some western states such as California and Arizona employ ASR systems that use exclusively recycled waters. Greskowiak et al. (2005) simulated carbon cycling and biogeochemical changes during the operation of an ASR system at Bolivar, South Australia. They found through modeling that during the storage phase, dynamic changes in bacterial population can affect the local geochemistry around the injection/extraction wells. Farther away from the injection wells, breakthrough of cations was strongly affected by exchange reactions. Calcite dissolution affected calcium concentration.

Seasonal variations in redox reactions have not been extensively studied in the context of ASR. Temperature-dependent pyrite oxidation in a deep (1000 ft) anaerobic aquifer in the Netherlands was simulated by (Prommer and Stuyfzand (2005). They found that pyrite oxidation around the injection well was dependent on the temperature of the injectant, which in-turn controlled other reactions. Greskowiak et al. (2006) examined the variability in the degradation of pharmaceutical phenazone (present in the wastewater of Berlin, Germany) as a function of season. They found that the degradation was redox sensitive and breakthrough of phenazone in monitoring wells occurred in warmer summer months when anaerobic conditions developed.

Methods, Procedures and Facilities Used

The study was carried out by collating information, analyzing the available data and literature from various sources, building a conceptual model and carrying out numerical modeling with parameters and scenarios using standard methods, procedures and computers.

For this study, we examined various areas of Georgia for ASR feasibility. The coastal zones were excluded as the current regulations do not allow for ASR systems in the immediate future (until the prohibition for ASR expires). Areas north of the “fall line” that runs northeast from Columbus, GA to Augusta, GA were eliminated because of geological constraints. Most recently, the Flint and Chattahoochee basins experienced drought conditions that reduced stream flows significantly. Because there exists a good hydraulic connection between the surface water in the rivers of these basins and the groundwater, the Georgia EPD asked the farmers to stop withdrawing groundwater for irrigation in return for a cash rebate (Wilson, 2007).

Cities that are located in the area also face limitations of growth because of restrictions of additional pumpage from surface or ground water sources. One possible solution was to consider withdrawing water from the Flint or the Chattahoochee rivers during periods of high flows (above some base flow condition) and then treating this water and storing in a deeper aquifer for future use. The needed treatment before injection could be regular treatment of surface water in a conventional water treatment plant, natural filtration such as river bank filtration without additional treatment, or a combination of both. Such a mechanisms would allow the cities to capture excess runoff at a period of no or minimal restrictions and storing that water in deep aquifers for later use.

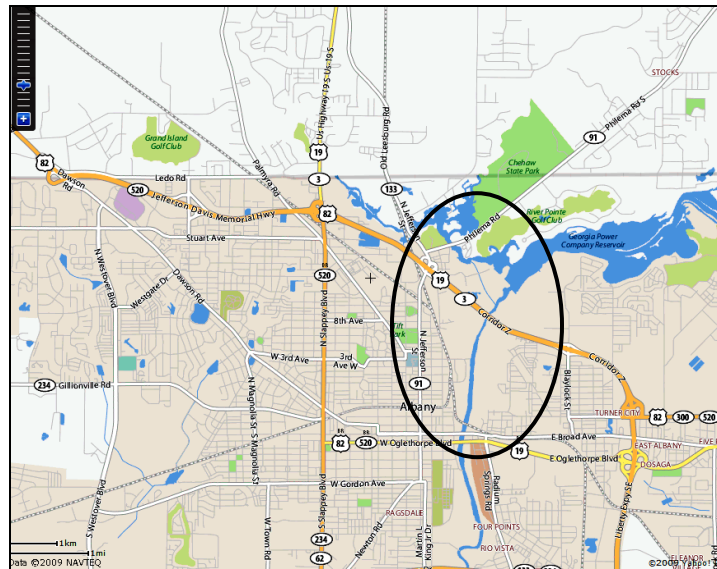


Fig 1: Possible location of the ASR site east/north-east of Albany.

For this study, we selected an area in vicinity of the City of Albany, GA, where the Water Planning and Policy Center (h2opolicycenter.org) had developed a feasibility assessment of an ASR (conceptual stage) of such an extraction and injection scenario for the future expansion of the local industries or for inviting new industries to the area (Water Resource Solutions, 2006). The paper suggests extracting enough water from the Flint River and treating it and storing in a deeper aquifer so that an industry could pump at a sustained rate of 10 million gallons per day (MGD). Water for injection could be obtained by directly pumping surface water or obtaining it from riverbank filtration (RBF) schemes, and the latter has been recommended as the more attractive one. It was expected that the RBF scheme would be cheaper with reduced initial and O&M costs and not be susceptible to heavy metals leaching during sub-surface storage.

The area lies on the Floridan Aquifer system, having multiple aquifers and confining layers and the geohydrology is well documented (Hicks et al., 1981). A generalized stratigraphy and the water-bearing properties of formations underlying the study area are shown in Figure 2. Our aquifers of concern are:

- i) Upper Floridan Aquifer or the Ocala Limestone, and
- ii) Clayton Aquifer of the Midway Group.

The first aquifer will be harvested when the surface waters exceed the demand and this extracted water will be used to recharge the second aquifer. This in turn can be used to augment water supply during dry summer months. An area to the east/north-east of the City of Albany appears suitable for a RBF and ASR scheme as suggested by the feasibility study (Water Resource Solutions, 2006).

For the simplified purpose of this study, water is drawn from the river/aquifer for the six months of October to March and recharged into the deeper aquifer and withdrawn from this storage for the remaining six months of April to September when the water demand is higher. The water from storage could be directly used for municipal or agricultural uses, or released into the river which could augment the environmental flows and recharge the depleting aquifer. Study of the available materials and maps indicate that suitable areas for the project would be located adjacent to the river, north east of the City of Albany. A linear parcel along the river would facilitate placing about 10 RBF wells, each of about 1 MGD capacity, at a spacing of 200 ft. This could draw water from Upper Floridan Aquifer (also called the Ocala aquifer) which is hydraulically connected to the Flint River (see Fig 2).

A 3-D numerical model using MODFLOW (Harbaugh et al., 2000) was set up to explore the flow condition in the aquifers and this information was used to prepare computationally more efficient 2-D models. Separate models were set up for obtaining water from the river (named the RBF model) and for the subsequent storage and retrieval of the pumped water (named ASR). Geochemical transport of the different species in the model with multi-component reactions was carried out by using the PHT3D code (Prommer et al., 2003) which couples the transport simulator MT3DMS (Zheng and Wang, 1999) with the geochemical model PHREEQC-2 (Parkhurst and Appelo, 1999).

ERA	SYSTEM	SERIES	GROUP, FORMATION, AND MEMBER		AQUIFER OR CONFINING UNIT		
			Northwest	Southeast			
Cenozoic	Quaternary	Holocene	Undifferentiated overburden	Undifferentiated overburden	Surficial aquifer/upper semi-confining unit		
		Pliocene	Miocene	Oligocene		Undifferentiated sediments	
						Suwannee Limestone	
	Tertiary	Upper Eocene	Ocala Limestone	Ocala Limestone	Upper Floridan aquifer		
			Clinchfield Sand				
			Lisbon Formation	Lisbon Formation			
		Middle Eocene	Clalborne Group		Lisbon confining zone		
			Tallahatta Formation				
		Paleocene	Wilcox Group	Tusahoma Formation	Wilcox confining unit		
				Baker Hill Formation			
			Porters Creek Clay				
			Midway Group	Clayton Formation		Clayton aquifer	
				Clayton-Providance confining zone			
	Mesozoic	Upper Cretaceous	Providence Sand (upper unnamed sand member)		Providence aquifer		
			Providence Sand (Perote member)		Providence-Ripley confining zone		
			Ripley Formation		Cusseta aquifer		
			Cusseta Sand				
			Blufftown Formation		Blufftown aquifer		
Eutaw and Tuscaloosa Formations (undivided)							

¹ Gibson, 1982
² Ripy and others, 1981

EXPLANATION

 Sediments comprising the Upper Floridan aquifer
 Missing rocks

Figure 2: Aquifers in the Albany area (source: <http://ga.water.usgs.gov/projects/albany/stratcol.html>)

The RBF model was setup with a dimension of 520 feet length, 1 feet width, and 160 feet deep including the confining layer at the bottom as shown in Figure 3. The vertical discretization, with 14 layers, is refined at the river portion so that the river hydrograph could be captured and the cells would not go dry at any time during the simulation.

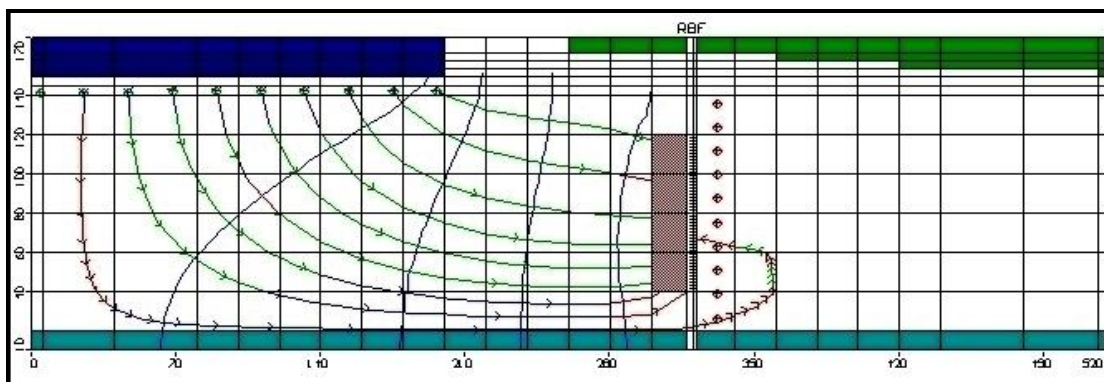


Fig 3: Two dimensional model depicting riverbank filtration.

The pumping well was located 120 feet away from the river bank. The river stage data and the aquifer data were obtained/deduced from USGS sites for surface water and groundwater data. The model is subjected to a time variant hydraulic boundary (constant head) of the river and a general head boundary corresponding to regional piezometric heights of the aquifer at about 5000 ft from the site at both the ends. The pumped well is subjected to a withdrawal of 5000 GPD (per unit width of aquifer corresponding to 1 MGD over a 200 feet distance) for six months, starting October till March, and then is turned off for the rest of the year. All simulations are run with a 50 day spin up period so as to remove any bias from arbitrarily chosen starting conditions.

The river water quality and stage data is obtained for the station ID 02352560 (Flint River at Albany) from the USGS surface water data inventory. The groundwater quality data of the nearest well in the Upper Floridan Aquifer was obtained for the well ID 12K129 and that for the lower aquifer, the Clayton aquifer, was obtained from well ID 12L020. Water quality and hydrology data of the other adjacent wells (12M002, 13L002) were also looked into to determine the regional flow, if any, or the required aquifer chemistry. It was essential that the water quality data used as inputs in to a numerical model be charge balanced, it was done so using the PHREEQC-2 code (Parkhurst and Apello, 1999). The charge balanced water quality parameters used in defining the model are shown in Table 1.

Note that the streamline escaping to the right of the RBF well in Figure 2 is very slow-moving; each arrow interval is 5 days. Almost all of the water pumped out from the well is bank filtrate from the river.

Table 1: Aqueous components as model inputs from charge balanced data set.

Aqueous Component	Flint River (mol/L)	Upper Floridan Aquifer (mol/L)	Lower Floridan Aquifer (mol/L)
Orgc	0.00035	0	0
Tmp	9.8-30.6	20.4	0.023
O(0)	4.4e-4 to 6.9e-4	5.44E-04	0
Ca	5.24E-04	9.68E-04	2.99E-04
Mg	5.76E-05	2.17E-05	2.47E-04
Na	2.94E-04	9.18E-05	1.44E-03
K	4.60E-05	8.19E-06	7.16E-05
Fe(3)	1.38E-06	5.37E-08	3.22E-06
Mn(3)	7.81E-07	1.82E-08	9.10E-08
Si	1.09E-04	1.33E-04	3.33E-04
Cl	7.48E-04	1.44E-04	1.23E-03
C(4)	5.98E-04	1.76E-03	1.34E-03
S(6)	9.68E-05	1.87E-06	1.35E-04
N(5)	2.71E-05	2.04E-04	2.86E-06
N(3)	2.14E-07	7.14E-08	0
Amm	1.61E-06	0	0
pH	7.3	7.9	7.2

Units: mol/l except Temp ($^{\circ}\text{C}$) and pH is dimensionless.

Site-specific time series data essential for a detailed and accurate analysis were not available and only a few parameters such as river stage, temperature and dissolved oxygen in the river water were found to be recorded sporadically. So, single point data were used to emulate time series data and other reasonable approximations were made where site-specific data were not available.

The ASR wells are assumed to be laid at 350 ft spacing, compared to the RBF wells at 200 feet spacing, in view of the target aquifer and, more importantly, the flow reversals taking place. So the pumping rates for the deep aquifer model will be lower. Furthermore the model is set up to simulate one-half of the symmetrical area, the pumping rate is halved to a total of 1450 GPD per foot width of the aquifer as shown in Table 2.

Table 2 Pumping Schedule

Start time (days)	End time (days)	RBF well (GPD)	ASR well (GPD)	remarks
0	50	-5000	1450	Start up period
50	230	-5000	1450	to storage
230	410	0	-1450	to supply
410	590	-5000	1450	to storage
590	770	0	-1450	to supply

The deeper aquifer storage and recovering part includes the injection/extraction well into the Clayton aquifer located at 625 feet to 750 feet below the ground surface. The hydraulic conductivity is estimated to be about 66 ft/day from aquifer transmissivity figures. A 2-D vertical model, with one half of the symmetrical area, is set up with the well at one end and a general head boundary with specified ambient concentrations at 900 ft from it (see Fig. 4). The left boundary cells are set as point sources for injecting and extracting water, i.e. a well with reversible pumps. The length of the model domain is selected in an iterative manner so that the right boundary chemistry remained unchanged. The vertical grids are finer near the well and placed farther apart towards the right boundary as more rapid reactions are assumed to take place in vicinity of the wells.

The cells on the right boundary are general head boundaries and the left is a well with point source. The source water obtained from the RBF, in the previous model is injected into this well. Two observation wells are placed at 50 feet and 400 feet from the well. The initial head is set at -150 feet, i.e. 150 feet below the ground surface. The pressure head variation with time for the ASR model is given in Figure 5.

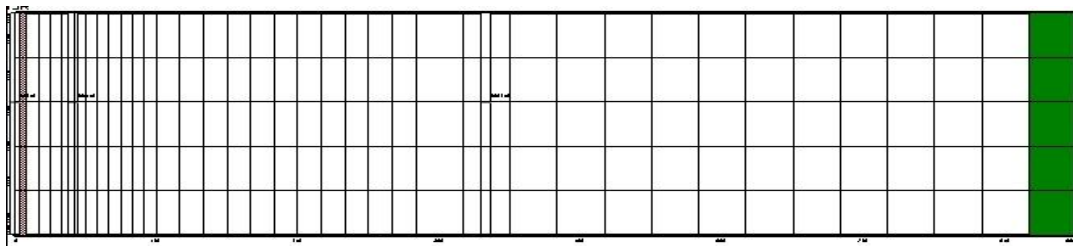


Fig 4: Rectangular grid model with a finer mesh of cells near the injection/extraction well at right and observation wells at 50 feet and 400 feet from the well.

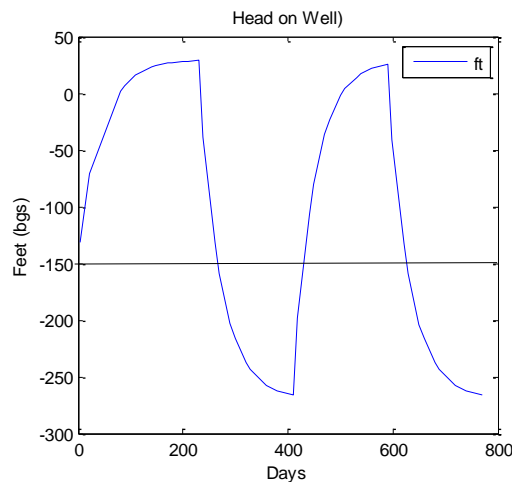


Fig 5: Hydraulic head exerted on the well head. (-150 ft bgs is the ambient condition)

Both the upper and the lower aquifers are limestone aquifers, so the model was first set up to run equilibrium and dissolution reaction with oxidation of the organic carbon and other species using

the transport engine PHT3D v 1.46 with sorption described by linear isotherm and the reaction module defined by the PHREEQC-2 database (Parkhurst and Appelo, 1999).

Results/Findings

The simulation results for investigation into organic carbon redox reactions, calcite dissolution and the general equilibrium reactions show that the organic carbon degradation is the first and predominant reaction that takes place. The modeling process was ensured that some organic carbon is present as “not-so-easily” degradable organic carbon. Some organic carbon is always said to remain as a less degradable carbon (Greskowiak et al., 2005). The simulation plots are shown in Figure 6.

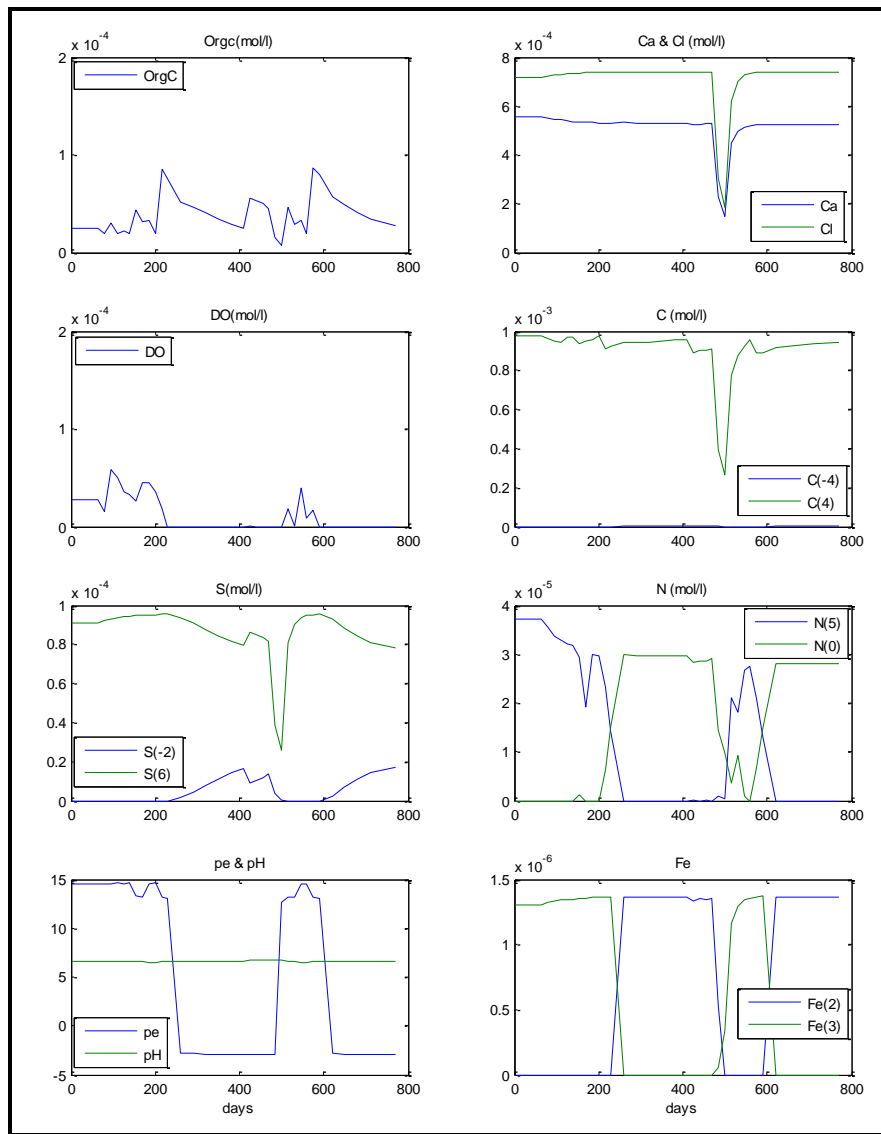


Fig 6: Concentration time series data at the RBF pumping well. The pump is turned off during the periods 230 – 410 and 590 – 770 days.

The denitrification process starts, around time period 200 days after pumping – N(5) to N(0). This is again followed in tandem by Iron reduction in presence of low pe and Fe(3) at around 210 days. During the period when there is no pumping, the redox potential (pE) reverses itself to lower values indicating increased electron activities that promote reductive mechanisms on oxidized species.

A closer look at the Sulphate and S(-2) behavior after the pumping stopped shows that the sulphate reduction occurs giving off sulphide and bicarbonates. This process ceases once the pump is turned on, at 410 days, the conversion of S(6) to S(-2) stops, but S(6) decreases dramatically. It is seen that cations also reduce dramatically. This indicates that formation of some negatively charged complexes (including sulphates, carbonates) that attract the positively charged metal ions and precipitate them out. This can also explain the reduced inorganic carbon around that time (500 days) when Ca-carbonates or CaMn-carbonates can precipitate out.

The pumped filtrate water is then again pumped into the deeper aquifer in the aquifer storage and recovery (ASR) part. The concentration in the observation wells in the injecting/extracting well is shown in Fig 7.

It is seen that the organic carbon is persistent and anoxic conditions develop most of the time. The water extraction period is from 230-410 and 590-770 days. The species concentrations of the water produced is shown in Table 3.

Table 3: Aqueous components of extracted water

Aqueous Component	ASR extraction water (mol/L)
Temp	14.05 to 12.2
Ca	3.77E-04 to 4.94E-04
Mg	4.97E-04 to 6.48 E-04
Na	2.54E-04 to 3.4E-04
K	3.71E-04 to 4.46E-04
Fe(3)	0 to 1.97E-07
Mn(3)	4.33 E-7 to 6.82E-7
Si	9.31E-05
Cl	6.01E-04
C(4)	7.64E-04 to 9.3E-04
N(5)	0-1.32E-05
pH	6.6
pe	-3.03 to 11.71

Units: mol/l except Temp (^oC) and pH is dimensionless.

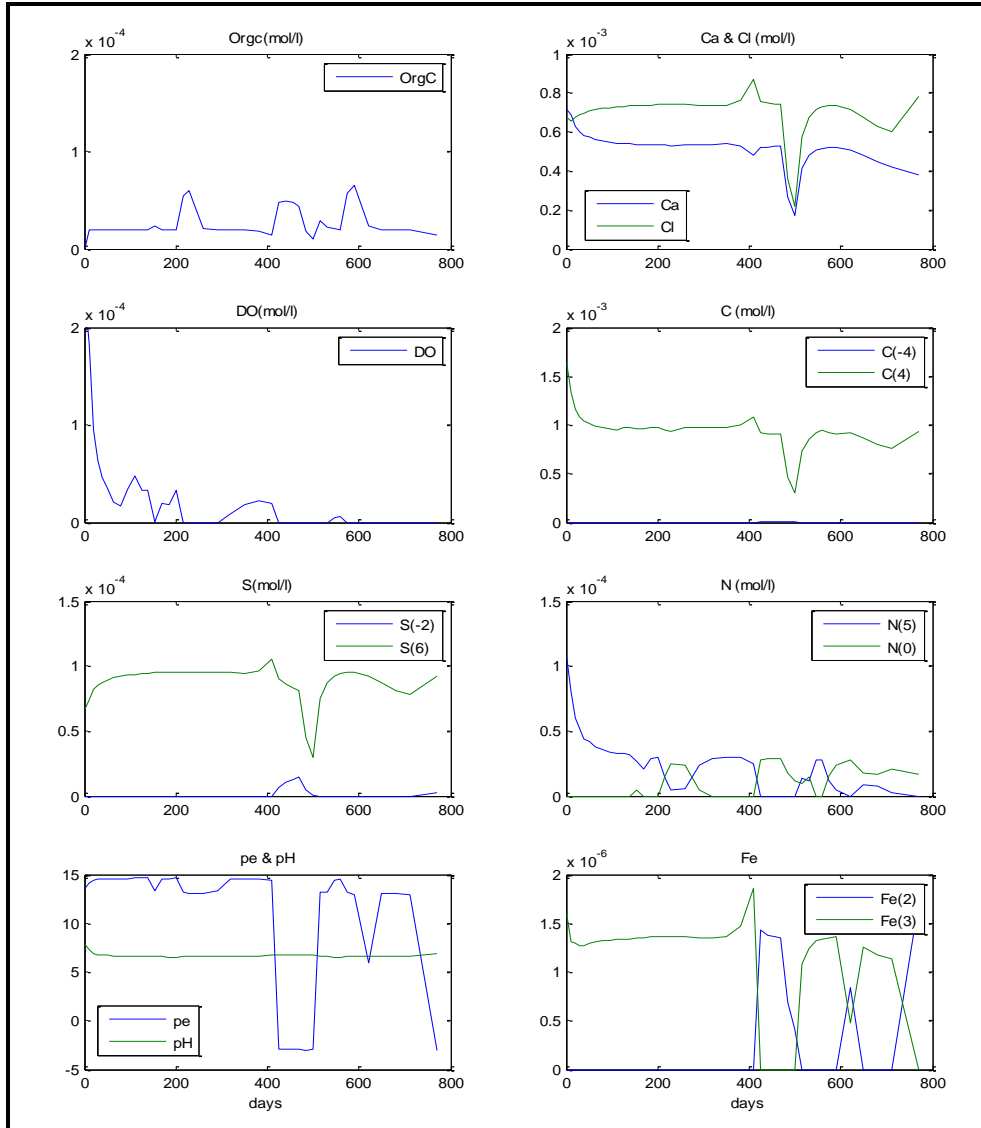
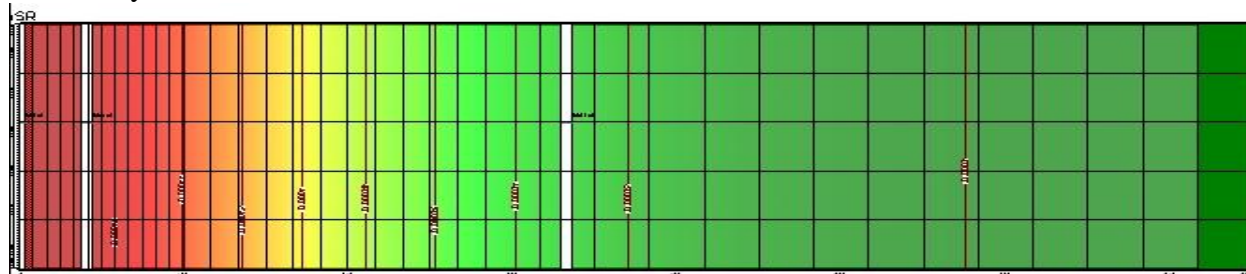


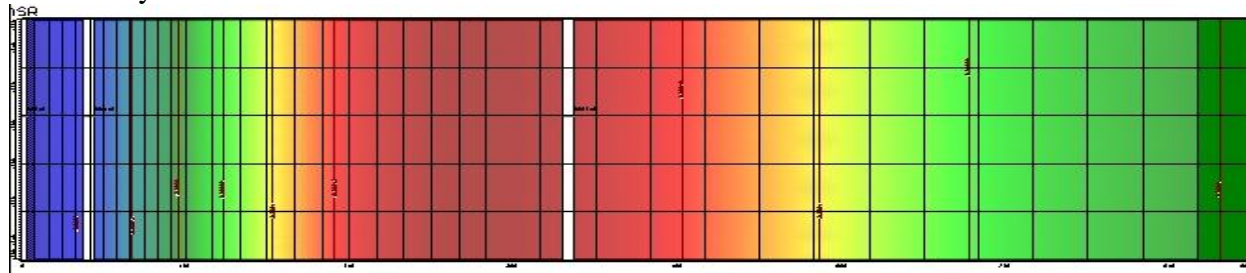
Fig 7: Concentration time series plot at the ASR well. The pump is extracting during the periods 230 – 410 and 590 – 770 days and injecting in other times.

One important aspect in limestone aquifers is the possibility of the calcite dissolution with repeated flow reversals and further aided by dissolution facilitating environments such as suitable pH. The dissolution of calcite is estimated to occur at the vicinity of the reversible wells as seen in the following three figures at different times.

t= 410 days



t = 500 days



t= 530 days

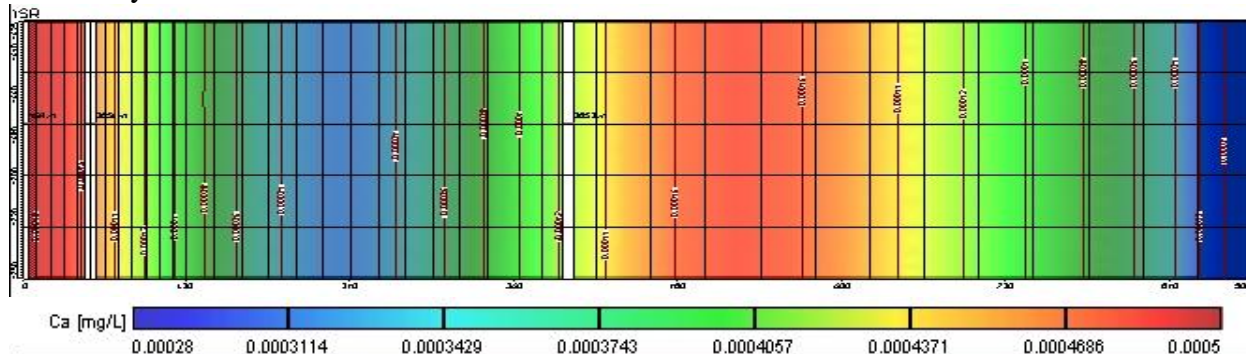


Fig 8: Successive fronts of Ca²⁺ ions showing dissolution of the Calcite Aquifer.

The above movement of Ca²⁺ is occurring during the injection of water into the aquifer. So the calcite dissolution takes away the calcium ion further away from the pump well. It is understood that this mechanism can help offset the well clogging phenomenon that can occur due to precipitates near the well or deposition of other organic complexes. It should be noted that microbial activities also take place in complex mechanism and this has not been considered here, which needs to be considered thoroughly in a detailed study when site specific data are available.

Another set of runs were made with a different set of assumptions on the geochemistry of the aquifer. It was assumed that the aquifer mass contained some pyrites (kinetic version) that could leach arsenic containing compounds into the aquifer when pyrite is subjected to oxidation. The ratio of arsenopyrite, the compound containing arsenic to the pyrite mass was assumed to be 1 in 1000, so that one mole of pyrite will be accompanied by dissolution of 1 mmole of arsenopyrite. The results of the geochemical modeling done in a manner similar to the deep well injection

experiment of Prommer and Stuyfzand (2005) show that the As (3) and As (5) are present in the low range of 4E-09 and 1.2E-13 mol/L.

This low concentration of Arsenic is because the Arsenite (As(3)) and As(5) adsorb strongly to iron oxides, clays and silicates or onto iron (hydro)oxides or sulfides in a narrow pH band around 7. If these conditions are prevalent then leaching of As will probably not take place. Because the Arsenic leaching is such a complex issue that is easily perturbed by other stressors, it is very important that a detailed hydro-geochemical data of the concerned site is available before any estimates can be made with confidence.

Conclusions and Future Research Recommendations

The study shows that a coupled RBF and ASR scheme is possible and would help alleviate the water scarcity problems in the drier seasons. It is seen that the complex set of different mechanisms and reactions can be modeled to determine the quality of water pumped out. It was determined this would be viable option to store and pump water. The particular questions of leaching of Arsenic and other heavy trace elements can be accurately modeled if it is backed by accurate in-situ geochemical data. Transport and fate of arsenic is an immediate concern for the field of RBF and ASR schemes. A better elucidation backed by benchmark studies is essential to restore confidence in these schemes.

The extent of dissolution and clogging of the aquifer, specially in the vicinity of the aquifers need to be looked at more carefully to estimate the ease of injection and efficiency of aquifer recovery.

The modeling did not look at the aspects of transport and fate of microorganisms and other chemicals of concern such as disinfection by-products (DBPs) and pharmaceuticals and personal care products which are pressing issues that need to be looked at in the immediate future.

References

Arthur, J.D., Dabous, A.A. and Cowart, J.B., 2002. Mobilization of arsenic and other trace elements during aquifer storage and recovery, southwest Florida, US Geological Survey Artificial Recharge Workshop Proceedings, Sacramento, CA, pp. 2-4.

Eckert, P. and Appelo, C.A.J., 2002. Hydrogeochemical modeling of enhanced benzene, toluene, ethylbenzene, xylene (BTEX) remediation with nitrate. *Water Resources Research*, 38(8): 1130.

EPD, 2007. Georgia's Water Resources: A Blueprint for the Future, Environmental Protection Division of Georgia, Atlanta, GA.

EPD, 2008. Georgia Comprehensive State-wide Water Management Plan, Georgia Water Council, GA.

Greskowiak, J., Prommer, H., Massman, G. and Nutzmann, G., 2006. Modeling seasonal redox and dynamics and the corresponding fate of the pharmaceutical residue phenazone during artificial recharge of groundwater. *Environ. Sci. Technol.*, 40(21): 6615-6621.

Greskowiak, J., Prommer, H., Vanderzalm, J., Pavelic, P. and Dillon, P., 2005. Modeling of carbon cycling and biogeochemical changes during injection and recovery of reclaimed water at Bolivar, South Australia. *Water Resources Research*, 41(10): -.

Harbaugh, A.W., Banta, E.R., Hill, M.C. and McDonald, M.G., 2000. MODFLOW-2000, the U.S. Geological Survey modular ground-water model -- User guide to modularization concepts and the Ground-Water Flow Process, US Geological Survey.

Hicks, D. W., Krause, R. E., and Clarke, J. S., 1981. Geohydrology of the Albany Area, Georgia. Prepared in cooperation with the U.S. Geological Survey and the Albany Water, Gas, and Light Commission, Georgia Geologic Survey, Environmental Protection Division, Department of Natural Resources, Atlanta, GA.

Meyer, K.U., 1999. A numerical model for multicomponent reactive transport in variable saturated porous media, University of Waterloo, Waterloo, Canada.

Mirecki, J.E., Campbell, B.G., Conlon, K.J. and Petkewich, M.D., 1998. Solute changes during aquifer storage and recovery testing in a limestone/clastic aquifer. *Ground Water*, 36(3): 394-403.

NRC, W.S.T.B., 2007. Prospects of Managed Underground Storage of Recoverable Water. The National Academies Press, Washington, D.C., 256 pp.

Parkhurst, D.L. and Appelo, C.A.J., 1999. User's guide to PHREEQC (version 2)-A computer program for speciation, batch-reaction, one-dimensional transport, and inverse geochemical calculations. US Geol. Survey, Water-Resour. Inv. Rep. 99-4259, 312 p. {websites: <http://www.geo.vu.nl/users/posv/phreeqc.html> or http://wwwbrr.cr.usgs.gov/projects/GWC_coupled/phreeqc/index.html}

Pyne, D., 2005. Aquifer storage recovery: A guide to groundwater recharge through wells. ASR Systems, Gainesville, FL.

Prommer, H., Barry, D.A. and Zheng, C., 2003. MODFLOW/MT3DMS-based reactive multicomponent transport modeling. *Ground Water*, 41(2): 247-267.

Prommer, H. and Stuyfzand, P.J., 2005. Identification of temperature-dependent water quality changes during a deep well injection experiment in a pyritic aquifer. *Environ. Sci. Technol.*, 39(7): 2200-2209.

Rinck-Pfeiffer, S., Ragusa, S., Sztajn bok, P. and Vandeveld, T., 2000. Interrelationships between biological, chemical, and physical processes as an analog to clogging in aquifer storage and recovery (ASR) wells. *Water Research*, 34(7): 2110-2118.

Smedley, P.L. and Kinniburgh, G.D., 2002. A review of the source, behavior, and distribution of arsenic in natural waters. *Applied Geochemistry*, 17: 517-668.

Stuyfzand, P.J. (Editor), 1998. Quality changes upon injection into anoxic aquifers in the Netherlands: Evaluation of 11 experiments. *Artificial Recharge of Groundwater*. A. A. Balkema, Brookfield, VT, 283–291 pp.

Vanderzalm, J.L., Le Gal La Salle, C. and Dillon, P.J., 2006. Fate of organic matter during aquifer storage and recovery (ASR) of reclaimed water in a carbonate aquifer. *Applied Geochemistry*, 21(7): 1204-1215.

Wilson, D., 2007. The feasibility of using aquifer storage and recovery to manage water supplies in Georgia. In: T. Rasmussen (Editor), *Proceedings of the 2007 Georgia Water Resources Conference*. University of Georgia, Athens, GA, pp. 3.

Zheng, C. and Wang, P.P., 1999. MT3DMS: A Modular Three-Dimensional Multispecies Transport Model for Simulation of Advection, Dispersion, and Chemical Reactions of Contaminants in Groundwater Systems; Documentation and User's Guide. Vol. Contract Report SERDP-99-1, U.S. Army Engineer Research and Development Center, Vicksburg, MS.

Disclaimer

The contents of this report are those of the authors and do not necessarily reflect the views of the Georgia Water Resources Institute, the United States Geological Survey, or the State of Georgia.

Tidal Streams: A Renewable Energy Source for Georgia

Basic Information

Title:	Tidal Streams: A Renewable Energy Source for Georgia
Project Number:	2008GA180B
Start Date:	3/1/2008
End Date:	2/28/2009
Funding Source:	104B
Congressional District:	5th
Research Category:	Engineering
Focus Category:	Water Use, Surface Water, Models
Descriptors:	
Principal Investigators:	Kevin A Haas, Hermann Marc Fritz

Publication

Tidal Streams: A Renewable Energy Source for Georgia

March 1, 2008 – February 28, 2009

PI: Dr. Kevin A. Haas - Georgia Tech Savannah,
School of Civil and Environmental Engineering,
khaas@gatech.edu

Co-PI: Dr. Hermann M. Fritz - Georgia Tech Savannah,
School of Civil and Environmental Engineering,
fritz@gatech.edu

SUMMARY

In this study an advanced method for assessing the tidal power potential with a three dimensional numerical model is developed and applied along the coast of the state of Georgia. This region has the largest tidal range for the southeast United States, with low to moderate average tidal currents along most of the coast, but with the possibility of very strong local currents within its complex network of tidal rivers and inlets between barrier islands. In order to resolve the changes in magnitude and the flow pattern of the tidal flows the currents are modeled with the Regional Ocean Modeling System (ROMS). Digital sounding data from the National Ocean Service (NOS) Hydrographic Data Base is used for the bathymetry information. The tidal forcing for the model is acquired from the tidal elevations and constituents information from the ADCIRC tidal database. The model results are incorporated into a Geographical Information System (GIS) database to document local regions which might be used for energy conversion and distributed energy production in the future. Data from the tidal current stations and the modeling efforts show that there are locations with as much as five times larger tidal currents than the average for the region. The results of modeling show that the Georgia coast has numerous locations with high tidal power density. However, not all of these locations have enough power that can be converted to useful energy within the current technological limits. Also the availability of these locations diminishes more once the depths requirements for placing the converters are considered. Findings from this study indicate that only a few locations limited within the Cumberland, St. Catherines, and Ossabaw Sounds and Savannah River could be considered for further investigation.

TABLE OF CONTENTS

SUMMARY	2
2. METHODS AND PROCEDURES.....	6
2.2. Numerical Modeling	6
3. RESULTS/FINDINGS	9
3.1. Verification of the tidal model results	9
3.3. Resource Mapping with GIS.....	18
3.3.1. Bathymetry Filter	18
3.3.2. Mean/ Maximum Tidal Currents and Maximum Tidal Power Density	19
4. CONCLUSION AND FUTURE WORK	22
5. PRODUCTS.....	23
6. REFERENCES	24

LIST OF FIGURES

Figure 1. Examples of (a) different computational grids and (b) different offshore extents used for ROMS simulations of the tidal currents along the Georgia coast.	8
Figure 2. Map of the three final computational grids used for ROMS simulations of the tidal currents along the Georgia coast.	8
Figure 3. Measured and modeled tidal constituents at station 8670870 at Fort Pulaski, GA.	11
Figure 4. Measured and modeled tidal constituents at station 8677344 at the entrance to St. Simons Sound, GA.	12
Figure 5. Water level (WL) and current magnitude (CUR) prediction comparison locations at the entrance of Cumberland Sound, GA.	14
Figure 7. Magnitude of the tidal current from model predictions and NOAA predictions to the Northeast of Fort Clinch at the entrance to Cumberland Sound, GA.	14
Figure 6. Water levels from model predictions and measurements in the entrance to Cumberland Sound, GA.	15
Figure 8. Tidal current predictions by NOAA and by the model at Ogeechee River Florida Passage, GA.	16
Figure 9. Water Level predictions by NOAA and by the model at Ogeechee River Florida Passage, GA.	16
Figure 10. Tidal current comparison with USACE measurement (1A) and the model grid point (1709).	17
Figure 11. Water level comparison with USACE measurement (TLR7) and the model grid point (1711).	18
Figure 12. Images of (a) the raw bathymetry layer and (b) filtered bathymetry ($h_{min} = 7$ m) layer for the southern Georgia coast.	19
Figure 13. Images of the (a-b) mean and maximum tidal current speeds along the Georgia coast.	20
Figure 14. Images of the maximum tidal density along (a) the southern coast and the (b) northern coast of Georgia.	21
Figure 15. The maximum power density using depth filter $h_{min} = 7$ m, and a minimum power density of 0.5 kW/m^2 for (a) the southern and (b) the northern Georgia coast.	22

LIST OF TABLES

Table 1. Spacing of the computational grids used in modeling the tidal currents along the Georgia coast.	9
Table 2. Quantitative comparison of tidal constituents at station 8670870 at Fort Pulaski, GA.....	11
Table 3. Quantitative comparison of tidal constituents at station 8677344 at the entrance to St. Simons Sound, GA.....	13

1. PROJECT SCOPE AND OBJECTIVES

The purpose of the project was to identify and evaluate potential locations as a source of tidal stream energy to enhance the ability of Georgia to position itself at the forefront of the utilization of clean energy technologies in the United States. Despite the large tidal range on the Atlantic coast of Georgia, the state has not been considered as a location of significant tidal energy due to the relatively weak currents on the shallow depths of the continental shelf. However, this does not take into account the large currents that are generated inside the complex network of tidal rivers and creeks that make up the Georgia coast line. To accomplish the primary objective of the project which was to evaluate the tidal flows along the Georgia coast for suitability of ocean energy conversion, the entire coast of Georgia was simulated with a numerical model to identify and quantify regions which are suitable for tidal stream energy conversion. A GIS tool was developed for assisting in the analysis of tidal energy potential.

2. METHODS AND PROCEDURES

In this study we are using state-of-the art modeling and mapping tools to assess the tidal energy potential along the coast of Georgia while satisfying some of these criteria. The Georgia coast stretches between the latitudes 30° 42' N and 32° 3' N along the Atlantic Ocean. It is characterized with its complex network of tidal rivers and inlets between barrier islands. This complex geometry of the coast with many interconnecting channels is anticipated to create favorable conditions for strong local currents. Therefore, it is important to be able to create the full three-dimensional geometry of a region and run a numerical model that can accommodate the complete physics of the problem. This approach provides means to evaluate the water levels and water currents more comprehensively rather than depending on measurements or calculations limited to a number of specific points. For this purpose, first the existing data and then the tidal modeling results are used to calculate the power from the tidal currents in the region. The tidal power per unit area or the power density is calculated using the equation

$$P_{tide} = 1/2 \cdot \rho \cdot V^3 \quad (1)$$

where P_{tide} is the tidal power density, ρ is the density of water and V is the magnitude of the depth averaged velocity.

2.2. Numerical Modeling

The Regional Ocean Modeling System (ROMS) is a member of a general class of three-dimensional, free surface, terrain following numerical models that solve three dimensional Reynolds-averaged Navier-Stokes equations (RANS) using the hydrostatic and Boussinesq assumptions (Haidvogel et al. 2008; Shchepetkin and McWilliams 2005). ROMS uses finite-difference approximations on a horizontal curvilinear Arakawa C grid (Durran 1999) and vertical stretched terrain-following coordinates. Momentum and scalar advection and diffusive processes are solved using transport equations and an equation of state computes the density field that accounts for temperature, salinity, and suspended-sediment concentrations. The modeling system provides a flexible framework that allows multiple choices for many of the model components such as several options for advection schemes (second order, third order, fourth order, and positive definite), turbulence models, lateral boundary conditions, bottom- and surface-boundary layer submodels, air-sea fluxes, surface drifters, a nutrient-phytoplankton-zooplankton model, and a fully developed adjoint model for computing model inverses and data assimilation. The code

is written in Fortran90 and runs in serial mode or on multiple processors using either shared- or distributed-memory architectures (Open Multi-Processing or Message Passing Interface).

To produce accurate simulations of tidal currents, the model requires detailed bathymetric data for the generation of the computational grid. The coastline and bathymetry information is obtained from the National Geophysical Data Center (NGDC). NOAA's Medium Resolution Shoreline (1/70,000) dataset is used for the coastline information. The coastline dataset is extracted using the coastline extractor available at the NGDC website (NGDC 2008) and the bathymetry data downloaded through the ArcIMS (NOS 2008) interface provided by NGDC, which is the official source for National Ocean Service (NOS) bathymetric maps. The vertical datum for the bathymetry data is adjusted using the Mean Lower-Low Water (MLLW) and Mean Tidal Level (MTL) values reported by local tidal stations (NOAA 2008).

The computational grid is generated using the SeaGrid orthogonal grid maker for Matlab (Denham 2008). The bathymetric data is used to generate depths for each grid point. Grid points within the computational domain which remain permanently "dry" are determined and marked by using a masking feature utilizing the coastline data. The grid is examined manually to ensure that all computational points are interconnected with at least two other points. Finally, the vertical datum for the grid is adjusted to the MTL. In order to simulate the tidal flows inside the estuaries, rivers, inlets and bays in more detail numerical grid resolution is kept to be as small as tens of meters. For this reason, to keep the computational domain to a manageable size, the coast is broken up into subgrids, each being used for separate simulations. Sensitivity analyses of both tidal current velocities and the water level changes to under various computational grid extents and the computational cell sizes are studied (Figure 1). The computational cell sizes are designed as small as possible within the limitations of the grid generator. The final computational cell sizes for each computational are fine enough to model the most of the tidal creeks and interconnection between the tidal estuaries. The offshore extent of each computational domain is limited based on the sensitivity analysis by comparing the predicted constituents for tidal water elevation and tidal currents in each case. Finally the Georgia coast has been modeled with 3 overlapping subgrids with computational cell sizes varying between 42 and 320 m (Figure 2 and Table 1). Wherever possible, natural barriers are selected as boundaries between the different grids; estuaries or bays are contained in their entirety within a single computational domain. The neighboring grids contain overlaps of several kilometers to ensure full coverage.

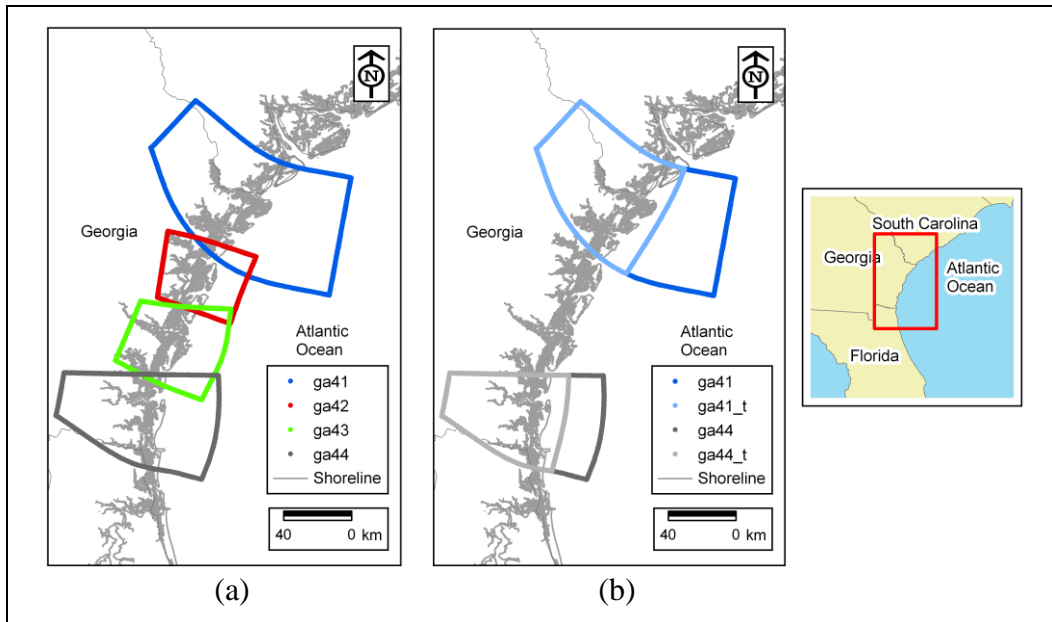


Figure 1. Examples of (a) different computational grids and (b) different offshore extents used for ROMS simulations of the tidal currents along the Georgia coast.

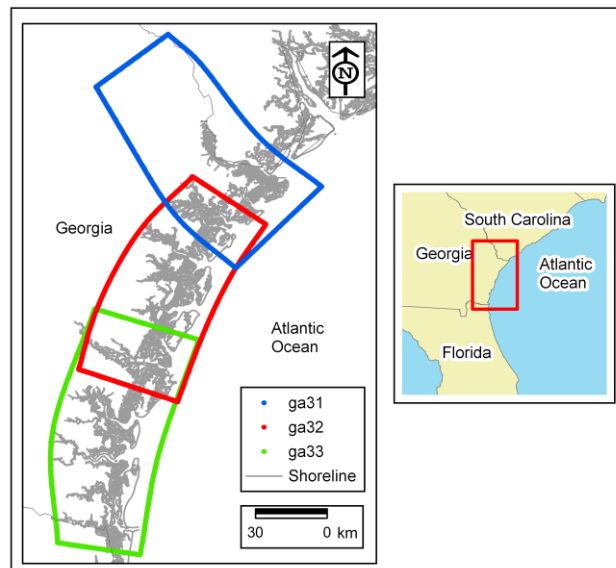


Figure 2. Map of the three final computational grids used for ROMS simulations of the tidal currents along the Georgia coast.

Table 1. Spacing of the computational grids used in modeling the tidal currents along the Georgia coast.

Grid Name	X-grid spacing (m)		Y-grid spacing (m)		Z-grid spacing (m)	
	Min	Max	Min	Max	Min	Max
ga31	70	258	84	320	0.1	3.0
ga32	42	173	84	225	0.1	3.1
ga33	71	241	78	261	0.1	4.4

In order to produce simulations of the tidal currents, the model requires tidal forcing along the boundaries of the computational domain. This forcing can be derived from a variety of sources including measurements, model simulations or the harmonic constituents provided by the NOAA CO-OPS. The tidal forcing comes from the ADCIRC tidal database created by the numerical model ADCIRC for the Western North Atlantic Ocean (Mukai et al. 2002). This database includes the M2, S2, N2, K2, O1, K1, P1, Q1, M4, M6 and STEADY tidal constituents. Although the M4, M6 and STEADY components in ADCIRC database have not been verified, M4 and M6 constituents are still included in the model tidal forcing to incorporate the effect of the overtides. The constituents are extracted from the tidal database and applied at the open boundary of the computational grids to force the ROMS simulations of the tidal currents.

The model is run to simulate 32 days, encompassing an entire lunar cycle, for each computational domain. Currents and water levels are retained at 1 hour intervals for all points within the domain to allow for harmonic analysis using the T_Tide harmonic analysis toolbox for Matlab (Pawlowicz et al. 2002) of both the water levels and the velocities.

3. RESULTS/FINDINGS

3.1. Verification of the tidal model results

Starting from November 1, 2005, 32 days worth of tides were simulated with the model. The model results compared with available data for the water levels are shown in Figure 3 and 4. The water level data has been obtained from the CO-OPS website and run through the harmonic analysis toolbox to extract the same tidal constituents as used in driving the model. Differences between the model and measurements are evident in the first few tidal cycles as the model goes through its spin-up phase beginning from a cold start. The spin-up of the model was successfully contained within the first two days of the model runs. After the initial startup, the model and measurements are quite similar, clearly demonstrating the ability of the model to reproduce the tidal water levels. The model results are compared with the tidal elevation constituents, water level predictions and current predictions from NOAA CO-OPS. Wherever it is available, historic data from field measurements in the area is also used to verify the model findings.

Comparison of Tidal Elevation Constituents

Nine of the water level tidal constituents obtained from CO-OPS and computed from the model for station are compared for verification purposes. The constituents from the model are computed while

neglecting the first 48 hours to eliminate startup effects in the model. Comparison of the tidal elevation constituents for the model grid ga33 at station 8670870 at Fort Pulaski is shown in Figure 3 and a quantitative comparison is given in Table 2. It is seen that the difference between the model and the measured values are kept in less than 10% for the five most energetic constituents, whereas it is much higher for the remaining less energetic ones. However, the overall effect of the difference in these constituents on the tidal amplitude is less than 3 cm and can be neglected when compared to the more energetic constituents. As an example to verification efforts for model grid ga33 the results for station 8677344 at the entrance to St. Simons Sound are shown in Figure 4 and in Table 3. Similar to the verification results for model grid ga31, the difference between the tidal elevation constituents from the measurements and the model are kept below 10%, the combined contribution from the less energetic constituents to the tidal elevation amplitude also being less than 3 cm. Tidal elevation constituents for model grid ga32 cannot be verified against measured data since there is no tidal constituent measurement available from CO-OPS. Therefore, the results from this grid are still verified using various maximum current predictions and high/low tidal elevation predictions available from NOAA. In conclusion, even though the model is only using 30 days worth of data to compute the harmonics, the comparison with the measurements show that the computed amplitude and phase results are reasonably close to the measured values.

Table 2. Quantitative comparison of tidal constituents at station 8670870 at Fort Pulaski, GA.

Name	Period (hrs)	Measured Amplitude (m)	Model Amplitude (m)	Measured Phase (min)	Model Phase (min)
Q1	26.87	0.02	0.01	891	862
O1	25.82	0.08	0.08	889	879
K1	23.93	0.11	0.11	801	768
N2	12.66	0.22	0.20	5	745
M2	12.42	1.01	0.91	37	8
S2	12.00	0.16	0.16	92	51
K2	11.97	0.04	0.04	92	57
M4	6.21	0.04	0.03	257	334
M6	4.14	0.01	0.02	42	22

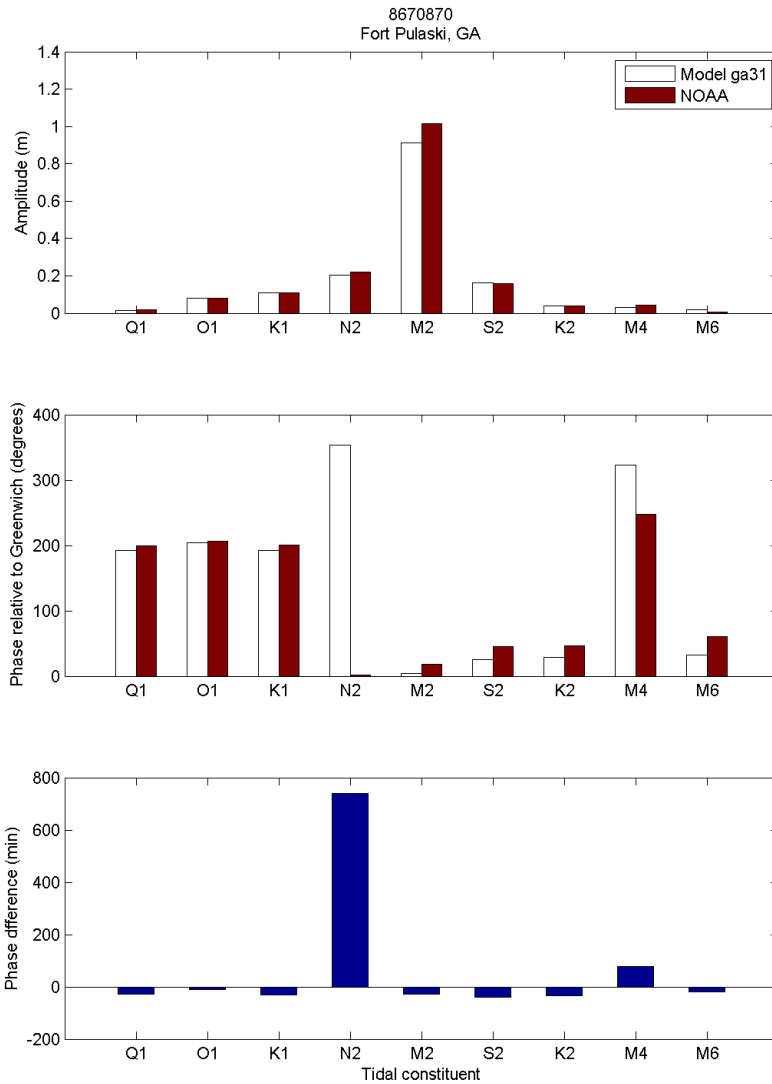


Figure 3. Measured and modeled tidal constituents at station 8670870 at Fort Pulaski, GA.

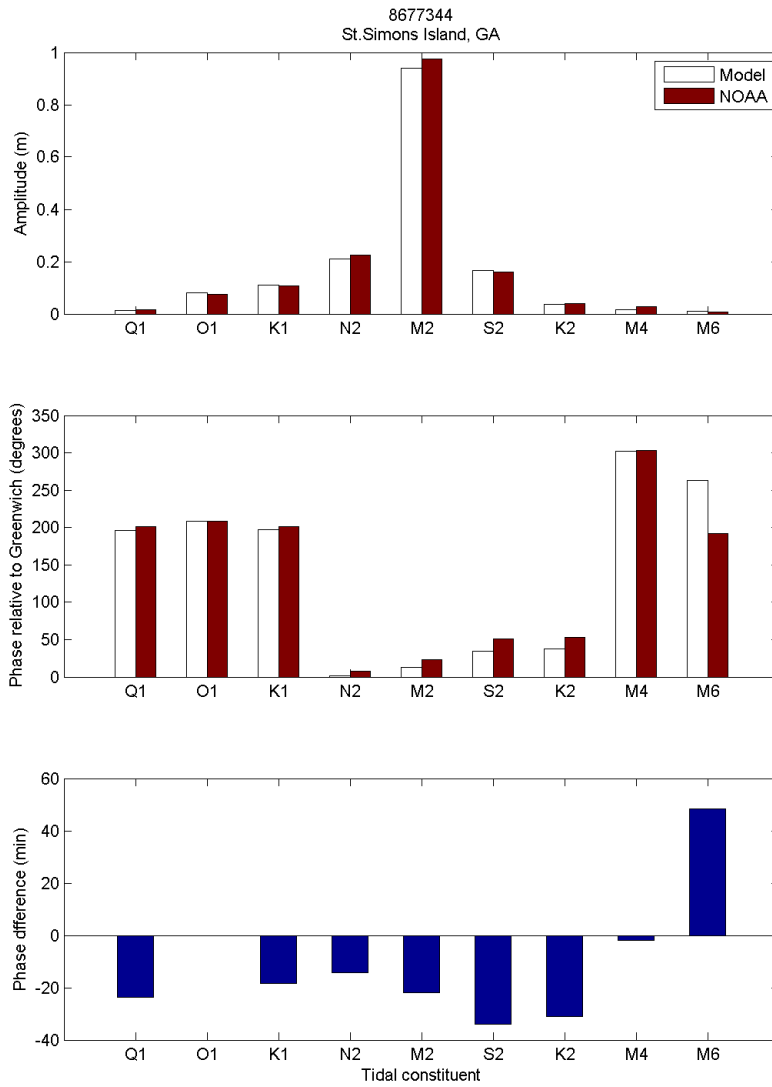


Figure 4. Measured and modeled tidal constituents at station 8677344 at the entrance to St. Simons Sound, GA.

Table 3. Quantitative comparison of tidal constituents at station 8677344 at the entrance to St. Simons Sound, GA.

Name	Period (hrs)	Measured Amplitude (m)	Model Amplitude (m)	Measured Phase (min)	Model Phase (min)
Q1	26.87	0.02	0.01	903	879
O1	25.82	0.08	0.08	895	895
K1	23.93	0.11	0.11	803	784
N2	12.66	0.23	0.21	17	3
M2	12.42	0.98	0.94	48	26
S2	12.00	0.16	0.17	102	68
K2	11.97	0.04	0.04	106	75
M4	6.21	0.03	0.02	314	312
M6	4.14	0.01	0.01	133	181

Comparison of Predicted Maximum Currents and Predicted High/Low Tidal Elevations

The accuracy of the velocities for the tidal currents is also evaluated by comparing the computed velocities with available data. A time series may be constructed utilizing information from the tidal current prediction gauges and compared directly to the model predictions of the magnitudes of the tidal currents.

A comparison of the maximum tidal current magnitudes for selected locations (Figure 5) inside the entrance channel for Cumberland Sound in Georgia is shown in Figure 6 for verification of model results from model grid ga33. The maximum envelope from the station is shown with solid red line, and the tidal current time series obtained by generating a time series from the harmonic constituents calculated by the model are shown in blue. The reproduction of the tidal currents is quite good for this station. The time series constructed from the tide table has 1 hour resolution for the velocity outputs may not resolve the precise slack water time. At many locations the tidal velocity may never entirely vanish, because the velocity actually follows an elliptical pattern as it turns from flood to ebb and not simply flop back and forth in a collinear pattern. This explains the apparent mismatch between the model and measurements for low current speeds. It is important to note that tide station measurements often include components from fresh water runoff or river flow and atmospheric effects, which are not included in the tidal model. The tidal elevation comparison at this location is also in agreement with the predictions by NOAA (Figure 7).

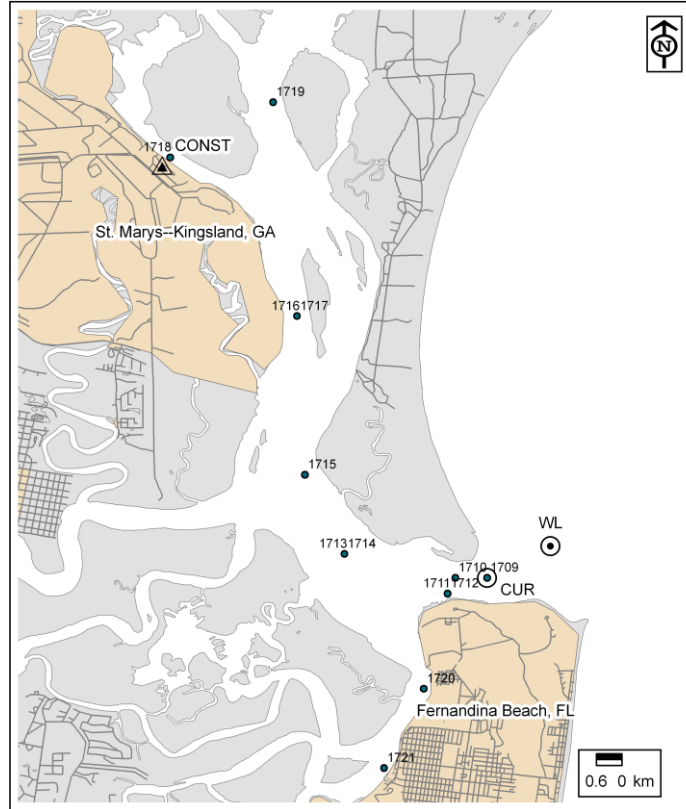


Figure 5. Water level (WL) and current magnitude (CUR) prediction comparison locations at the entrance of Cumberland Sound, GA.

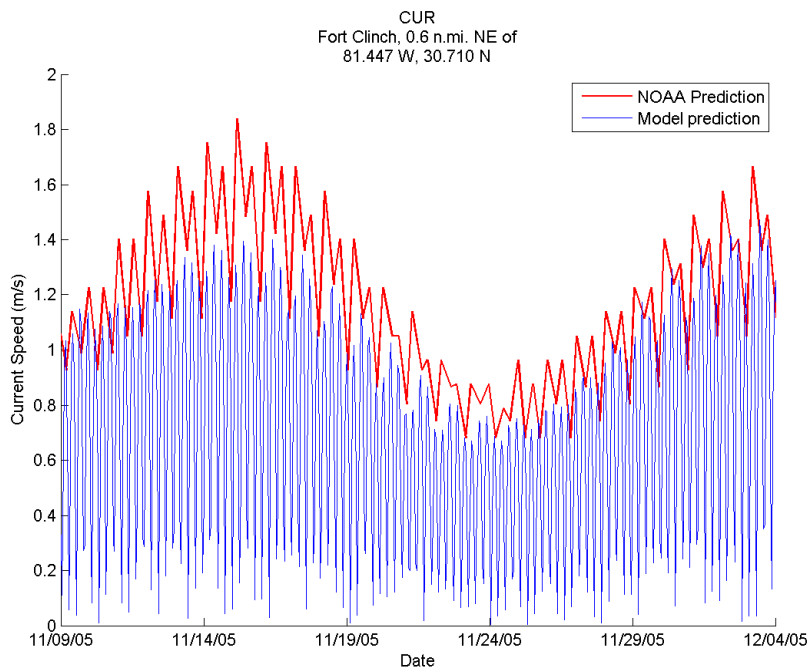


Figure 6. Magnitude of the tidal current from model predictions and NOAA predictions to the Northeast of Fort Clinch at the entrance to Cumberland Sound, GA.

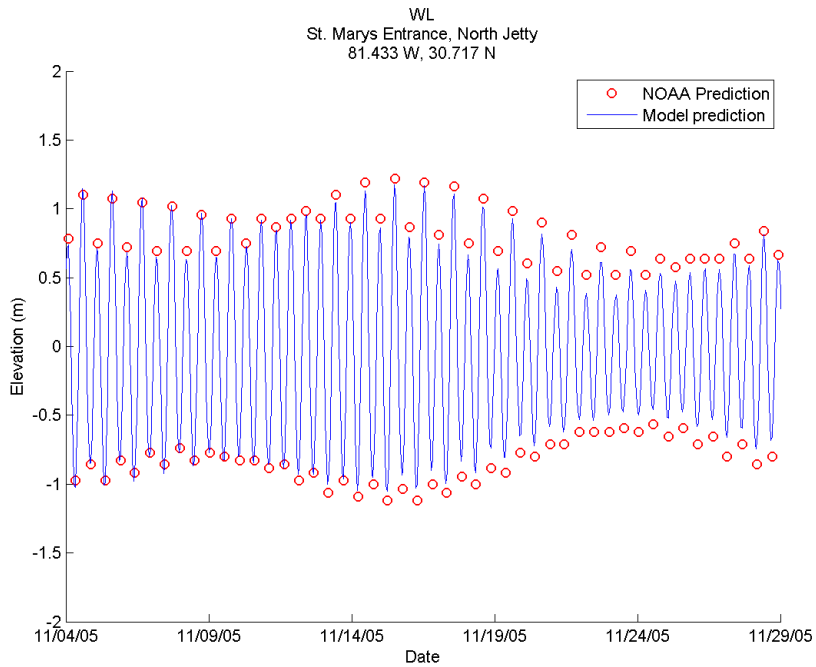


Figure 7. Water levels from model predictions and measurements in the entrance to Cumberland Sound, GA.

Similarly the results for the model grid ga32 are shown in Figure 8 and 9. This time only the envelope for the maximum tidal current magnitudes obtained by the model and published by NOAA are shown. It is seen that the model predictions agree with the NOAA predictions, but the model falls short in reproducing the large differences between the maximum flood and maximum ebb currents. This is an expected issue for models that do not include the wetting and drying of the computational cells in modeling the tidal flows (Huang et al. 2008). The smoothing of the bathymetry for model stability degrades the model accuracy in predicting tidal water elevations and tidal current magnitudes. Moreover, the approximation of the channel width in plane coordinates due to the fixed size of the computational grid introduces some error in the flow cross-section, hence the currents and water levels. This is especially a larger relative impact on the narrower channels as can be seen in the difference between the model and the predicted tidal elevations in Figure 9.

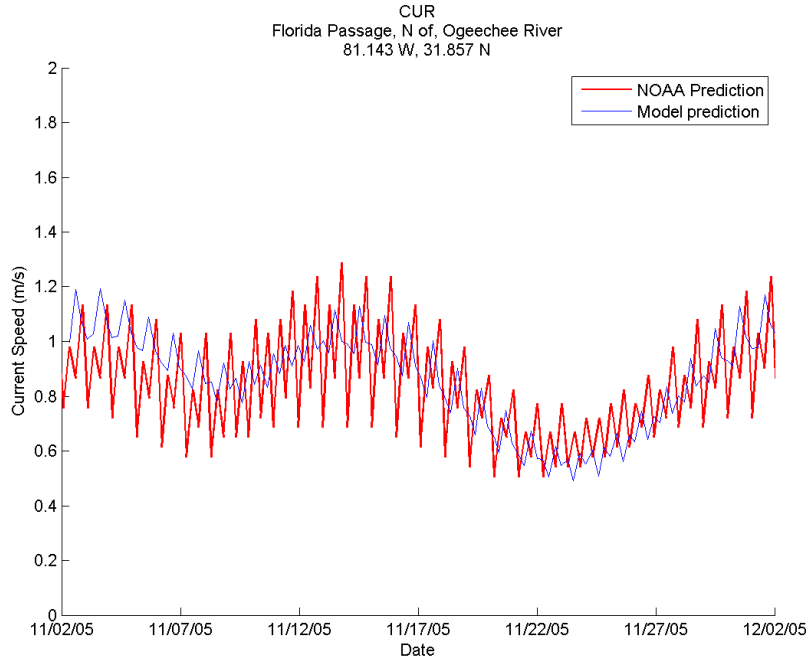


Figure 8. Tidal current predictions by NOAA and by the model at Ogeechee River Florida Passage, GA.

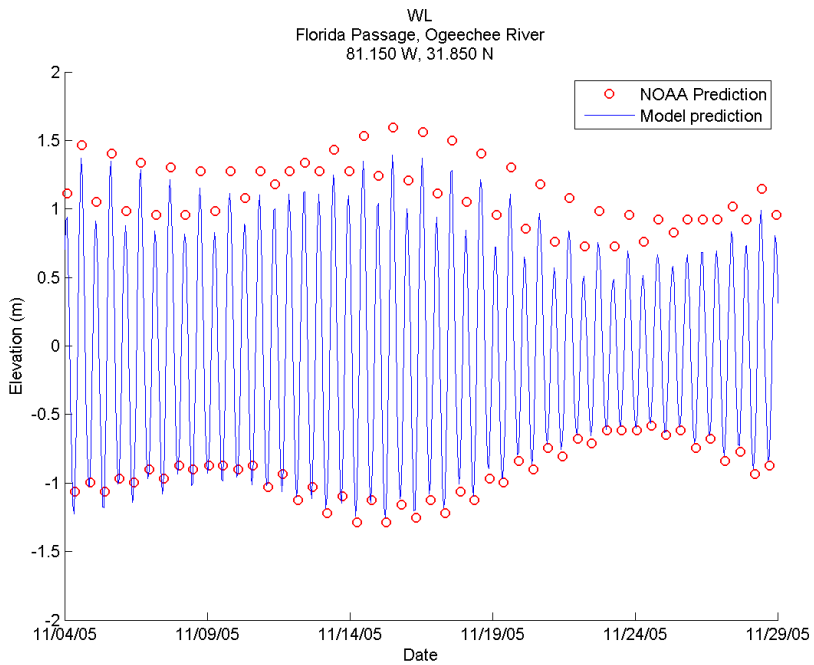


Figure 9. Water Level predictions by NOAA and by the model at Ogeechee River Florida Passage, GA.

Comparison of Results with Field Measurements

The Hydraulics Laboratory of the US Army of Engineer Waterways Experiment Station performed a field measurement of hydrodynamics at the Cumberland Sound in 1990 as a part of the Cumberland Sound Monitoring Program of the Department of the Navy (Charlier 2003). The water level and tidal current measurements at the Cumberland Sound entrance from this study are compared to the model results for verification of model results. Two of the closest model output points (1709 and 1711) are used for this purpose. Comparison of the depth averaged measured currents to the depth averaged currents from tidal constituents computed by the model shows that the model does a good job in predicting the currents with a maximum error margin of 5 -10 cm/s difference in the current magnitudes (Figure 10). The difference between the measured data and the model is more pronounced in the case of phase differences. The model results are more symmetrically distributed around the time of occurrence of maximum currents, whereas the measurements show that the currents are biased towards the ebb or flood flow. However, the duration of the measured data is not long enough to make a conclusion on the difference between flood and ebb flow. The water level predictions from the model and the measurements fall in close range with a magnitude difference of 10 cm and a better agreement in the measured and the computed phases when compared to the phase difference between the measured and computed tidal current time series (Figure 11).

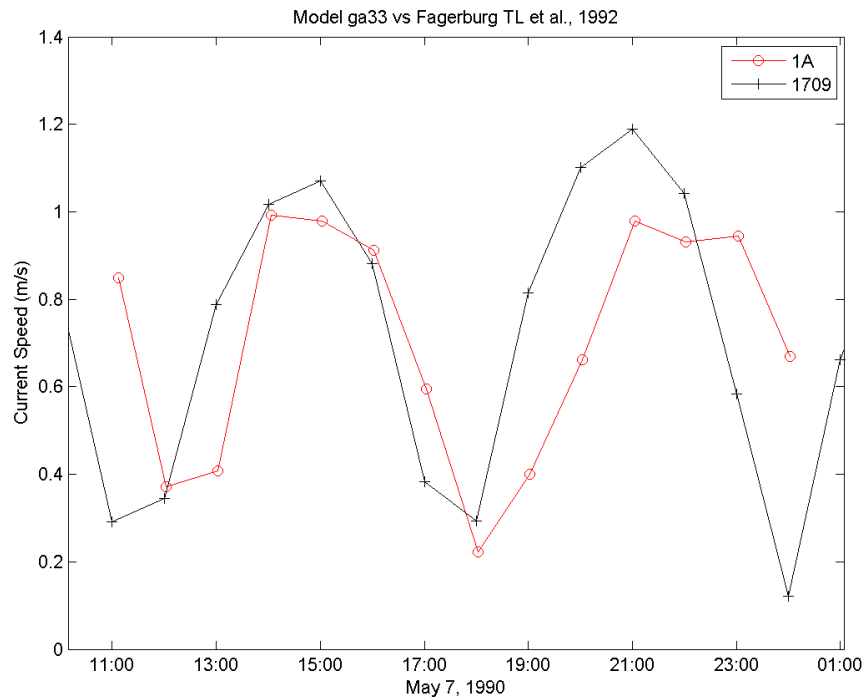


Figure 10. Tidal current comparison with USACE measurement (1A) and the model grid point (1709).

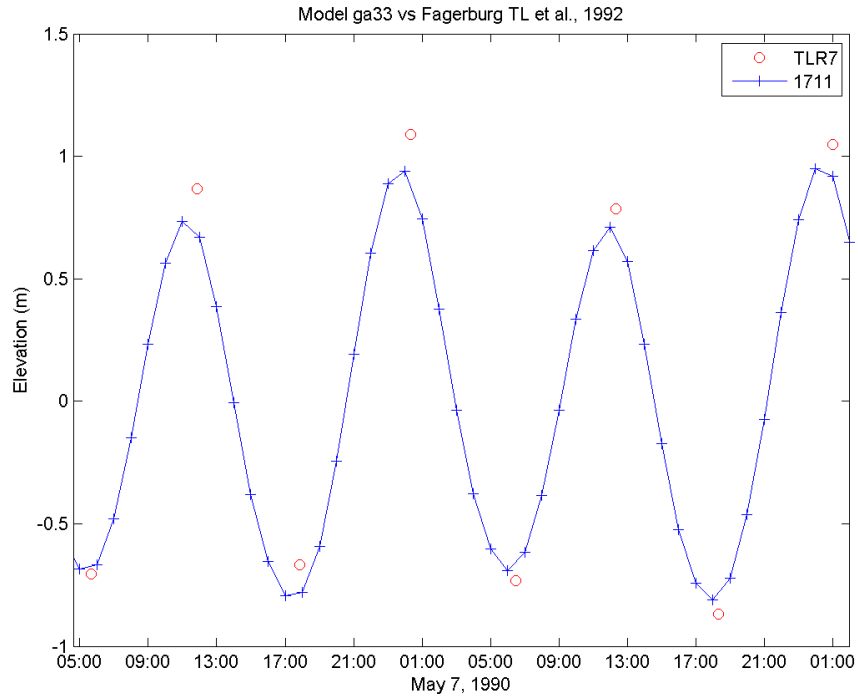


Figure 11. Water level comparison with USACE measurement (TLR7) and the model grid point (1711).

3.3. Resource Mapping with GIS

ESRI's ArcView (ESRI 2008) package with the Spatial Analyst extension has been used for resource mapping in this study. The spatial masking according to the minimum depth and minimum tidal power density using ArcView package is explained in details in the following subsections.

3.3.1. Bathymetry Filter

Tidal stream energy converters are currently limited in their variety and are primarily classified in vertical and horizontal axis devices with open or shrouded rotors. Independent of their design all the devices have depth requirement based on their dimensions. The first step for a site selection scheme for any of these energy converter projects is to determine which locations will meet the minimum depth requirements. The minimum depth is usually given as

$$h_{min} = h_b + h_s + d_p \quad (3.1)$$

where h_{min} is the minimum depth, h_b is minimum height of the prototype above the bed, h_s is the minimum clearance of the prototype below the surface and d_p is the device dimensions. As an example, if the minimum height above the bed was set at 2 m, the minimum clearance below the MLLW was 2 m and the propeller diameter was 3 m, the minimum depth becomes 7 m. Figure 12(a) shows the raw bathymetry layer and Figure 12(b) shows the filtered bathymetry layers for the Georgia coast with $h_{min} = 7$ m created in ArcView. All depths below the h_{min} have been removed from this layer as evident by the white areas, leaving only the depths in the offshore region and within the channels in the nearshore region. This layer is used to mask the map for the available tidal power.

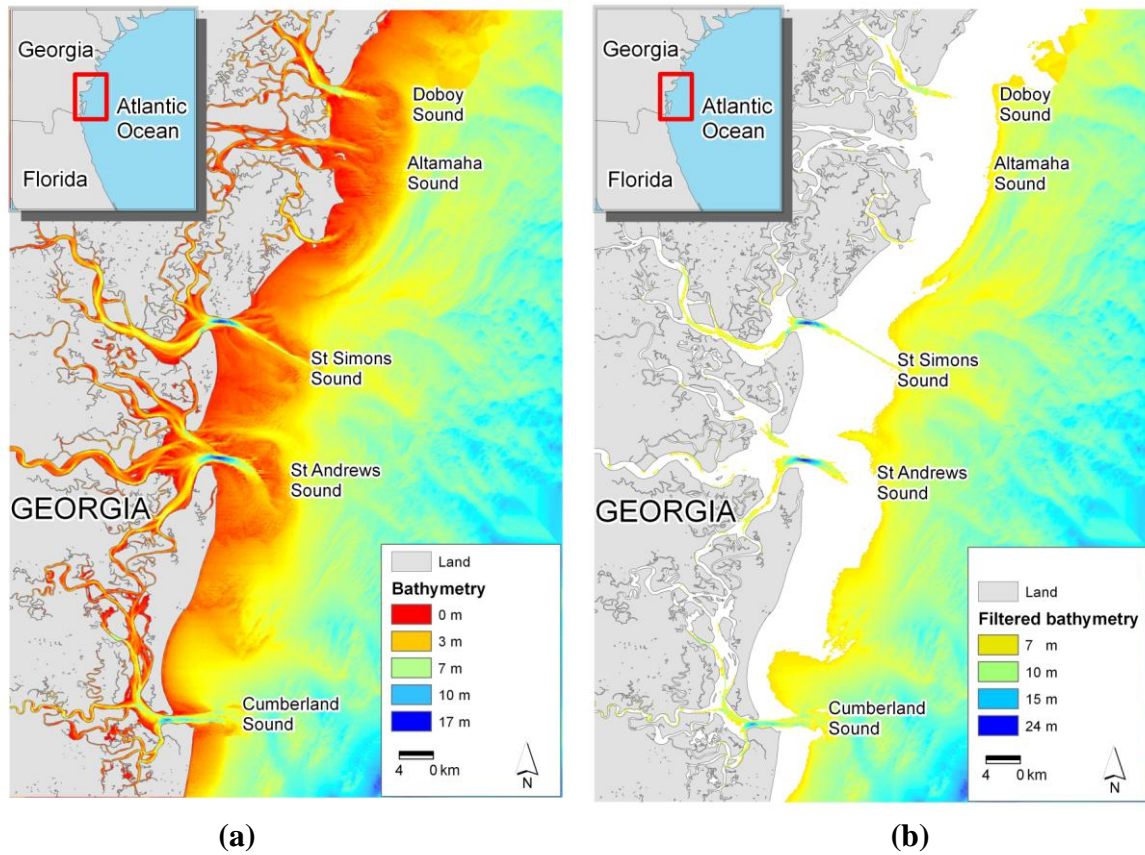
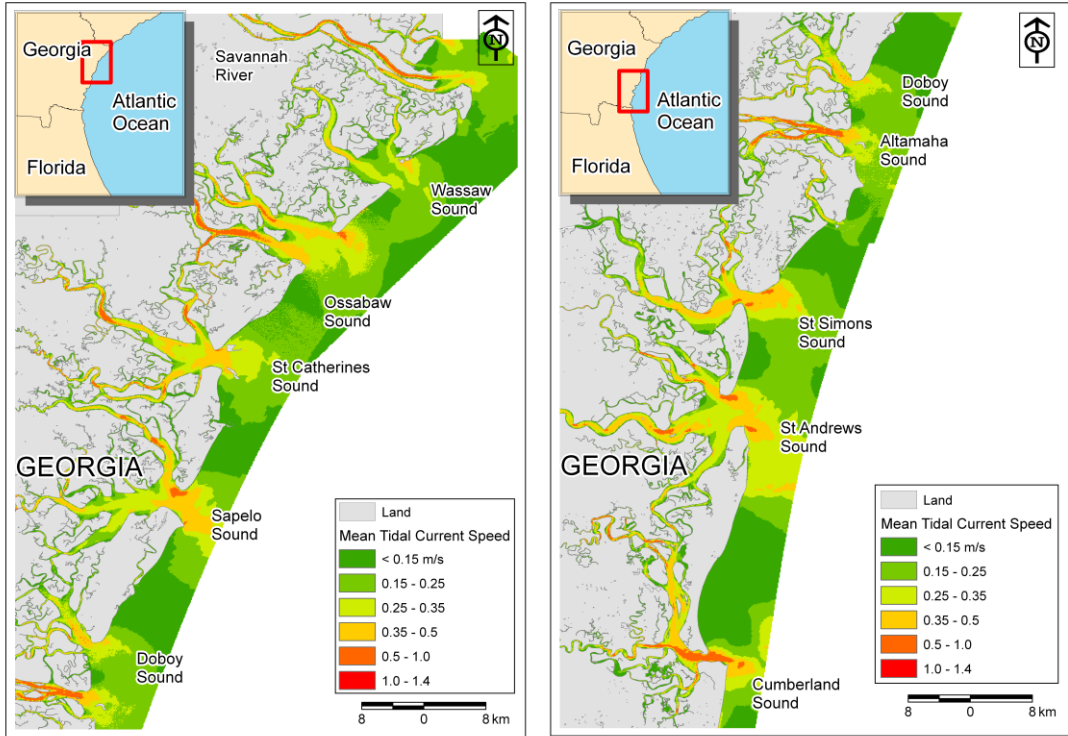


Figure 12. Images of (a) the raw bathymetry layer and (b) filtered bathymetry ($h_{min} = 7$ m) layer for the southern Georgia coast.

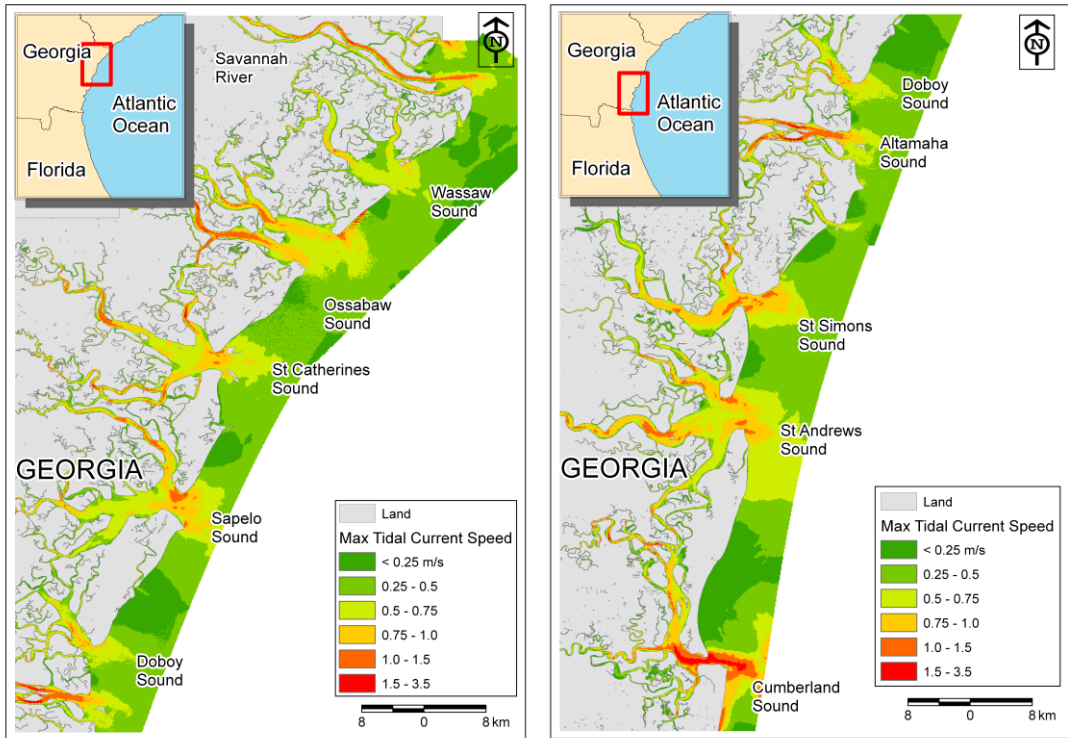
3.3.2. Mean/ Maximum Tidal Currents and Maximum Tidal Power Density

The mean and maximum tidal currents along the Georgia coast are shown in Figure 13. The strongest currents seem to occur mainly at the entrance of the tidal rivers and sometimes at the entrance to the main Sound. The maximum current magnitudes are observed to be usually 2 to 3 times higher than the mean current magnitudes. Figure 14 shows the annual maximum power for the southern coast of Georgia taken from the model simulations shown in Figure 2. Figure 14 is the total available power as computed from the model output.



(a)

(b)



(c)

(d)

Figure 13. Images of the (a-b) mean and maximum tidal current speeds along the Georgia coast.

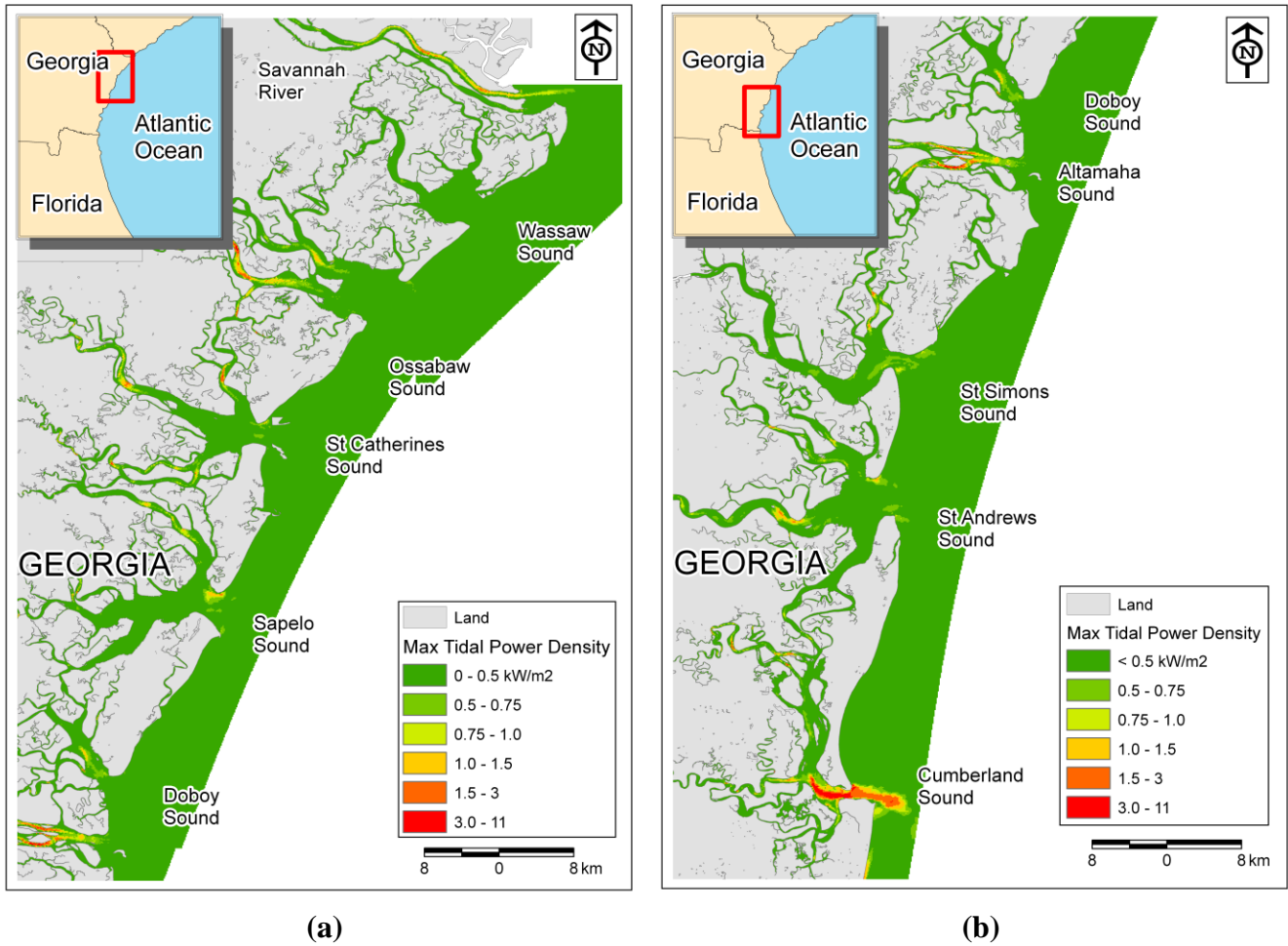
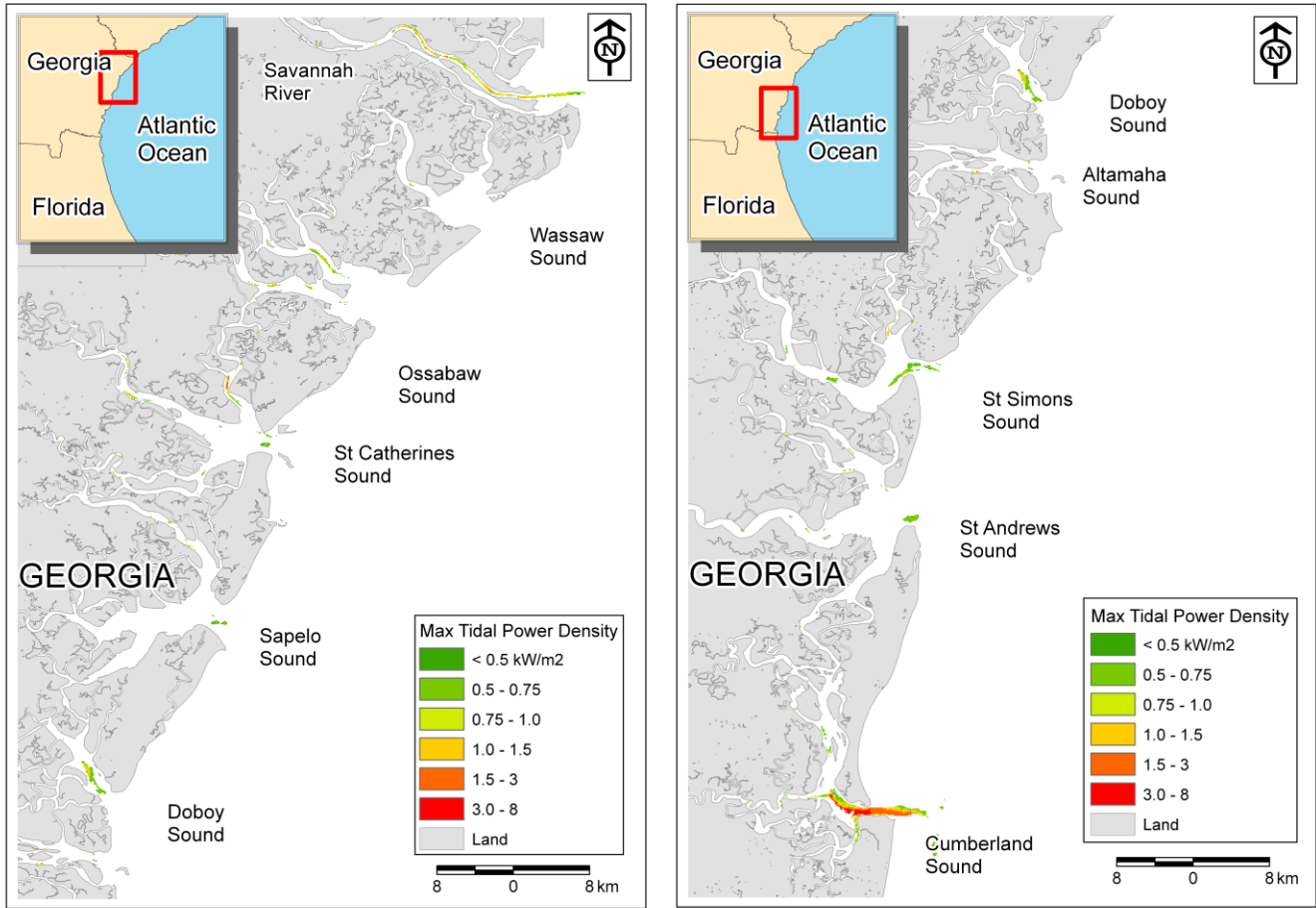


Figure 14. Images of the maximum tidal density along (a) the southern coast and the (b) northern coast of Georgia.

The annual maximum power density is then filtered by the bathymetry threshold and also is filtered by a minimum required power ($> 0.5 \text{ kW/m}^2$) in order to facilitate the identification of regions with useful tidal energy potential. The filters have reduced the data to just a few specific locations where there is significant tidal power available for extraction. The concentration of available power density is clearly located within the channels between the islands. In particular, the entrance to Cumberland Sound has extensive power density highlighting the importance of the tidal modeling for the entire coastline to identify potential sites. In Figure 15(a) it is seen that the maximum power density in the Cumberland sound entrance can be as large as 11 kW/m^2 , which is much larger than the average in the region. St. Andrews and Altamaha Sounds also have a few locations which qualify the minimum depth and minimum power density criteria. The tidal power densities in these areas are in the order of 0.1 kW/m^2 . It is also possible to see the surface area of the maximum tidal power density for each location in the same figure. According to this, about 1.5 km^2 of the suitable area at the Cumberland Sound entrance has a power density between 1.0 and 11 kW/m^2 . The total suitable area at Cumberland Sound is about 7.9 km^2 , with depths varying between 7 and 24 m , and widths ranging from 0.9 to 1.6 km across the channel.

The average maximum tidal power density map for the northern part of the Georgia coast is given in Figure 15(b). Savannah River, Ossabaw and St Catherines Sounds have areas with more than 1.0 kW/m^2 tidal power densities. Amongst these Ossabaw sound has the largest suitable area of 9.5 km^2 with depths between 7 and 9 m for average maximum tidal power densities higher than 1.0 kW/m^2 . The width of this suitable area changes from 0.3 to 1 km across the channel. At the Savannah River entrance and further inland of Ossabaw and St Catherines Sounds it is possible to find areas where maximum tidal power density levels go up to $3\sim 8 \text{ kW/m}^2$, but these are very small areas ($< 0.3 \text{ km}^2$) when compared to the others.



(a) (b)
Figure 15. The maximum power density using depth filter $h_{min} = 7 \text{ m}$, and a minimum power density of 0.5 kW/m^2 for (a) the southern and (b) the northern Georgia coast.

4. CONCLUSION AND FUTURE WORK

The Georgia coast of the USA has a complex geometry with many inlets between barriers. The 133 tidal current prediction stations in the region are not sufficient to resolve all of the flow patterns in this complex network of channels. Modeling results show that the largest tidal power density with a water column depth higher than 7 m is at the entrance of Cumberland Sound near the border to Florida. The average maximum tidal power density at this location can be as large as 11 kW/m^2 . However, the mean

tidal current magnitudes are known to be 2 to 3 times smaller than the available maximum tidal current magnitudes and certain physical constraints such as the allowable space in the vertical for an energy converter limit the extent of areas that are available for energy conversion. Moreover, one should note that the final usable power will further diminish in regards to the efficiency of the energy converters. St. Andrews, Altamaha, St. Catherines, Ossabaw Sounds and Savannah River are the other locations that have patches of areas that satisfy the minimum depth (> 7 m) and minimum tidal power density (> 0.5 kW/m²) criteria. The maximum tidal power density in these areas is in the level of 100 W/m² based on a typical efficiency curve shown in Figure 7. There are also very small areas at St Catherines Sound, Ossabaw Sound and at the entrance of Savannah River where the average maximum tidal power density levels go up to 1.5 kW/m².

Although the modeling provides better spatial resolution, it needs to be verified with any available measurements to make sure that it represents the real physics of the problem. The effect of the riverine flows and the drying and wetting of the computational cells are additional efforts that can be integrated into the existing modeling methodology in order to obtain more sophisticated methodology. Also the effect of energy extraction at a location on the flow regime and other location should be considered for more accurate assessment of the tidal power potential. Nevertheless, modeling provides means to integrate information from different sources such as bathymetry, efficiency of energy conversion devices and many others that have not been discussed here with the tidal modeling results. In the end the data set can be filtered with appropriate tools to provide more elucidative findings.

5. PRODUCTS

Defne, Z., Haas, K. A., Fritz, H. M., and Cambazoglu, M. K. (2008). "Assessment of Tidal Currents along the Atlantic Coast of the Southeast USA for Energy Conversion: Case Study for Georgia." International Conference on Ocean Energy (ICOE) 2008, Brest, France, In Press.

Defne, Z., Haas, K. A., Fritz, H. M. (2008). "Assessment of Tidal Currents along the Georgia Coast for Energy Conversion." TechFest 2008, The Creative Coast Alliance, Savannah, GA.

Haas, K., Fritz, H., Defne, Z., Jiang, L., French, S., Shi, X., and Smith, B. (2009) "Assessment of Energy Production Potential from Tidal Streams in the United States" Poster presentation at the Global Ocean Renewable Energy Conference. Washington DC.

Provided support for PhD student Zafer Defne. Expected Graduation Summer 2009.

6. REFERENCES

- Charlier, R. H. (2003). "A "sleeper" awakes: tidal current power." *Renewable and Sustainable Energy Reviews*, 7(6), 515-529.
- Defne, Z., Haas, K. A., Fritz, H. M., and Cambazoglu, M. K. (2008). "Assessment of Tidal Currents along the Atlantic Coast of the Southeast USA for Energy Conversion: Case Study for Georgia." International Conference on Ocean Energy (ICOE) 2008, Brest, France, In Press.
- Denham, C. R. (2008). "SeaGrid Orthogonal Grid Maker for Matlab."
- Durran, D. R. (1999). *Numerical methods for wave equations in geophysical fluid dynamics*, Springer, New York.
- ESRI. (2008). "GIS Mapping Software, ArcView."
- Haidvogel, D. B., Arango, H., Budgell, W. P., Cornuelle, B. D., Curchitser, E., Di Lorenzo, E., Fennel, K., Geyer, W. R., Hermann, A. J., Lanerolle, L., Levin, J., McWilliams, J. C., Miller, A. J., Moore, A. M., Powell, T. M., Shchepetkin, A. F., Sherwood, C. R., Signell, R. P., Warner, J. C., and Wilkin, J. (2008). "Ocean forecasting in terrain-following coordinates: Formulation and skill assessment of the Regional Ocean Modeling System." *Journal of Computational Physics*, 227(7), 3595-3624.
- Huang, H., Chen, C., Blanton, J., and Andrade, F. (2008). "A numerical study of tidal asymmetry in Okatee Creek, South Carolina." *Estuarine, Coastal and Shelf Science*, 78(1), 190-202.
- Mukai, A. Y., Westerink, J. J., and Luettich, R. A. (2002). "Guidelines for Using Eastcoast 2001 Database of Tidal Constituents within Western North Atlantic Ocean, Gulf of Mexico and Caribbean Sea." US Army Corps of Engineers.
- NGDC. (2008). "Coast Line Extractor." National Oceanic and Atmospheric Administration.
- NOAA. (2008). "Tidal Datums." National Oceanic and Atmospheric Administration.
- NOS. (2008). "Office of Coast Survey US Bathymetric & Fishing Maps." National Ocean Service, NOAA.
- Pawlowicz, R., Beardsley, B., and Lentz, S. (2002). "Classical tidal harmonic analysis including error estimates in MATLAB using T_TIDE." *Computers & Geosciences*, 28(8), 929-937.
- Shchepetkin, A. F., and McWilliams, J. C. (2005). "The Regional Ocean Modeling System (ROMS): A split-explicit, free-surface, topography-following coordinates ocean model." *Ocean Modelling*, 9, 347-404.

A Comprehensive Evaluation of the Mandatory Drought Responses in Georgia

Basic Information

Title:	A Comprehensive Evaluation of the Mandatory Drought Responses in Georgia
Project Number:	2008GA184B
Start Date:	3/1/2008
End Date:	2/28/2009
Funding Source:	104B
Congressional District:	5
Research Category:	Social Sciences
Focus Category:	Drought, Conservation, Law, Institutions, and Policy
Descriptors:	
Principal Investigators:	Susan E. Cozzens, Hyun Jung Park

Publication

An Evaluation of Mandatory Drought Responses in Georgia, Focusing on Water Utilities

Basic Information

Title:	An Evaluation of the Mandatory Drought Responses in Georgia, Focusing on Water Utilities
Project Number:	2008GA184B
Start Date:	3/1/2008
End Date:	2/28/2009
Funding Source:	104B
Congressional District:	5
Research Category:	Water Quantity
Focus Category:	Drought, Conservation, Law, Institutions, and Policy
Descriptors:	drought, water conservation, performance, water utilities
Principal Investigators:	Susan E. Cozzens, Hyun Jung Park

**A Comprehensive Evaluation of the Mandatory Drought Responses in
Georgia: Focusing on Water Utilities**

Final Report

Hyun Jung Park

Post-Doctoral Fellow

Technology Policy and Assessment Center, Georgia Institute of Technology¹

¹ Current position: Programme Officer, SDM Programme, United Nations Framework Convention on Climate Change - secretariat Martin-Luther-King-Strasse 8, D-53175 Bonn, Germany Tel. +49-(0)228-815-1142 Fax. +49-(0)228-815-1999 HPark@unfccc.int

Executive Summary

Due to continuous extreme weather conditions, North Georgia has suffered drought since 2007. During the drought, the Georgia government imposed mandatory drought responses and encouraged conservation practices among water utilities. The purpose of this study was to help improve the performance of water conservation and the effectiveness of drought responses by providing better understanding and analytical explanations of the drought responses.

Through both qualitative and quantitative analyses, this research attempted to evaluate the performance levels of water conservation and identify key determinants. This research also explored how the Georgia water utilities complied with the mandatory drought responses, whether through self-improvement or customer-relations approaches.

Eight-six water utilities responded to a questionnaire on their water conservation responses out of 162 contacted (a response rate of 53%). Utilities usually implemented multiple water conservation approaches, with customer education being the most widely used. About half the approaches were either promoted more strongly or newly implemented in response to the mandatory reduction targets. The largest increase was in customer relations rather than self-improvement programs.

Many utilities perceived that customer education and leak control were quite beneficial as compared with their costs. Hiring conservation coordinators, recycling support, and operating adjustments were not seen to be cost-effective, although there were differences of opinion on the balance of costs and benefits within each conservation measure. Many utilities could not make a judgment on the balance of costs and benefits, an interesting finding in itself. The utilities perceived that leadership and customer cooperation were the most important factors for success of their programs.

When the views the utilities expressed on the questionnaire were compared with their reported performance and organizational characteristics from other data sets, most of the explanatory factors tested in the study showed a statistical relationship to performance. Large utilities, however, were no more likely to reduce use than small ones, and the effect of leak control programs was not statistically significant. Systems that purchased water showed particularly strong improvements, and previous system inefficiency and the presence of a strong internal advocate were also positive influences. Seasonal rate structures and number of customer complaints were both negatively related to performance. The poverty rate in the service area was also negatively correlated.

Water use reductions increased between the period of mandatory restrictions and the immediately following period, suggesting that there may be long term benefits from the measures implemented during the mandatory restriction period.

The results suggest that water regulators should consider special help for utilities in high poverty areas and tools to help utilities judge the cost-effectiveness of the measures they adopt under their particular conditions. These steps could help increase the overall impact of the water restrictions.

Table of Contents

Executive Summary	3
Table of Contents	4
Introduction	5
Background: Georgia Mandatory Drought Responses	5
Project Scope and Objectives.....	7
Past Relevant Work	9
Research Methods	10
Conceptual Model:.....	10
Data Collection Methods:	11
Results	13
Survey Outcomes: Descriptive Analyses.....	13
Analytical Results:	19
Conclusions	22
References	23
Appendix 1: Description of the Variables in the Statistical Model	25
Appendix 2: Detailed Results of the Statistical Model	26

List of Tables

Table 1. Results of the Analytical Model for Performance Evaluation.....	20
Table 2. Self-improvement vs. Customer-Relations.....	22

List of Figures

Figure 1. Georgia Drought Monitor, 2006 vs. 2007	5
Figure 2. Drought Impacts & Interactions of Key Players.....	8
Figure 3. Two Mechanisms for Water Utilities' Compliance with Drought Responses and Most Influential Internal/External Factors	11
Figure 4. Water-loss management vs. end-user conservation.....	13
Figure 5. Total number of water utilities using each conservation program.....	14
Figure 6. Total number of water conservation programs by approach	15
Figure 7. Influence of programs on water conservation by utility's approach.....	15
Figure 8. Cost-Benefit Analysis of Water Conservation Program.....	17
Figure 9. Cost-Benefit Analysis of Water Conservation Program by Approach	18
Figure 10. Benefits of Water Conservation.....	18
Figure 11. Success Factors for Water Conservation.....	19

Introduction

Background: Georgia Mandatory Drought Responses

Due to enormous rainfall deficits, the entire state of Georgia was very dry in 2007. Especially, across north Georgia the drought conditions were extreme (refer to Figure 1). Lake and stream levels were far below average and surface soil moisture deficits had also become worse, a situation that imposed substantial negative environmental impacts, social hardships, and economic losses.² According to the Drought Impact Reporter, Georgia had 67 reported drought impacts including two environmental and 31 social ones -- the largest number in the records of the October in 2007.³ Furthermore, the long-term outlook for the drought was not optimistic. This severe drought conditions triggered conflicts between water users across the South. Even mussel species in Florida competed with Georgia's population for water.

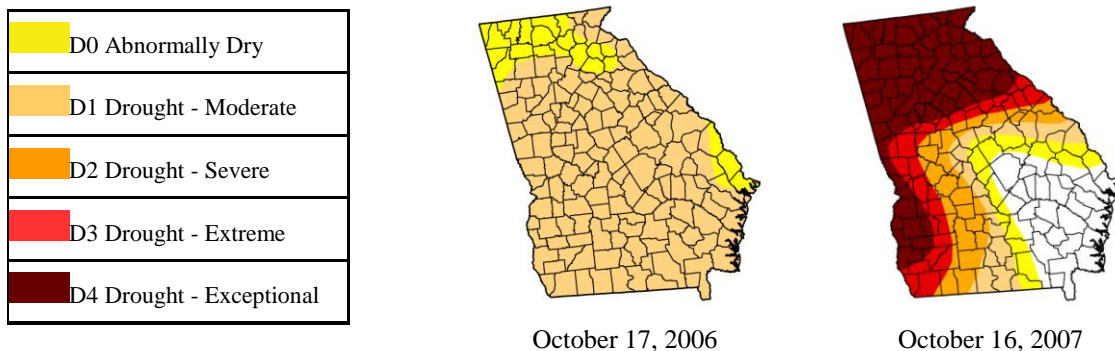


Figure 1. Georgia Drought Monitor, 2006 vs. 2007 (source: <http://www.ndmc.unl.edu/dm/archive.html>)

Drought occurs almost everywhere – not only in the dry western states but also several eastern states. Therefore many states have so-called drought management plans that allow governors to declare a ‘Drought Emergency’ and to order measures to mitigate drought. These measures include voluntary water conservation as well as mandatory water restrictions. Pennsylvania, New Jersey, Virginia, Maryland, Delaware, and many western states have issued Executive Orders related to drought over the last decade.

² National Drought Mitigation Center. 1998. *Impacts of Drought*. Available at: <http://enso.unl.edu/ndmc/impacts/impacts.htm>

³ See: <http://droughtreporter.unl.edu/map.jsp>

On October 20, 2007, the Governor of Georgia signed an Executive Order declaring a ‘Drought Emergency’ and imposing mandatory water restrictions and conservation practices. Based on the Governor’s Order, the Georgia Environmental Protection Division (EPD) enforced new permit restrictions along with fines for noncompliance. All non-farm water permit holders in the 61 North Georgia counties covered under the Level 4 drought designation were required to reduce their water use by 10 percent against the baseline monthly average. This Georgia mandatory water-use reduction for permit holders was exceptional in terms of the strictness and scope of the enforcement. Many other states also implemented mandatory water restrictions such as outdoor watering and car washing bans and imposed mandatory conservation practices to target groups such as new permit holders, but they have usually relied on voluntary participation of various water users in reducing water consumption. Georgia, however, took the unprecedented action of setting a mandatory target goal applied to the majority of water users. The Georgia state government hoped that these aggressive mandatory drought responses would mitigate the disastrous drought conditions and help ensure sufficient and sustainable water resources in the long term as well as in the short term.

The Governor of Georgia also announced an Executive Order to reduce water consumption by 10 to 15 percent at state owned facilities. This order prohibited several water kinds of water use at state facilities and directed agency heads to develop plans to conserve water in a wiser way, to encourage the leadership of the state government in water conservation efforts. However, there were no systematic procedures for evaluation of their leadership and performance, while there was a system established to gather water-use data from water permit holders and to share the information about their general performance with the public. Due to a lack of performance data from the state government, the present study excluded the evaluation of their leadership in conserving water.

The state Environmental Protection Department (EPD) recommended several conservation practices, but water users usually chose appropriate measures to achieve the

target goal by themselves. There were a variety of water conservation practices and tools available, and it seemed relatively easy to obtain general information about costs, performances, and operations. Each water user implemented different measures and generated different outcomes. But the same measures are often associated with different levels of performance outcomes. There was a specific goal (10% reduction), but there were no specific instructions applicable for a certain condition or appropriate by user type. Most water users are not conservation experts and would not spend a lot of their resources identifying the most appropriate measure for them. That is, it may not have been efficient to give them many choices without more specific guidelines. This issue provides the rationale for research to develop more comprehensive guideline for water conservation and drought responses.

Project Scope and Objectives

This research was designed to evaluate the mandatory drought responses by exploring how the key players complied with the requirement and identifying the key factors distinguishing successful performance. The study was designed to provide useful information to develop water conservation guideline for users and help state governments in establishing target goals and groups, as well as to help in developing further policy options for water conservation. That is, the objective of this research was to help improving the performance of water conservation and effectiveness of drought responses by providing better understanding and analytical explanations of those responses. Based on performance evaluation and systematic analyses of the mandatory drought responses in Georgia, this project was designed to answer the following questions:

- Which conservation programs have water utilities implemented and what are their experiences in those programs?
- What are the key factors for successful performance?
- Which approaches are most effective?
- What causes the different levels of performances?
- What are the long-term impacts and policy implications of the mandatory drought responses?

As we see the below (Figure 2), drought often causes various changes from affected players. To deal with drought more effectively, governments may change or develop policies including regulated orders as well as voluntary programs; water users may be required to change their behaviors towards less usage or more efficient consumption in accordance with different price signals and policy changes; and water utilities may need to improve or implement water conservation programs and change prices in order to control water uses. Each player is not affected only by drought itself but also by responses from other players. Although it is not easy to assert which player is most important, this study assumes that water utilities are the central players because they are the major water withdrawal holders who are directly required to reduce water uses by the Georgia order. In order to comply with the 10%-reduction requirement, water utilities reduced waste and improved efficiency in their own systems as well as encouraged and assisted their customers to save more water. That is, water utilities have been playing important roles in water conservation, so this research focused the evaluation of the mandatory drought responses of Georgia water utilities.

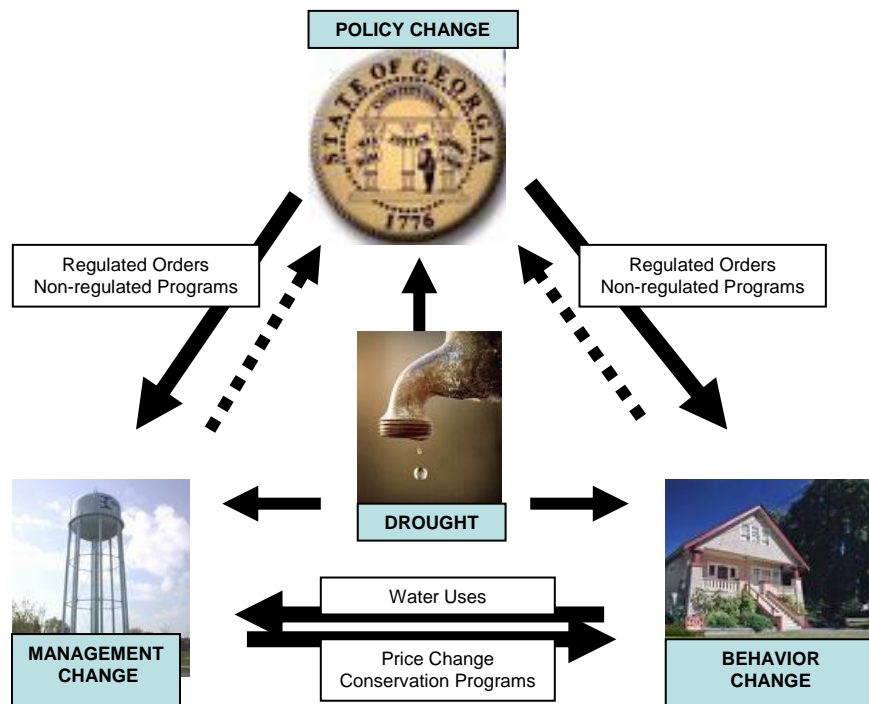


Figure 2. Drought Impacts & Interactions of Key Players

Water conservation is usually beneficial but there are many obstacles to adopting conservation practices actively, such as lack of interest, lack of incentives, lengthy payback periods, costs, a low level of water price, and other social factors. Drought conditions and regulated orders will promote water conservation, but the levels of performance of water conservation will be different in accordance with the types of measure, conditions, and performers. To better understand the different levels of performance, this research recognized the importance of relevant factors as well as the levels of performance of water conservation.

Conservation measures initiated in times of drought often result in a long-term reduction of water consumption (Anderson-Rodriguez, 1996). According to Wang and his colleagues (1994), investment in water conservation may not be recovered in the short-term period. That is, evaluations of short-term performances can be biased and are likely to miss some impacts of the mandatory drought response. However, the GA 10%-reduction requirement only started in late 2007 and data for only an 11-month period were available for this research. Therefore, this research assessed only potential long-term impacts in an approximate way. Later research will be needed to address the long-term effects of water conservation promoted or initiated by the mandatory drought responses.

Past Relevant Work

Even though there has been a significant amount of research focusing on water conservation, this study could be considered unique in its scope, because the Georgia mandatory drought responses were unprecedented. Recently, demand management has been a central issue for water conservation and customers' key roles in saving water have been emphasized. Many researchers have studied behaviors and attitudes of customers related to water conservation including their responses to price or policy changes. However, there has not been much research focused on the roles of water utilities, in particular their roles in a comprehensive framework (Park, 2006).

Some studies have focused on program comparisons in order to evaluate the effectiveness or the efficiency of various programs (White & Fane, 2002; Maddaus, 2001; Renwick & Green, 2000; and Campbell et. al., 1999) while others have tried to identify key factors of successful conservation (Keyes et. al., 2004). There were a few case studies on Georgia water conservation: Elfner (2003) introduced several Georgia water conservation efforts by different water use sectors and Power (2003) presented a success story of water conservation in one of the Georgia counties. Those studies were useful to design our research. That is, our research utilized their research outcomes, considered their research scopes, and also combined their different research methods, such as program comparisons, systematic analyses of key factors, and descriptive analyses.

One interesting study is Inman and Jeffrey's research (2006). They reviewed the performance of various water conservation tools and identified influences on implementation effectiveness, an approach that is similar to ours. However, they focused only on residential conservation measures and utilized only recent conservation literature in the western world, so the scope of the research and application of their results could be limited. Our research also evaluated the performance of conservation measures in an empirical framework, focusing on the performance of key players and categorizing them by approach in a comprehensive and innovative research framework.

Research Methods

Conceptual Model:

Since this research focused on water utilities, we categorized conservation programs based on the utilities' roles in conservation. The "self improvement" mechanisms, which saved water through improvement of performance in their own systems, included conservation practices such as leak control, meter upgrades, unauthorized-use control, energy conservation, operating adjustments, hiring conservation specialists or coordinators, and auditing. "Customer relations" mechanisms, which targeted water-saving changes in customers' behaviors, included practices such as rate increases, conservation-oriented rate structures, customer education, water-efficient

appliance incentives, and recycling supports. Most utilities exercised both mechanisms but some utilities relied on only one.

There were many potential factors that determined the performance level of water utilities. These can be categorized as internal or external. While utilities usually have significant power to control internal factors, this was not true of external factors. The most important external factors were water resource availability and the socioeconomic characteristics of customers. Among internal factors, operation and maintenance (O&M), water prices, and organizational characteristics were identified as most important in previous research (Park, 2006).

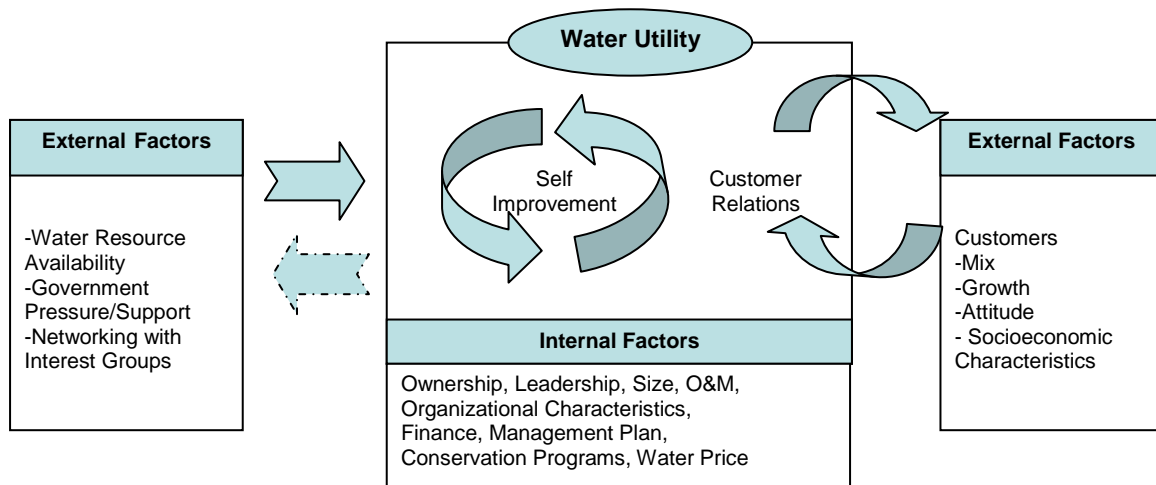


Figure 3. Two Mechanisms for Water Utilities' Compliance with Drought Responses and Most Influential Internal/External Factors

Data Collection Methods:

To evaluate the responses to the mandatory drought measures in a comprehensive framework, it was vital to gather and combine a variety of data. The most important data came from the Environmental Protection Division of the Department of Natural Resources (hereafter, the GA EPD). EPD tracked the water withdrawals of permit holders monthly to see if the permit holders achieved the target goal and evaluate their performance focusing on total water savings. In November 2007 when the 10%-reduction requirement took effect, 61 counties in North Georgia were affected and 855 water

withdrawal permit holders started reporting their use levels along with the baseline monthly average. (Although the requirement expired in the end of March 2008, 166 water utilities in the 55 northern Georgia counties that used more than 100,000 gallons of water per day were still required to report their water use as of September 2008.) The 855 permit holders were potential targets for our project, but we limited that number to 162 to match data availability from other major data sources. The Environmental Finance Center (EFC) provided several key internal financial, demographic, and socioeconomic indicators for water utilities and their service areas, while external financial support data were obtained through the Georgia Environmental Facilities Authority (GEFA). The climatic data was extracted from www.georgiadrought.org and other basic information about water utilities was extracted from the GA EPD website.

To identify key factors which determined the level of conservation performance and to recognize the ways in which water utilities complied with the GA state requirement, we needed more detailed data, so we conducted a web-based survey along with a following-up mail survey of water conservation among Georgia water utilities. The survey questionnaire was designed to gather data from water utilities on organizational characteristics, conservation measures, success factors, and managers' perspectives on water conservation. As mentioned above, this research categorized conservation programs into two mechanisms/approaches: self improvement and customer relations. In order to understand water utilities' approaches to the mandatory drought responses, the survey included five customer-relations and seven self-improvement programs (refer to Figure 5).

The data were analyzed in both qualitative and quantitative ways. We tried to better understand the GA water utilities in terms of conservation activities and opinions, and answer some of our research questions through descriptive analyses of survey results and others through a statistical model. The level of performance (reduction in the amount of water consumption) was a dependent variable and a variety of independent variables (internal and external) were considered in the statistical model. The statistical analyses utilized the combined data from all data sources and survey results.

Results

Survey Outcomes: Descriptive Analyses

We distributed the survey questionnaire to 162 target water utilities and received 86 responses (response rate = 53.09%). Although 16 answers were anonymous, we were able to use some of them in the descriptive analyses. The other 70 respondents were identified and could be combined with other data, and they were analyzed in the statistical model. Most respondents were managers, so their responses were likely to represent their organization's experience and opinions of water conservation rather than personal views.

Figure 4 shows the most important question in our survey. Based on this question, the water utilities were categorized into one of two groups.⁴ Sixty-four percent of the utilities were categorized into a self-improvement group, which considered the self-improvement approach most effective. Another important question was how the utilities weighed public education as against public involvement; this question helped us better understand water utilities in terms of customer relations. It is well-known that customer cooperation is one of the most important factors in successful water conservation; our survey result confirmed that again (see Figure 11). To promote customer cooperation, most utilities responded that they preferred public education over public involvement.

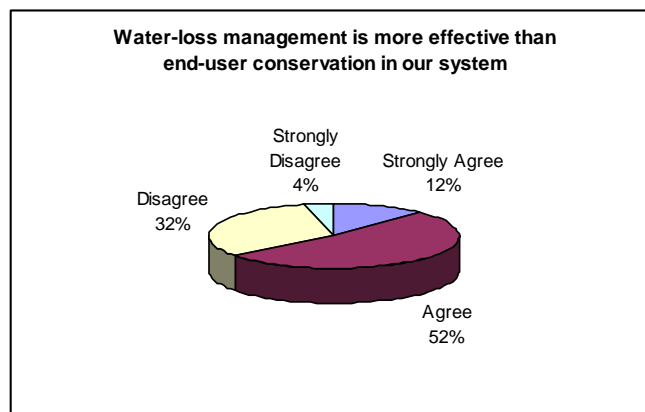


Figure 4. Water-loss management vs. end-user conservation

⁴ Assumption: Utilities that consider the effectiveness of water-loss management (a representative practice of self-improvement approach) more significantly than that of end-user conservation would likely to implement self-improvement approach more.

Seventy-nine utilities had implemented at least one of the twelve water conservation programs. The most popular program was customer education; all utilities except one had implemented it. Hiring conservation specialists or coordinators was not popular among the Georgia water utilities. Figure 5 shows how many utilities employed conservation measures by program. As it implies, the utilities usually implemented multiple programs. The total number of conservation programs that these 79 utilities implemented was 733, of which 43% were promoted (194) or newly implemented (121) to comply with the 10%-reduction requirement. More utilities relied on self improvement than on customer relations before the GA EPD required the 10% reduction. However, after the mandatory reduction was in effect, more utilities started new programs that relied on customer relations rather than self improvement. When they promoted existing programs more energetically, they focused more on the self-improvement approach to comply with the reduction requirement.

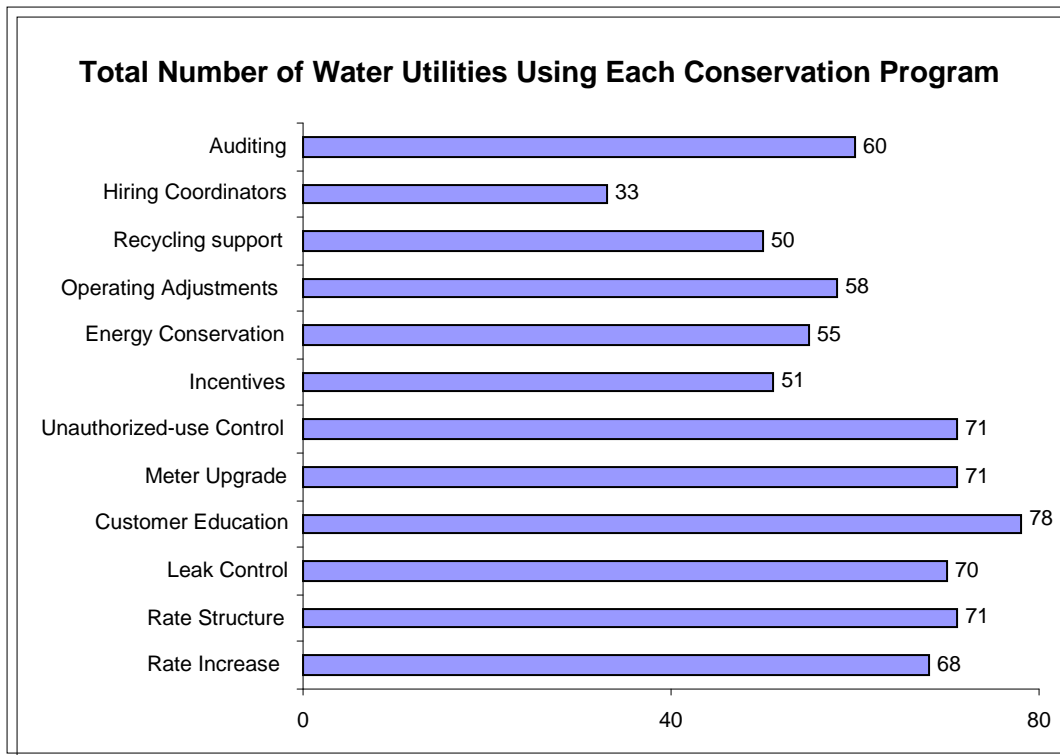


Figure 5. Total number of water utilities using each conservation program

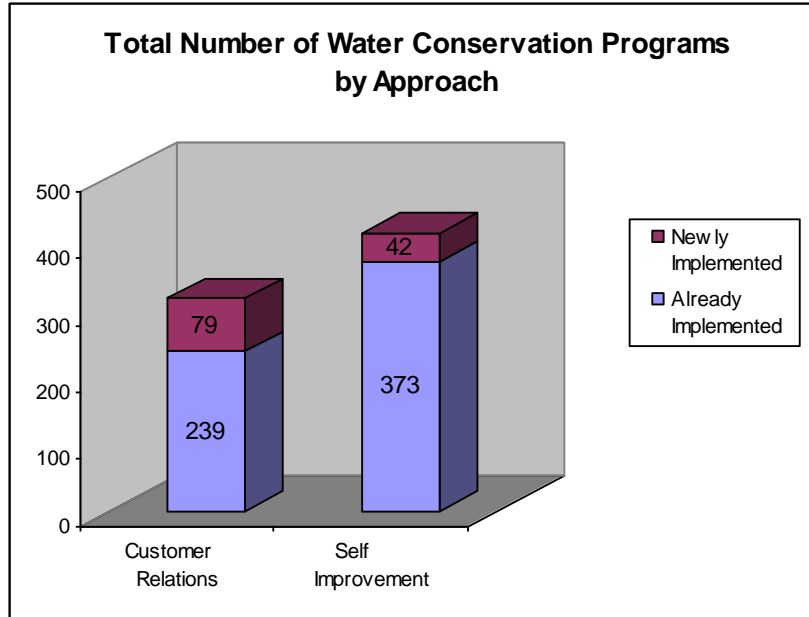


Figure 6. Total number of water conservation programs by approach

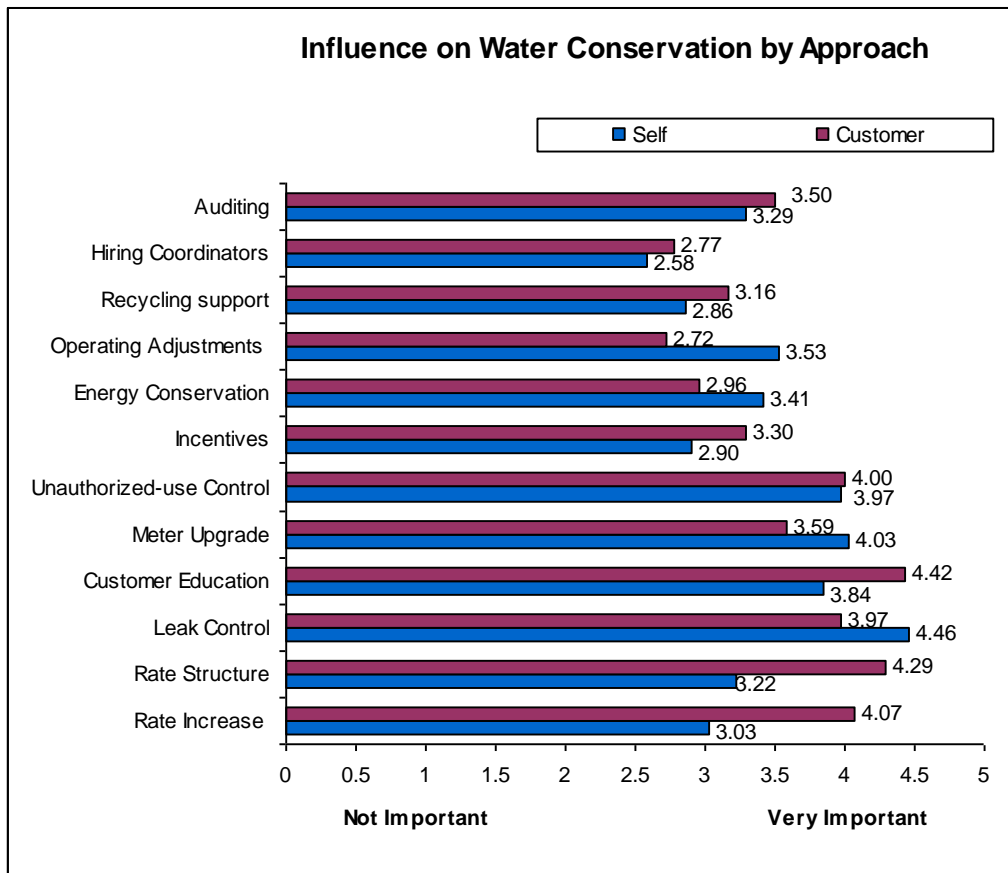


Figure 7. Influence of programs on water conservation by utility's approach

Figure 7 shows how differently water utilities weighed the influence of each program on water conservation by their approach. The respondents in the self-improvement group considered water-leak control to be the most significant conservation measure, followed by meter upgrades and control of unauthorized uses. For those in the customer-relations group, customer education, conservation-oriented rate structures and rate increases were seen to have the most substantial impacts on water conservation.

The survey provided some information on the costs and benefits of various conservation measures as they operated under general conditions and average values. However, most utilities often operate under different conditions so the cost-benefit analysis of each conservation program would vary in accordance with utility's conditions. Most respondents found customer education to be a very cost-efficient conservation measure along with leak control. As expected, utilities had different opinions about the efficiency of the same programs. One of the most interesting outcomes of this survey was that many water utilities could not judge whether their conservation programs were cost efficient or not. This result might come from lack of experience of the utilities with certain programs, or it might imply that many of the utilities did not conduct cost-benefit analyses of their conservation programs. Regardless of approach, a majority of utilities thought conservation programs were cost beneficial, but there were some different evaluations between customer-relations and self-improvement programs (Figure 9).

There are numerous benefits of water conservation; some may be more important to certain utilities than others. Since these water utilities were required to reduce water use, they felt that the most important benefit of water conservation was to comply with the legal requirement.⁵ Many utilities seemed to consider that water conservation increased system efficiency, protected the environment, and achieved their organizational goals. However, many of them did not agree that conservation programs would create new conservation jobs or reduce the pressure of system augmentation.

⁵ Although a little more than 50% of the utilities did not agree that the 10% reduction target of the state government was reasonable, they seemed to make efforts to comply with the legal requirement anyway.

Many utilities selected leadership and customer cooperation as the most important factors associated with successful water conservation. Financial feasibility, long-term plans, qualified employees, and clear purposes/ targets seemed to be also success factors for water conservation. Both internal and external factors were given similar weight (Figure 11).

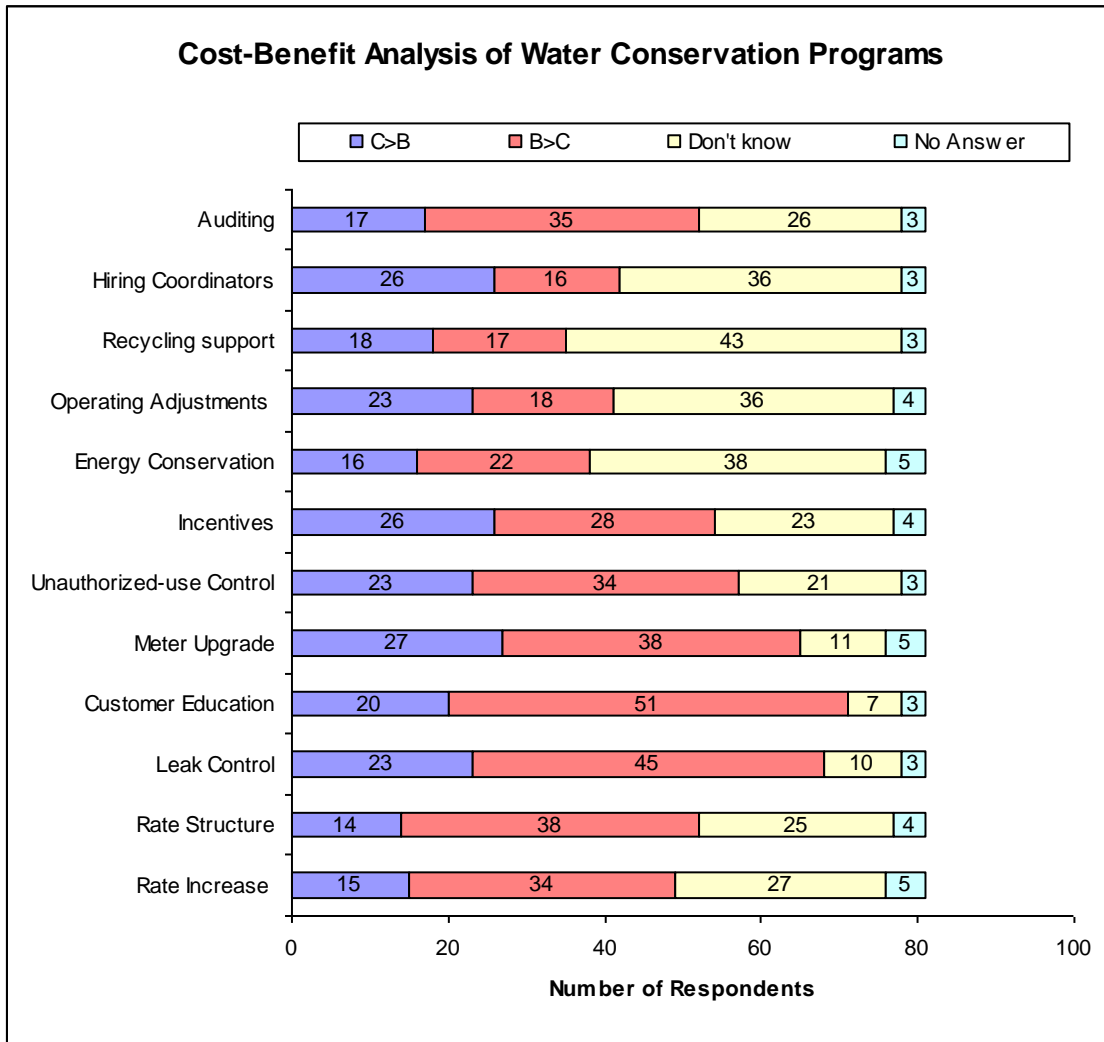


Figure 8. Cost-Benefit Analysis of Water Conservation Programs

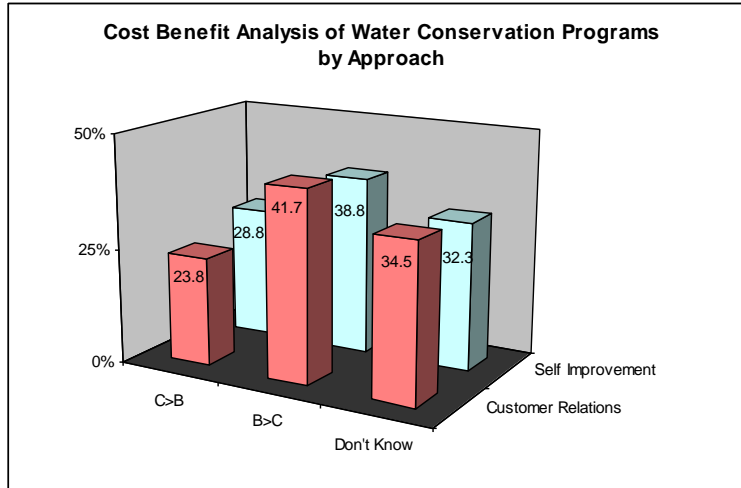


Figure 9. Cost-Benefit Analysis of Water Conservation Program by Approach

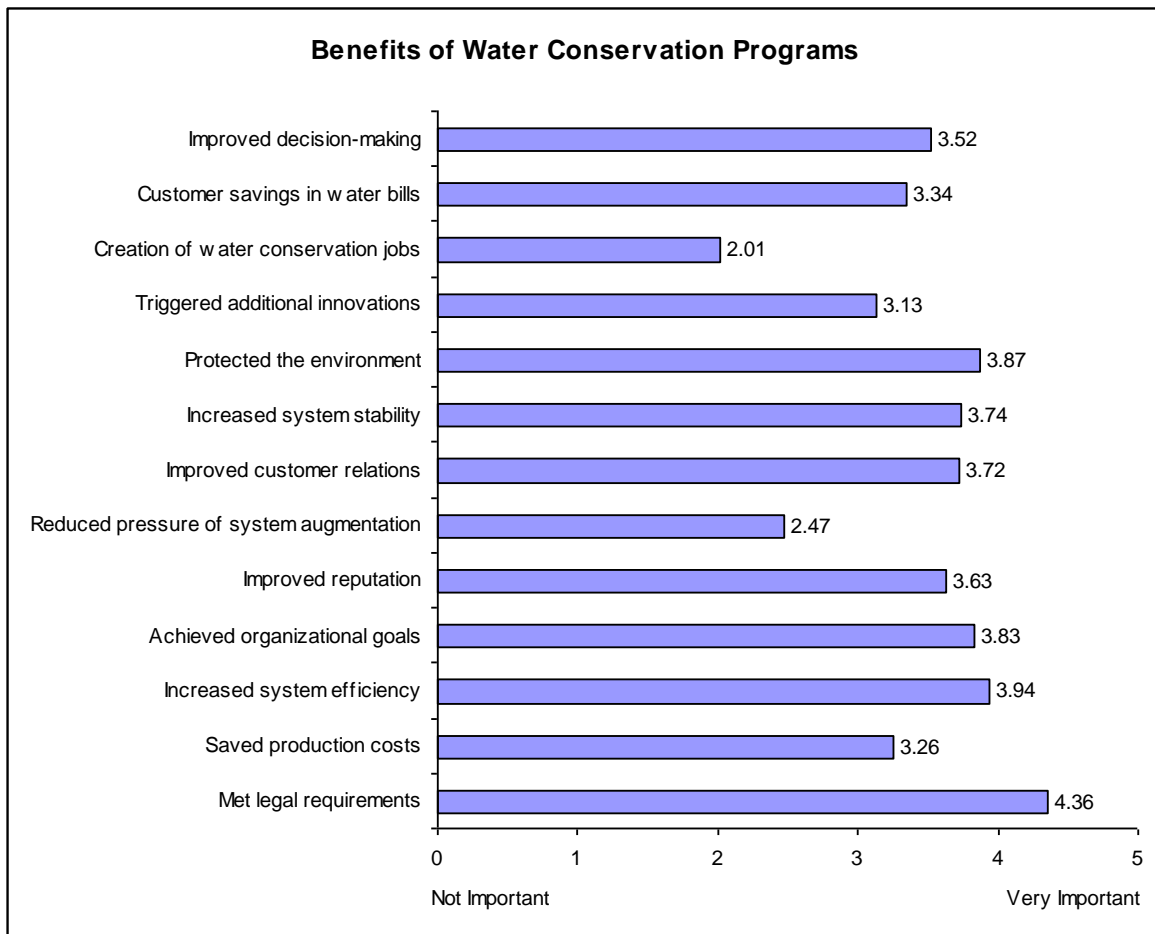


Figure 10. Benefits of Water Conservation

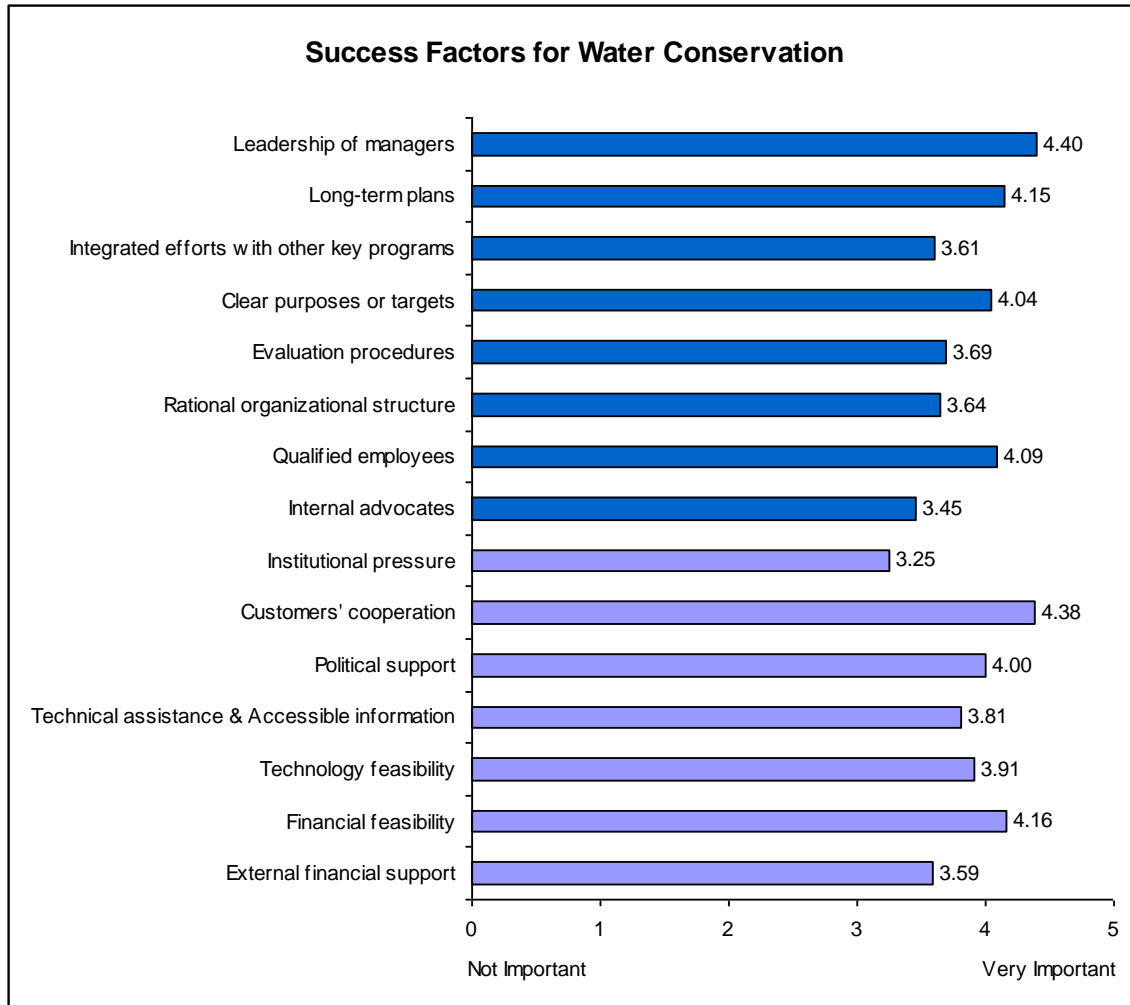


Figure 11. Success Factors for Water Conservation

Analytical Results:

The analytical model was developed to evaluate the performance of mandatory drought responses measured as the reduced amount of water use (MGD) per population served by each utility. Due to some missing data, only 50 utilities were analyzed in this model. At a significance level of 0.05, this study confirmed that most of the independent variables considered in this model were related in some way to levels of performance. Water utilities that had strong internal advocates, higher frequency of the compliance, or higher residential water rates were likely to perform better, as expected. Utilities that used purchased water as a primary source or faced drier conditions (low water balance)

also performed better. The results confirm that the type of water source and water availability affects the level of water conservation.

Table 1. Results of the Analytical Model for Performance Evaluation

Linear regression		Number of obs	= 50
		R-squared	= 0.8804
		Root MSE	= 121.56
Internal/ External	Independent Variables	Increase/ Decrease	Significant
Internal	Ownership (Authority)	+	Marginally
	Internal Advocates	+	Yes
	Large Size	+	No
	No. Compliance	+	Yes
	System Inefficiency	+	Yes
	Leak control	-	Marginally
	Self Improvement_8	-	Yes
	Customer Relations Influence	-	Yes
	Self Improvement (promoted)	-	Yes
	Bill_6000	-	Yes
	Seasonal Rate Structure	-	Yes
External	Inter-government Relations (-)	+	Yes
	Purchased	+	Yes
	Water Balance (July, 2008)	-	Yes
	Customer Complaints (+)	-	Yes
	Poverty Rate	-	Yes
	Water Rate (residential)	+	Yes
	Water Rate (commercial)	-	Yes

One of the interesting findings was that utilities that had higher levels of water losses (system inefficiency) were likely to save more water. This result might be explained by higher marginal costs associated with additional water conservation for highly efficient utilities. Another interesting finding was that utilities with a negative opinion of inter-government relations or lower levels of customer complaints were likely to produce better performance in water conservation. That is, the results suggest that the utility's relationship with external players influences its level of performance in terms of water conservation. The higher the poverty rate in the utility's service area, the lower the performance on water conservation, probably because the utilities were more likely to have financial problems that made it difficult to invest their limited resources in water conservation.

Water utilities that were categorized into the self-improvement group or promoted primarily self-improvement programs to comply with the legal requirements produced lower levels of conservation performance. However, utilities that recognized the significant influence of customer-relations approach were also associated with the low levels of conservation performance. There were some additional unexpected results; for example, utilities that had higher levels of water prices, conservation-oriented rate structures, or higher levels of commercial water rates were more likely to produce poor performance in water conservation.

Table 2. Self-improvement vs. Customer-Relations

	Self Improvement		Customer Relations	
	Obs.	Mean	Obs.	Mean
Reduction/Pop served	45	190.78	23	305.92
Reduction Target (Reasonable)	45	0.47	23	0.38
Response Time (Decreasing)	40	0.28	23	.065
System Inefficiency	37	2.17	20	1.35
Resistance against Changes	40	0.28	23	0.52

Most utilities had implemented both self-improvement and customer-relations programs and their performance levels were determined by the mixed impacts of both approaches. Thus, it was hard to determine the performance levels influenced by only one approach, but it would be interesting to find out which approach might be associated with better performance in water conservation. Table 2 showed some differences of two groups of water utilities, based on their dominant approaches to water conservation (self-improvement vs. customer-relations). More utilities were categorized into the self-improvement group in our data sample and their average amount of reduced water was much smaller than the amount saved by the other group. Even though more utilities in the self-improvement group seemed to consider the 10% target reasonable, their performance levels were not that high. Water utilities in the customer-relations group were likely to perform better in system efficiency as well as water conservation and create better relationships with their customers. However, they seemed to encounter higher levels of

resistance against changes. These simple group comparisons might be not sufficient to confirm the effectiveness of the customer-relations approach, but the results imply that the customer-relations approach seemed to respond more effectively to the GA mandatory drought responses.

To assess the potential long-term impacts of the mandatory drought responses, we selected water utilities that had been reporting their water uses ever since the legal requirement took effect. We then compared performance levels during the period when the legal requirement was on effect with those during the period after the requirement had expired. During the previous period, the total reduction levels against the baseline monthly average ranged from 10% to 18% per month. During the next period, the total reduction levels ranged from 15% to 33% per month. The results thus suggest that the mandatory drought responses could have long-term impacts on water conservation.

Conclusions

The purpose of this study was to help improve the performance of water conservation and the effectiveness of drought responses by providing better understanding and analytical explanations of what utilities did in response to the restrictions. This research explored how the Georgia water utilities complied with the mandatory drought responses, based on a new categorization of their approaches into self-improvement vs. customer-relations methods. The research also identified the factors the utilities associated with successful performance and the factors associated with high conservation performance levels. The analysis evaluated differences between the two approaches and provided a rough approximation of the potential long-term impacts of the legal requirement. Although the study attempted to analyze the mandatory drought responses in a state-wide framework, the sample size was quite small and biased towards large utilities. In addition, the survey generated some inconsistent results. It is therefore difficult to generalize from our findings. However, the research provided detailed information to help better understand utilities' responses to drought and some interesting findings for that later studies can explore.

Most water utilities consider implementing water conservation programs in their systems and developing supporting programs to encourage customer-side conservation an important part of their business. However, it is arguable whether they undertake water conservation efficiently. This research found that many utilities could not identify the efficiency of many conservation programs. This lack of information means that utilities cannot choose the most efficient options to deal with extreme conditions such as drought. Cost-benefit analysis is complicated for many utilities, and state water authorities may want to develop easy guidelines and provide training.

The results of the statistical analysis suggest that utilities with high levels of system efficiency or those serving poor areas might have difficulty making efforts for further water conservation. Therefore, it might be necessary to provide them some kind of support system including financial and technical assistance. This research attempted to develop the new approach to understand water utilities, but still faced challenges in categorizing and measuring them in a comprehensive framework. Further studies are needed to develop the measures further and provide on the ground data for the efficiency and effectiveness of the various conservation measures.

References

1. Anderson-Rodriguez, Lynn. 1996. Promoting Efficient Water Use. *Journal of the American Water Works Association*. Jan., Vol. 88, No. 1: 8.
2. Elfner, M. A. 2003. Water conservation in Georgia: who's doing what and where do we go from here? Available at:
<http://gwri.ce.gatech.edu/GAConf/Proceedings/Papers/2003/Elfner.PDF>
3. Inman, D. & P. Jeffrey. 2006. A review of residential water conservation tool performance and influences on implementation effectiveness. *Urban Water Journal*. 3(3): 127-143.
4. Keyes, A. M., M. Schmitt, and J. L. Hinkle. 2004. Critical Components of Conservation Programs that Get Results: A National Analysis. *American Water Works Association, Water Conference Proceedings*.

5. Maddaus, L. A. 2001. *Effects of Metering on Residential Water Demand*. Masters Project. University of California, Davis.
6. National Drought Mitigation Center. 1998. *Impacts of Drought*. Available at: <http://enso.unl.edu/ndmc/impacts/impacts.htm>
7. Park, Hyun Jung . 2006. *A Study to Develop Strategies for Proactive Water-Loss Management*. Georgia Institute of Technology.
8. Power, C. 2003. Water conservation in coastal Georgia: a success story. Available at: <http://gwri.ce.gatech.edu/GAConf/Proceedings/Papers/2003/Power.pdf>
9. Renwick, M. A. and R. D. Green. 2000. Do Residential Demand Side Management Policies Measure Up? An Analysis of Eight California Water Agencies. *Journal of Environmental Economics and Management*. 40: 37-55.
10. Wang, Young-Doo, et al. 1994. *Integrated Resource Planning Framework For Water Utilities: Applicability and Issues*. Newark, DE: Center for Energy & Environmental Policy, University of Delaware.
11. White, S. B. and S. A. Fane. 2002. Designing Cost Effective Water Demand Management Programs in Australia. *Water Science and Technology*. 46(6-7): 281-8.

Appendix 1: Description of the Variables in the Statistical Model

Dependent Variable	
Reduction/SvsPop	Total amount of water reduction per Population served (MGD)
Independent Variables	
No. Compliance	Total number of compliance with legal requirement (1-11)
System Inefficiency	Water loss per employee (%/employee)
Bill_6000	Water bill for 6,000 gal
Seasonal Rate Structure	1 if a utility had seasonal rate structure, 0 otherwise
Leak control	1 if a utility implemented leak control in the system, 0 otherwise
Self Improvement_8	1 if a utility responded that water-loss management was more effective than end-user conservation, 0 otherwise
Inter-government Relations (-)	1 if a utility recognized inter-government relations negatively, 0 otherwise
Customer Complaints (+)	1 for a utility with increasing customer complaints, 0 otherwise
Poverty Rate	Poverty Rate in Service Area (%)
Purchased	1 if the major water source was from purchased, 0 otherwise
Water Balance (July, 2008)	Differences between precipitation and evaporation (inch): Proxy for water resource availability
Water Rate (residential)	Residential Water Rate for basic service (0 gal)
Water Rate (commercial)	Commercial Water Rate for basic service (0 gal)
Customer Relations Influence	Degree of the average influence of customer-relations programs on water conservation that each utility evaluated
Ownership (Authority)	1 if ownership of a utility was authority, 0 otherwise
Internal Advocates	Degree of the importance as a success factor for water conservation
Large Size	1 if a utility used 100,000 gal per day, 0 otherwise
Self Improvement (promoted)	Total number of the promoted conservation programs relied on self improvement

Appendix 2: Detailed Results of the Statistical Model

Linear regression		Number of obs	=	50
		R-squared	=	0.8804
		Root MSE	=	121.56
Reduction/SvsPop	Coef.	Robust Std. Err.	t	P>t
No. Compliance	39.65123	8.20177	4.83	0.000
System Inefficiency	39.10591	12.04644	3.25	0.003
Bill_6000	-13.24993	4.028011	-3.29	0.003
Seasonal Rate Structure	-219.5222	85.51275	-2.57	0.015
Leak control	-63.08496	35.16552	-1.79	0.083
Self Improvement_8	-129.2005	46.8632	-2.76	0.010
Inter-government Relations (-)	114.6114	42.15656	2.72	0.011
Customer Complaints (+)	-213.6315	78.50775	-2.72	0.011
Poverty Rate	-9.94408	3.721891	-2.67	0.012
Purchased	150.556	62.14342	2.42	0.021
Water Balance (July, 2008)	-50.52084	19.19763	-2.63	0.013
Water Rate (residential, 0 gal)	27.52579	6.640864	4.14	0.000
Water Rate (commercial, 0 gal)	-13.20376	3.451394	-3.83	0.001
Customer Relations Influence	-49.92219	22.814	-2.19	0.036
Ownership (Authority)	100.9634	56.56277	1.78	0.084
Internal Advocates	60.99806	16.14093	3.78	0.001
Large Size	87.95594	78.46038	1.12	0.271
Self Improvement (promoted)	-23.52186	10.51941	-2.24	0.033
constant	190.4309	137.2032	1.39	0.175

Information Transfer Program Introduction

None.

GWRI Information Transfer Activities

Basic Information

Title:	GWRI Information Transfer Activities
Project Number:	2008GA189B
Start Date:	3/1/2008
End Date:	2/28/2009
Funding Source:	104B
Congressional District:	5
Research Category:	Not Applicable
Focus Category:	None, None, None
Descriptors:	None
Principal Investigators:	Aris P. Georgakakos

Publication

USGS Summer Intern Program

None.

Student Support					
Category	Section 104 Base Grant	Section 104 NCGP Award	NIWR-USGS Internship	Supplemental Awards	Total
Undergraduate	1	0	0	0	1
Masters	5	0	0	0	5
Ph.D.	12	0	0	0	12
Post-Doc.	1	0	0	0	1
Total	19	0	0	0	19

Notable Awards and Achievements